Tesi di Dottorato

Stochastic models for phytoplankton dynamics in marine ecosystems

Modelli stocastici di dinamica di fitoplancton negli ecosistemi marini

Tutor:
Prof. Davide Valenti

Dottorando:
Dott. Ing. Giovanni Denaro

Coordinatore:
Prof. Bernardo Spagnolo

SSD: Fis03

Università degli Studi di Palermo - Dipartimento di Fisica e Chimica

---

Corso di DOTTORATO DI RICERCA INTERNAZIONALE in FISICA APPLICATA
XXIV CICLO - 2014

To my family members who have always been close to me in times of difficulty,
To all whom believed in my skills,
To my cousin Giacomo with the hope that he can win the battle more hard of his life.

Acknowledgements

First and foremost, I would like to thank my advisor, Prof. Dr. Davide Valenti, for giving me the opportunity to work on this interesting project. I thank Davide for giving me the freedom to explore, sharing his critical insights and monitoring me throughout this years of research. Moreover, I thank him for encouragements and inspirations, unyielding support and vision that drives this research program forward. Without his organizational and scientific skills, I would not have had the opportunity to venture as researcher in the amazing field of the *Population Dynamics in Marine Ecosystems*.

By continuing ever in the *Department of Physics and Chemistry* (DIFIC) of the *University of Palermo*, my second thanking goes to Prof. Bernardo Spagnolo which has discovered my abilities as applied physicist during the SISSIS course of *Statistical Thermodynamics* about seven years ago. Without his initial support, probably I would not have begun to enjoy the taste of scientific research. Soon after, I would like to thank Dr. Pasquale Caldara, for his endless willingness to support me from a point of view technical during the first year of PhD course. Moreover, I want to thank Dr. Angelo La Cognata and Dr. Stefano Spezia who helped me to develop and to extend the numerical codes used in this thesis. Then, I thank to Professors of my qualification courses for the obtained skills through their lectures: Diego Molteni (Computational Physics), Angelo Bonanno (Oceanography and Physics of the Atmosphere), Bernardo Spagnolo (Physics of Complex Systems), Francesco Fauci (Image Processing Theory and Techniques), Salvatore Basile (Theoretical Physics), Leonardo Abbene, Maurizio Marrale and Fabio Principato (Experimental Physics).

I also wish to thank Prof. Dr. Lutz Schimansky-Geier at *Humboldt University* in Berlin and Prof. Dr. Horst Malchow at *University of Osnabrueck* in Osnabrueck (Germany) for valuable scientific discussions on some topics of this thesis and for the kind hospitality in their research institutes. Their knowledge of the mathematical physics, of the complex systems, and frank opinions are always appreciated. Again in Germany, I would like to thank the colleague PhD student Michael Bengfort for useful discussions and technical support during my visit in Osnabrueck. Finally, I wish to thank the colleague Tobias Schwarz and other students of Humboldt Uni-

versity who were always welcoming and helpful.

I would need to thank Prof. Dr. Salvatore Mazzola and members of the *Istituto per l'Ambiente Marino Costiero* at *Centro Nazionale delle Ricerche* in Capo Granitola (Italy) for giving me the opportunity to take part at the Oceanographic Survey on board the *Dalla Porta* in May 2011, and to use the experimental data sampled in Mediterranean Sea during last years. Moreover, I would like remind Dr. Christophe Brunet of the *Stazione Zoologica Anton Dohrn* in Naples (Italy) for the useful discussions on the mechanisms of marine ecosystems and the behaviour of the phytoplankton species.

A special thanking goes to my colleague Maria Antonietta Lodato who helped me in times of difficulty during these strenuous years. She have lived this PhD experience after me and with her I spent two years in the same laboratory. I hope that she can forgive me for prolonged absences in laboratory. I also remember with great enthusiasm Dr. Luciano Curcio, Dr. Angelo La Cognata, Dr. Stefano Spezia and Dr. Nicola Pizzolato, they have been the colleagues with whom I have spent the most hours of work in the laboratory during the previous experiences of grants, before to begin the PhD course. With them, I could discuss about many topics about physics, mathematics and also about our personal life.
I would like to mention the colleagues of the my PhD cycle, Dorotea Fontana, Accursio Antonio Turturici and Letizia Vivona. I would like to extend my thanks to all DIFIC's colleagues, and in particular to Dr. Maria Francesca Alberghina, Dr. Giuseppe Augello, Dr. Irina Balakhnina, Dr. Rosita Barraco, Dr. Onofrio Rosario Battaglia, Dr. Giuseppe Cannella, Dr. Anna Longo, Dr. Fabio Vizzini and Dr. Anna Zaitseva. Another special thanking goes to Claudio Guarcello and Luca Magazzú with my wish to get a long chain of successes in their research fields.

Finally, I would need to express my profound gratitude for my family: dad, mom and Andrea, for their love and unwavering support throughout these difficult years.

Commonly Used Abbreviations

Deep Chlorophyll Maximum: DCM
Modified Atlantic Water: MAW
Levantine Intermediate Water: LIW
Eastern Mediterranean Deep Water: EMDW
Western Mediterranean Deep Water: WMDW
High Performance Liquid Chromatography: HPLC
Upper Mixed Layer: UML
Upper Chlorophyll Maximum: UCM

Contents

Introduction

Population dynamics is that part of life science which studies the space-time evolution of biological species, considering also all phenomena, such as environmental processes, whose influence is of paramount importance for a complete description of the life processes within an ecosystem. Historically population dynamics was of interest in mathematical biology, just think of the Gompertz, Verhulst and Malthusian models, or the famous Lokta-Volterra equations [1, 2]. All these models are still widely used in various research fields. In particular, the most important are the epidemiological ones for the study of viral transmission [3], and the ecological ones on the migration and foraging strategies of animal species [4].

During last decades specific applications of population dynamics and theoretical models allowed to describe the behaviour of biological species in aquatic systems. In particular great attention was devoted to the analysis and prediction of the dynamics which govern the spatio-temporal distributions of planktonic species in marine ecosystems. A deeper knowledge of the mechanisms responsible for the dynamics of planktonic populations represents in fact one of the most pressing and, at the same time, fascinating challenges for ecological modeling, due to emergent problems such as global warming and reduction of the primary production, the latter being at the base of the food chain. During the 20^{th} century, biologists and naturalists devoted much effort to study spatio-temporal distributions of biological species and in particular the mechanisms responsible for the formation of complex patterns, in view of possible applications to the population dynamics in aquatic ecosystems. Despite of this, the field observations constitute yet a challenge for theoreticians and there is much work to be done before mathematical models, able to explain the complexity of these dynamics and to provide a satisfactory description of the planktonic spatio-temporal dynamics, are devised [5].

It is important to recall that the analysis of the spatio-temporal behaviour of phytoplankton species, in particular in marine ecosystems, is very worth for fishing activities, whose efficiency depends on the length of food chains, transfer efficiency and primary production, i.e. the process responsible for the phytoplankton biomass growth [6]. In particular the primary production, which constitutes the base of the metabolic activity of all aquatic ecosystems, is responsible for the amount of fish populations [7, 8, 9, 10, 11]. In fact the variations in the growth of fish species among different areas of the world are mainly explained by changes in the chlorophyll concentration, which is a marker of the presence of phytoplankton populations. For instance, due to a decrease in the biomass concentration during last years, it has been observed that the values of the anchovy growth in some regions of the world result to be in the low end of the range [12]. Therefore, the knowledge of the phytoplankton concentrations and their spatial distributions in marine ecosystem is of fundamental importance to understand the dynamics and structure of aquatic ecosystems [13, 14, 15, 16, 17, 18, 19, 20]. In fact the results obtained by using predictive model could be useful to forecast future changes in the phytoplankton distributions in marine ecosystems, contributing to prevent the decline of the phytoplankton production and the consequent decrease of fish species [18, 21, 22, 23].

In order to get a correct description and comprehension of these dynamics, it is worth considering that phytoplankton communities and their abundances depend on several phenomena of hydrological and biological origin, and involve different limiting factors [24]. The Mediterranean Sea, i.e. the marine ecosystem studied in this thesis, is generally characterized by oligotrophic conditions, and a previous work [25] suggested that there is a decreasing trend over the time in the chlorophyll concentration present in the Sicily Channel. This has been associated with an increased nutrient limitation resulting from reduced vertical mixing due to a more stable stratification of the basin, in line with the general warming of the Mediterranean Sea [25, 26, 27].

In marine ecosystems, the light intensity and nutrient concentration select different species and groups along the water column, contributing to determine the biodiversity of the ecosystem. The growth of all phytoplankton species is indeed limited by the light intensity I and nutrient concentration R [16, 19, 20, 28]. The light penetrates through the surface of the water and decreases exponentially along the

water column. The nutrients, which are in solution, come from deeper layers of the water column, near the seabed, and are characterized by an increasing trend from the surface waters to the benthic layer [13, 16, 17, 18, 29]. In Mediterranean Sea phosphorus, which is contained in phosphates present in solution, is the nutrient component playing the role of limiting factor for the growth of the phytoplankton populations [30, 31]. The mathematical models introduced in this thesis take into account both limiting factors, i.e. light intensity and phosphorus concentration, in order to better reproduce the vertical profiles of the phytoplanktonic species.

In particular, depending on the role assigned to these two environmental variables, i.e. natural light and food resources, the studies on this topic can be divided in two groups: (i) works based on light-limitation models, and (ii) studies based on models which include as limiting factors both light and nutrient. Initial investigations devoted to phytoplankton dynamics, such as the pioneering work by Riley et al. [32], exploited the first approach considering light as the only limiting factor for the phytoplankton dynamics. In this work authors introduce a model in which processes of vertical diffusion and settling are, for the first time, taken into account together with the growth and death processes of phytoplankton, considering only light-limitation phenomena without taking into account the self-shading effect of the algae. Detailed numerical models have been also developed to simulate the vertical profiles of phytoplankton concentration [33, 34, 35]. In these works, the role of the self-shading effect of the algae in phytoplankton dynamics is taken into account by modifying the analytical model by Riley et al. [32]. In particular, the non-linear term, that appears in the differential equation of phytoplankton dynamics, leads to an interesting mathematical problem on the steady-state solutions of the system, studied and solved by Shigesada and Okubo [35]. In the last two decades, extensive theoretical studies have been performed by using models which include the co-limiting effect of light and nutrient. Specifically, phytoplankton dynamics has been reproduced considering several systems and different effects such as vegetation patterns in water-limited habitats [16, 36], marine ecosystems with weakly mixed layer [17, 29, 37], well-mixed aquatic systems with a light gradient [13, 38], and non-uniform systems with two species in competition for two limiting resources [7, 18, 39, 40, 41, 42, 43]. In all previous works, however, the distribution of phytoplankton in oceans and lakes were obtained by using deterministic models to describe and reproduce the experimen-

tal data of biomass concentration. Conversely, very few authors applied stochastic approaches to describe the population dynamics of planktonic species. Finally, no authors converted the numerical results, obtained from mathematical models, in chlorophyll-a concentration in order to compare theoretical findings with experimental ones. On the base of these arguments two elements, representing a novelty, have been introduced in this thesis: i) the use of a stochastic approach to model the dynamics of one or more phytoplankton populations; ii) the comparison, between theoretical and experimental distributions of chlorophyll concentration, performed by the use of a conversion curve which allow to obtain, for each phytoplankton population, the equivalent chlorophyll content starting from the biomass concentration. It is important to recall that marine ecosystems, because of the presence as well of non-linear interactions among their parts as deterministic and random perturbations due to environmental variables, are complex systems [44, 45, 46, 47, 48, 49, 50, 51, 52, 53, 54, 55, 56, 57, 58, 59, 60]. Therefore, in order to better reproduce this non-linear and noisy dynamics, it is necessary that the models take into account the presence of external random fluctuations [61, 62].

The focus of this thesis is to study the population dynamics of phytoplankton species in the basin of the Mediterranean Sea, using stochastic advection-reaction-diffusion models in which random fluctuations are introduced by terms of multiplicative white Gaussian noise [29, 37, 51, 63]. In particular, the models presented are focalized on the spatio-temporal analysis of picophytoplankton, i.e. phytoplankton species whose linear size is less than 3 μm. This fraction of phytoplankton is formed by three groups, i.e. Prochlorococcus, Synechococcus and picoeukaryotes [64, 65, 66], and takes in account, on average, about 80% of the total chlorophyll-a ($chl\ a$) and divinil chlorophyll-a ($DVchl\ a$) in Mediterranean Sea [67, 68].

In this thesis three studies, conducted in two hydrologically stable areas of the Mediterranean Sea, i.e. Sicily Channel and Tyrrhenian Sea, are presented.
In particular, in the first part a stochastic advection-reaction-diffusion model, valid for poorly mixed waters, is introduced to describe the dynamics of a picoeukaryotes group in two different sites of the Sicily Channel. As a first step, a deterministic analysis [16, 17] is performed to obtain in stationary conditions the vertical profiles of the picoeukaryotes population, distributed along a one-dimensional spatial domain. Moreover the interaction of this population with the environment is assumed

to occur through both limiting factors, that is light intensity and concentration of nutrient, which in our ecosystem mainly consists of phosphorus. Therefore, intraspecific competition of the picoeukaryotes population for light and nutrients is also considered. As a second step random fluctuations, due to the interaction with the environment, are taken into account by adding a source of Gaussian multiplicative noise to the differential equation for the biomass concentrations. Finally, the indirect effects of environmental noise on picoeukaryotes dynamics are considered, by inserting a term of white Gaussian multiplicative noise in the differential equation for the nutrient concentration.

In the second part of the thesis the initial stochastic model [7, 17, 18] is modified to analyze the dynamics of two picophytoplanktonic groups, keeping to consider the light intensity and nutrient concentration as limiting factors. Moreover, in order to guarantee the coexistence of the two populations in the deep chlorophyll maximum (DCM), suitable values of biological and environmental parameters have been set. The main goal of this two-species analysis consists in the improvement of the results obtained by the one-species model, in order to obtain a better matching with the experimental data [17, 29, 37, 42]. Also in this case the spatio-temporal behavior and profiles of the biomass concentration of the two picophytoplakton groups, i.e. picoeukaryotes and Prochlorococcus, have been initially studied in the absence of noise sources. Afterwards, analogously to the procedure followed for the one-species model, in view of a better and more realistic description of the marine ecosystem considered, terms of multiplicative Gaussian noise have been introduced, obtaining also in this case a stochastic model. In particular, as a first step, the stochastic analysis has been performed inserting a source of white Gaussian noise in the differential equation for the nutrient dynamics. Afterwards, two Gaussian multiplicative noise terms have been added to the differential equations that describe the population dynamics of picoeukaryotes and Prochlorococcus. Statistical checks based on χ^2 and K-S tests have showed an agreement between theoretical results and experimental data better than that obtained by using the one-species model.

The last study presented in this thesis consists in devising a deterministic model which allows to describe the clorophyll-a concentrations obtained from data collected in a site of the Tyrrenian Sea at different times. In particular the model is able to reproduce the spatio-temporal behaviour of five picophytoplankton species

whose concentrations were sampled during different oceanographic surveys in the period from 24 November 2006 to 9 June 2007. Here, the competition between phytoplankton species for light and nutrient (phosphorus) has been modeled by using a system of coupled reaction-diffusion-taxis equations. Moreover in this analysis, in order to describe the water column stratification, it has been assumed that the vertical diffusivity is not constant, but takes a larger value in the upper part of the water column and a much smaller value in the deeper layers. Finally, to guarantee the coexistence among the five species along the water column, the invasion threshold criterion, devised by Ryabov and Blasius [7, 69], has been used. Preliminary results displayed a good agreement between numerical distributions and experimental profiles.

It is important to note that, in all systems analyzed in this thesis, the steady vertical distributions of the phytoplankton biomass have been obtained numerically solving the equations of the models by an explicit finite difference scheme. Moreover, in order to compare the numerical results with the experimental findings, the theoretical cell concentrations of the picophytoplankton species have been converted into *chl a* and *DVchl a* concentrations by using the curves of mean vertical profile obtained by Brunet et al. [68] for picoeukaryotes and Prochlorococcus, and assuming that the content per cell of Synechococcus is constant and equal to 2 fg/cell [70].

The plan of this thesis is as follows. In Chapter 1 we give a short presentation of the experimental and phytoplanktonic data collected during different oceanographic surveys in Mediterranean Sea. In Chapter 2 we introduce the deterministic and stochastic approaches (one-species model) adopted to describe the picoeukaryotes dynamics in Sicily Channel. Moreover, numerical results for the biomass concentration are compared with experimental data by using χ^2 goodness-of-fit test. In Chapter 3 we modify the previous one-species model to study the population dynamics of two picophytoplankton groups, i.e. picoeukaryotes and picoprokaryotes (Prochlorococcus). The agreement between theoretical results and experimental findings is checked by using two comparative methods: χ^2 goodness-of-fit test and Kolmogorov-Smirnov (K-S) test. In Chapter 4 we introduce a deterministic model used to perform the spatio-temporal analysis of five picophytoplankton species sampled in a site of the Tyrrhenian Sea: numerical results are compared with experimental data acquired during different oceanographic surveys in the period from

24 November 2006 to 9 June 2007. Finally conclusions and future prospects are discussed.

Chapter 1

Experimental data

In the first part of the chapter, we give some specific information on hydrological and chemical proprieties of Mediterranean Sea. Afterwards, sampling strategies and data collection methodologies, used during oceanographic surveys, are described in the two sub-sections dedicated to geographical areas studied in this thesis.

In the second section of the chapter, we use the study of taxonomic pigments to classify different phytoplankton groups and estimate their quantities. Moreover, the chlorophyll cellular content for every picophytoplankton species is obtained by using the experimental findings analyzed in previous works.

The last part of the chapter covers the description of vertical profiles of temperature and *chl a* concentration sampled in marine ecosystems during several oceanographic cruises.

1.1 Environmental data

In this section, we study the experimental data collected in Mediterranean Sea during last two decades. By analyzing data, it is possible to observe that Mediterranean basin is characterized by particular hydrological and chemical peculiarities described in the following.

From a hydrological point of view, the Mediterranean Sea is a three-layer system [31, 71, 72, 73]. Specifically, the upper layer (from the surface down to 200 m) is occupied by the Modified Atlantic Water (MAW), which enters through the Strait

of Gibraltar from the Atlantic Ocean, and flows from west to east by crossing the whole Mediterranean basin. The intermediate layer (from 200 m down to 600-700 m) is occupied by the Levantine Intermediate Water (LIW), which is formed in the easternmost part of the Mediterranean basin. The LIW crosses Mediterranean Sea up to reach the Strait of Gibraltar, where it is mixed with Atlantic Water. Finally, the deep layer (from 700 m down to the bottom of water column) is occupied by two different dense water masses corresponding to two sub-basins of Mediterranean Sea, i.e. Eastern Mediterranean Deep Water (EMDW) and Western Mediterranean Deep Water (WMDW). The first is formed in the Adriatic Sea and Aegean Sea during the winter season, while the latter is generated by strong northerly winds, which blow in the Gulf of Lions and Ligurian Sea during late winter and early spring.

In this thesis, the analysis of experimental data has been restricted to the upper layer which correspond to the euphotic zone, where the environmental conditions allow the growth of phytoplankton species. Here, the parameter used to identify the nutrient considered limiting factor is the Redfield stoichiometry, which gives the atomic ratios of chemical elements found in phytoplankton and throughout the deep oceans. In the top layer, chemical proprieties showed anomalous values of Redfieldian nutrient concentration ratios respect to other marine ecosystems [31, 72, 74]. Indeed, in Mediterranean Sea, both nitrate to orthophosphate ($N : P$) and orthosilicate to nitrate ($Si : N$) molar ratios are greater than the Redfieldian ones ($N : P$=16 and $Si : N$=0.9). In particular, the ratio $N : P$ decreases in the western basin, but it stays always above 20. Therefore, it has been chosen the phosphorous as the nutrient component that plays the role of limiting factor in our models.

After the description the main features of Mediterranean Sea, it is necessary to give some specific information on the marine ecosystems studied. In the following subsections we are going to introduce the sampling methods and environmental data of three sites located in the Strait of Sicily and Tyrrhenian Sea.

1.1.1 Strait of Sicily

The former two works presented in this thesis take into account the experimental data acquired in the period 12^{th} - 24^{th} August 2006 in the Sicily Channel area (Fig. 1.1) during the MedSudMed-06 Oceanographic Survey onboard the R/V Urania. The hydrological parameters, i.e. conductivity, temperature and density, were

sampled by means of the SBE911 plus CTD probe (Sea-Bird Inc.), while *chlorophyll a* and *divinil chlorophyll a* fluorescence measurements (*chl a/divinil chl a*, $\mu g\ l^{-1}$) were contemporary performed by using the Chelsea Aqua 3 sensor. The vertical profiles of temperature were used to localize the thermocline, which is the depth along the water column at which the gradient of temperature reaches a maximum. On the other side, the fluorescence measurements were used to estimate the total biomass concentration corresponding to all phytoplankton species present in the marine ecosystem.

The CTD stations were located on a grid of 12 x 12 nautical miles in the Strait of Sicily, and the values of the oceanographic parameters were acquired along a transect between the Sicilian and Libyan coasts. In our works, two stations out of the whole data set were considered. Specifically, the selected stations were located in the south of Malta (site L1105) and on the Libyan continental shelf (site L1129b). The experimental data were quality-checked and processed following the MODB instructions [75] using Seasoft software. The post-processing procedure generated a text file for each station where the values of the oceanographic parameters were estimated with a 1 m step. During the MedSudMed-06 Oceanographic Survey, hydrological conditions remained constant for the entire sampling period and were representative of the oligotrophic Mediterranean Sea in summer. Nitrate, nitrite, silicate and phosphate concentrations were not determined.

1.1.2 Tyrrhenian Sea

The third work introduced in this thesis considers the experimental data collected in the period from 24^{th} November 2006 to 30^{th} October 2010 in a sampling site (39^o 30.00′N,13^o30.00′E) localized in the middle of the Tyrrhenian Sea (Fig. 1.2). This is a hydrological stable area of Mediterranean Sea, where oligotrophic waters are mainly populated by picophytoplankton species during the whole year. Here, in order to study the seasonal variability of physical parameters, and nutrient and phytoplankton concentrations, the data were acquired in several times of the year, during three different oceanographic cruises (VECTOR-TM1, November 2006; VECTOR-TM2, February 2007; VECTOR-TM4, June 2007) performed on board of the R/V Urania of the Italian National Research Council (CNR).

In all oceanographic surveys similar sampling strategies and methodologies were

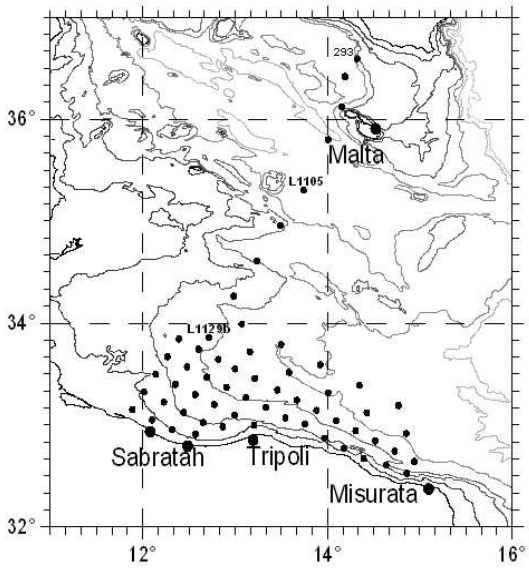

Figure 1.1: Locations of the CTD stations where the experimental data were collected.

used. In particular, vertical profiles of temperature, salinity and density were acquired by using a CTD probe equipped with fluorescence sensor, which measured total chlorophyll concentrations. The vertical profiles of temperature were used to study the displacement of the thermocline along the water column as a function of the time, and localize the depth of the upper mixed layer (UML). The vertical profiles of *chl a* were used to estimate the total biomass concentration of the phytoplankton species and find the position of the deep chlorophyll maximum (DCM) as in two previous works.

Nutrient concentrations and *chlorophyll a* (or *divinil chlorophyll a*) concentrations for every picophytoplankton species were obtained by analyzing the bottle samples collected at almost the same depths (0, 25, 50, ... 200 meters) during the sampling periods. Nitrate, nitrite, silicate and phosphate concentrations, collected in polyethylene vials and stored at $-20\ ^oC$, were determined within a few weeks after the end of each cruise by using classical methods of measurement with slight modifications [72, 73, 76]. The photosynthetic pigments samples were filtered to divide the picophytoplankton fraction from the rest of phytoplankton communities, and stored in liquid nitrogen for pigment analysis [72, 73]. Afterwards, in order to obtain the chlorophyll concentration for each phytoplankton species, high-performance

liquid chromatography (HPLC) analysis was used within two weeks of the sampling in according to the protocol described by Dimier et al.(2007) . Finally, the results of HPLC analysis were compared with those obtained by the fluorescence sensor, showing a qualitative agreement appearing between the values of total *chlorophyll a* and *divinil chlorophyll a* concentration measured by using the two methods.

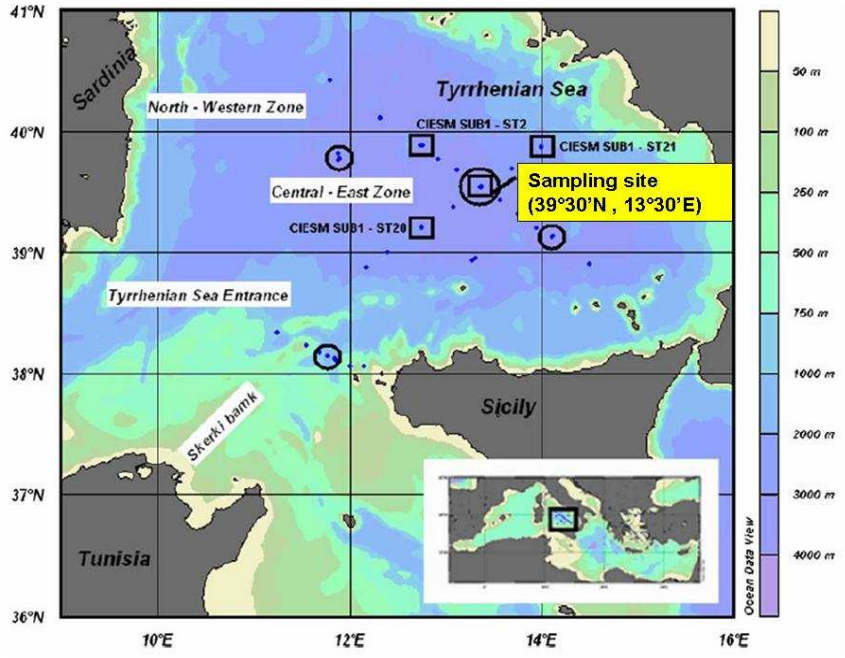

Figure 1.2: Location of the sampling site (39^o 30′.00N,13^o30′.00E) where the experimental data were collected during the period from 24 November 2006 to 30 October 2010 (Courtesy of Ribera d'Alcalà et al., 2009 (Ref. [72])).

1.2 Phytoplanktonic data

The quantity that indicates the presence of phytoplankton biomass in marine environment is the concentration of *chlorophyll a* and *divinil chlorophyll a* [67, 68]. In particular, the contribution of each phytoplankton group to the total phytoplankton biomass is obtained using group-specific conversion factors empirically determined, and based on the analysis of taxonomic pigments [65, 77]. These have been used as size class markers to identify two main size fractions: picophytoplankton ($< 3\mu m$)

and nano- and micro-phytoplankton ($> 3\mu m$).

The picophytoplankton size fraction accounts for 80% of the total *chl a* and *Dvchl a* on average in the Mediterranean Sea, and is mainly represented by two groups: picoprokaryotes and picoeukaryotes. The picoprokaryotes group is dominated by two species of cyanobacteria, i.e. Synechococcus and Prochlorococcus, while picoeukaryotes group is mainly represented by prymnesiophytes (or haptophytes) and pelagophytes [67]. Finally, diatoms, cryptophytes and dinophytes are present in traces.

Prochlorococcus, Synechococcus and picoeukaryotes are usually identified and measured based upon their scattering and autofluorescence [67]. This is due to the presence of *chl a* or *Dvchl a* molecules in their cells. In general, Synechococcus contributes more than 20% of the total chlorophyll concentration on average in the Mediterranean Sea. This species is mainly localized close to the surface water and is almost absent in DCM. Viceversa, Prochlorococcus and picoeukaryotes dominate deeper layers and contribute equally to the picophytoplankton biomass in terms of *chl a* and *Dvchl a* concentrations in DCM, even if Prochlorococcus are numerically more abundant than the picoeukaryotes group [68].

The nano- and micro-phytoplankton fraction amounts in average to 20% of the total *chl a* and *Dvchl a* and is dominated by prymnesiophytes, pelagophytes and diatoms. This size fraction is poorly present in DCM, and is almost uniformly distributed along the water column.

Picophytoplankton groups present eco-physiological properties [78, 79, 80, 81] that make them appropriate to be studied by the use of biological models. In fact, the small size of picoprokayotes and picoeukaryotes leads to a low package effect, which contributes to the light-saturated rate of photosynthesis that can be achieved at relatively low irradiances [78, 82, 83, 84]. This feature allows the growth of picoeukaryotes in deeper layers of the water column. Conversely, a low nutrient uptake of picoeukaryotes leads to an enough high nutrient concentration in shallower layers of the water column, where mainly picoprokayotes are localized and their growth is allowed. As a consequence, picoprokaryotes are dominant in the first 50 meters, but are replaced by picoeukaryotes in deeper water [68].

Experimental findings showed that Synechococcus prevails on others species inside the 0-30 m upper layer [70], where Prochlorococcus concentration remains constant

with depth. In deeper layers, between 50 and 90 m of depth, it has been observed that Synechococcus cells are replaced by Prochlorococcus ones [68]. In particular, the ratio between the cell concentration of Prochlorococcus and Synechococcus shows an significantly increase as a function of depth up to reach its maximum value at 90 m. Moreover the experimental data, acquired in Mediterranean Sea, showed that the vertical profiles of Prochlorococcus concentration have a bimodal distribution in the intermediate layers of the water column [68, 85], indicating the coexistence of two ecotypes of this species: high light-adapted (HL-) ecotype and low light-adapted (LL-) ecotype. The former is localized in the upper part of the euphotic zone between the surface water and 90 m of depth, while the latter is present at depths from 50 m downward [68, 85, 86]. However, the growth rate and the average cell concentration of LL ecotype are lower than those of HL ecotype in Mediterranean Sea. As a consequence, the biomass of Prochlorococcus is mainly located in shallower layers of the water column, between 30 m and 90 m of depth.
It is worth to underline that heterogenous composition is also a feature of picoeukaryotes group. In particular, in a previous work [66], it has been shown as a clear segregation along the water column of species belonging to the picoeukaryotes group is present in Mediterranean Sea. Specifically, Brunet et al. have found that prymensiophytes are more abundant in shallower layers of DCM, while pelagophytes dominate its deeper layers.
Therefore, because of their peculiarities and relevant role in the functioning of the ecosystem, picoprokaryotes and picoeukaryotes constitute two groups that can coexist in the same marine environment. In these conditions they are suitable to be described by a model of population dynamics [7, 17, 18, 29, 43].

The magnitude of the picophytoplankton cell concentration has been analyzed in previous works during the last two decades in Mediterranean Sea. In particular, the highest Synechococcus abundances (8.3×10^4 cell ml^{-1}) was observed in Gulf of Lions, while the maximum of Prochlorococcus concentration (1.84×10^5 cell ml^{-1}) has been found close to Lybia during the summer period [85]. However, Synechococcus concentration did not exceed, usually, the value of 1.9×10^4 cell ml^{-1} in all other areas of Mediterranean Sea. Finally, the maximum of picoeukaryotes (4.0×10^3 cell ml^{-1}) has been observed in the Sicily Channel during the winter [87].

In the last years, detailed analysis have been done on picophytoplanktonic groups

in the Strait of Sicily during the summer period [65, 67, 68]. Here, Synechococcus cell concentration showed a limited increase as a function of the depth down up to 50 m, with a relative peak of 1.05×10^4 cell ml^{-1}, which is about ten times lower than that found for Prochlorococcus species. The *chl a* cellular content of Synechococcus did not show appreciable variations with depth down up to 50 m [67, 68], even if its values changed in different areas of Sicily Channel. Because the *chl a* cellular content of Synechococcus in Mediterranean Sea has not been reported, exactly, in previous works, in this thesis has been used the value obtained by Morel in Mauritania coast, where the cellular content for this species was fixed equal to 2 fg *chl a* cell^{-1} [70].

In the Strait of Sicily, picophytoplankton is numerically dominated by Prochlorococcus with average concentrations of 5.2×10^4 cell ml^{-1}. This species is more concentrated in DCM, where it can reach the mean value of 12.5×10^4 cell ml^{-1}. In particular, the marker of Prochlorococcus is *divinil chlorophyll a*, whose molecular structure is almost identical to that of *chlorophyll a*. The *Dvchl a* cellular content of the total Prochlorococcus, which takes in account the presence of both ecotypes, ranges between 0.25 and 2.20 fg *Dvchl a* cell^{-1} along the water column, with a mean value exponentially increasing with depth (see Fig. 1.3a) [68].

Finally, in previous works, it is also possible to observe that the average picoeukaryotes concentration in the DCM is 0.6×10^3 cell ml^{-1}, and the mean value of *chl a* cell^{-1} ranges between 10 and 660 fg *chl a* cell^{-1} along the water column, with a significant exponential increase with depth (see Fig. 1.3b) [68]. The concentration of *chl a* per cell in picoeukaryotes is highly variable among different water masses, with significantly higher values in the DCM respect to the surface [66, 79, 83, 88].

It is worth noting that experimental analysis performed on samples collected in Sargasso Sea and Mediterranean Sea showed that the cellular content of *chl a* and *Dvchl a* increases in picoeukaryotes and Prochlorococcus with decreasing light conditions [68, 89]. In particular, with light intensity ranging from 1500 μmol photons m^{-2} s^{-1} near the surface to less than 1 μmol photons m^{-2} s^{-1} below the euphotic zone (approximately 100 m in Mediterranean Sea during the summer period), cells display a variety of differences. The most obvious ones are the concomitant increases in cell size and pigment content, which generally occur below the depth of the mixed layers [90]. On the other side, for depth greater than 100 m, the cell concentration of

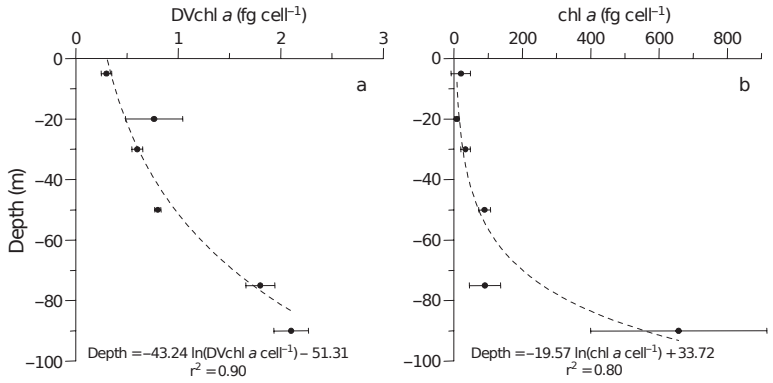

Figure 1.3: Mean vertical profile of *Dvchl a* content per Prochlorococcus cell (panel a) and *chl a* content per picoeukaryotes cell (panel b). Error bars are Standard Deviation. Equation and r^2 for the fit are reported on the plots. (Courtesy of Brunet et al., 2007 (Ref. [68])).

picophytoplankton shows a considerable decrease, due to the dramatic diminution of the light intensity, which becomes less than 1% of the light intensity at the sea surface. The consequent strong reduction of cell concentration below the euphotic zone allows to exploit the conversion curves shown in Fig. 1.3 also for depth below 100 m, describing, without significative errors, the increase in pigment content per cell. In general, these curves are not used for picophytoplankton species localized close to the surface water. Therefore, because Synechococcus are placed in shallower layers of the water column, the *chl a* cellular content of this species has been fixed constant in agreement with the experimental results obtained by other authors.

1.3 Experimental results

In this section, we describe the experimental data used to validate the theoretical results obtained by mathematical models. In particular, in the following sub-sections, we analyze the behaviour of hydrological parameters and *chl a* concentrations, along the water column, in two different marine ecosystems, i.e. Strait of Sicily and Tyrrhenian Sea.

1.3.1 Strait of Sicily

In the first ecosystem analyzed in this thesis, the vertical profiles, both for temperature and *chl a* concentration, have been acquired in order to be compared with numerical results obtained by using one-species and two-species models. The experimental data, collected in two different sites of the Sicily Channel during the MedSudMed-06 Oceanographic Survey, are shown in Fig. 1.4.

In site L1129b, the behaviour of the temperature along the water column indicates

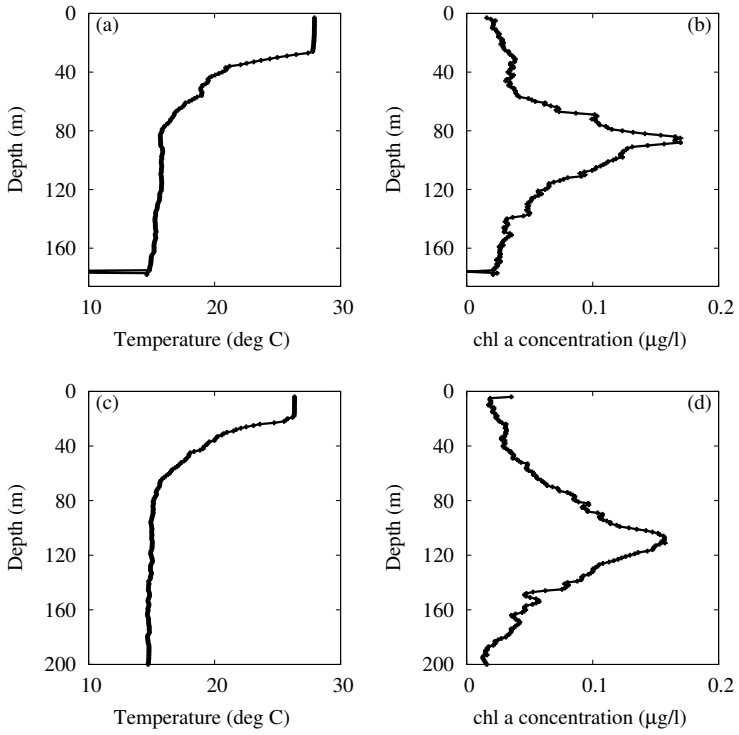

Figure 1.4: Profiles of temperature (panels a, c) and *chl a* concentration (panels b, d) measured in sites L1129b and L1105. The black lines have been obtained by connecting the experimental points corresponding to samples distanced of 1 meter along the water column. The total number of samples measured in the two sites is $n = 176$ for L1129b, and $n = 563$ for L1105.

the presence of an upper mixed layer (from the surface to 28 m of depth) characterized by a high value of temperature. Below the thermocline (28 m of depth) the temperature decreases up to 80 m, becoming uniform below this depth (Fig. 1.4a). The site L1105 shows an upper mixed layer over the first 24 m of depth, and a

sharp decrease of temperature from 24 to 75 m (Fig. 1.4c). Experimental data for *chl a* concentration show a nonmonotonic behaviour, as a function of the depth, characterized by the presence of DCM in both sites (see Fig. 1.4b,d). Specifically, fluorescence profiles show a similar behaviour in the two sites, with *chl a* concentration ranging between 0.010 and 0.17μg *chl a* l^{-1}, and a deep chlorophyll maximum (DCM) localized at 87 m (site L1129b) and 111 m (site L1105) of depth. Differences between the two sites are observed in the depth, shape and width of the DCM.

1.3.2 Tyrrhenian Sea

In the second ecosystem studied in this thesis, the experimental data have been collected in a site of the Tyrrhenian Sea during three different periods of the year, and compared with theoretical results obtained by a five-species model. The vertical distributions of temperature and *chl a* concentration are shown in Fig. 1.5.

The first sampling has been performed during VECTOR-TM1 Oceanographic Survey (24 November 2006). Here, the experimental profiles show the presence of an upper mixed layer, from the surface down to the thermocline, where the temperature is characterized by intermediate values. Below the thermocline (51 m of depth), the temperature decreases down up to 80 m, becoming uniform below this depth (Fig. 1.5a). The vertical profile of *chl a* concentration indicates an average value of 0.09 μg l^{-1} in the upper mixed layer, while a deep chlorophyll maximum is observed at 63 m, below the thermocline (Fig. 1.5b).

The experimental data, acquired during VECTOR-TM2 Oceanographic Survey (3 February 2007), indicates the presence of an upper mixed layer, from the surface to thermocline (69 m depth), where the temperature is characterized by low values (see Fig. 1.5c) and the *chl a* concentration ranges between 0.10 and 0.13 μg l^{-1}(see Fig. 1.5d). The temperature profile shows a uniform behaviour over the first 69 m of depth, while a weak decrease is observed within a water layer localized between 69 and 81 m of depth, below which the temperature returns to assume almost constant values (Fig. 1.5c). Viceversa, the fluorescence profile shows a non-monotonic behaviour with a DCM placed close to the thermocline, at 71 m of depth, where the chlorophyll concentration reaches a maximum value of 0.20 μg l^{-1}(Fig. 1.5d).

Finally, the experimental profiles collected during VECTOR-TM4 Oceanographic Survey (9 June 2007), showed a partially different behaviour respect to the previous

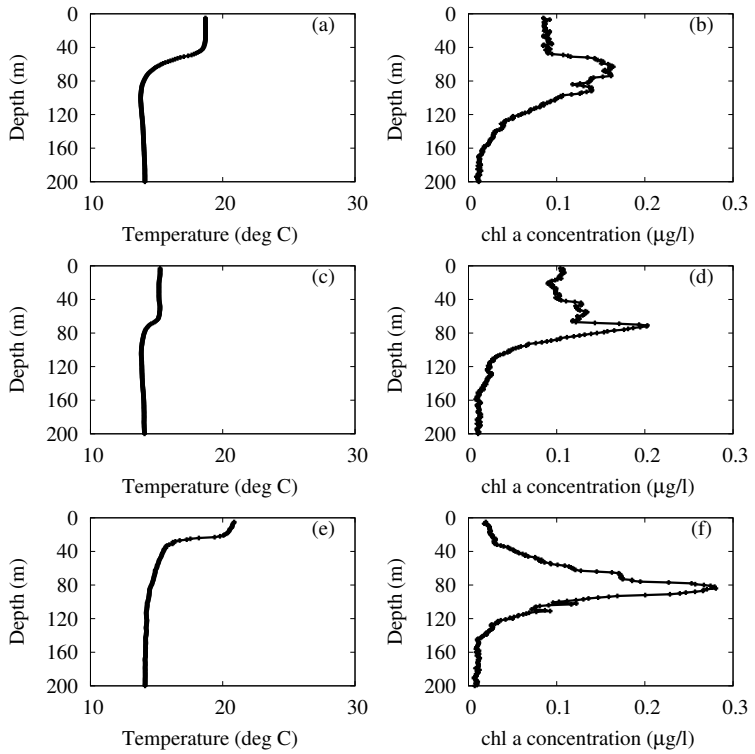

Figure 1.5: Profiles of temperature (panels a, c, e) and *chl a* concentration (panels b, d, f) acquired in the sampling site (39^o $30'.00$N, $13^o30'.00$E), during three oceanographic cruises (VECTOR-TM1, 24 November 2006 (panels a, b); VECTOR-TM2, 3 February 2007 (panels c,d); VECTOR-TM4, 9 June 2007 (panels e,f)). The black lines have been obtained by connecting the experimental points corresponding to samples distanced of 1 meter along the water column. The total number of samples measured in the site is $n = 3439$ for VECTOR-TM1, $n = 3439$ for VECTOR-TM2, and $n = 3488$ for VECTOR-TM4.

samplings. In particular, the vertical profile of the temperature indicates that the thermocline is localized at 24 m, in a position shallower than that observed in other periods of the year. Moreover, it is possible to note that the temperature of the upper mixed layer is much lower than that of the deeper layers (see Fig. 1.5e). As a consequence, due to the limited nutrient mixing generated by the stratification of the water masses, we expect that the *chl a* concentration is very low in the upper layer, and is very high in the DCM. This hypothesis is in agreement with the experimental results (see Fig. 1.5f). In particular the average *chl a* concentration, above the thermocline, is lower than that observed in other seasons, while the chlorophyll concentration reaches a maximum value of 0.28 μg l^{-1} in correspondence of the DCM. This is localized, during the late spring, in the deeper layers of the water column (84 m of depth), where the nutrient concentration is much higher than that of the surface layers.

In conclusion, the experimental profiles show a similar behaviour during the three samplings, even if the upper mixed layer and DCM show differences in the depth, shape and width.

Chapter 2

Models for population dynamics of a picophytoplankton group

In this chapter, we present an advection-reaction-diffusion model to describe the picophytoplankton dynamics in the basin of the Mediterranean Sea, characterized by poorly mixed waters. In particular, we analyze the population dynamics of the picoeukaryotes group by using two models based on two different approaches, i.e. deterministic and stochastic.

In the first section of the chapter, we introduce a deterministic model in order to simulate the vertical profile of the picoeukaryotes biomass concentration along the water column in our marine ecosystem. Afterwards, the numerical results obtained are compared with the experimental data collected in the two different sites of the Strait of Sicily.

In the second section of the chapter, in order to match better the theoretical results to the experimental data, the random fluctuations of the environmental variables are taken into account. In particular, a stochastic model is obtained from the deterministic one by inserting into the equations terms of multiplicative Gaussian noise.

2.1 Deterministic approach

In previous works the spatio-temporal dynamics of a phytoplankton community has been usually analyzed by using deterministic approaches. According to this, as a first step, a deterministic model has been chosen to study the behaviour of the picoeukayotes group in the marine ecosystems considered. In particular the growth of phytoplankton population is taken in account considering two limiting factors, i.e. nutrient and light, along the water column, reproducing the mechanism schematically shown in Fig. 2.1. Specifically, the mathematical tool used to simulate the phy-

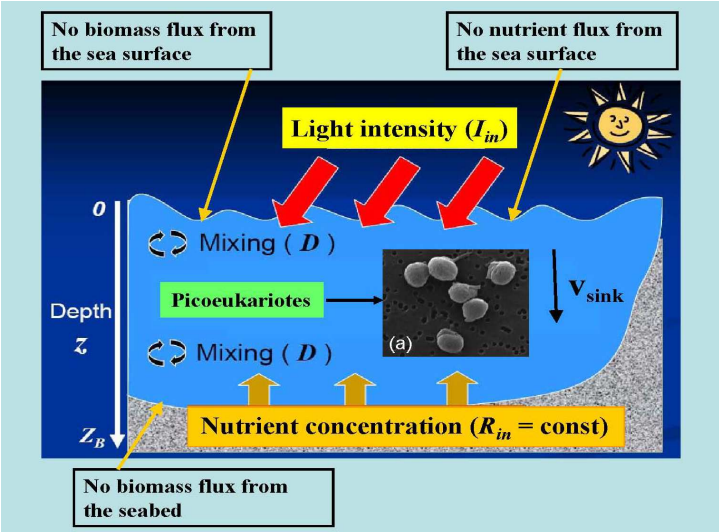

Figure 2.1: Scheme of the mechanism responsible for the phytoplankton dynamics (modified from original figure by Alexey Ryabov). (a) Image of Micromonas NOUM17 (courtesy of Augustin Engman, Rory Welsh, and Alexandra Worden.

toplankton dynamics is an advection-reaction-diffusion model. Moreover, according to real natural conditions, the light intensity decrease and nutrient concentration are assumed to decrease and increase, respectively, as a function of the depth.

2.1.1 Description of the model

In this paragraph, the model consisting of a system of differential equations, with partial derivatives in time and space (depth), is introduced by using a deterministic approach. The model allows to obtain the dynamics of the phytoplankton biomass

$b(z,t)$ and nutrient concentration $R(z,t)$. The light intensity $I(z,t)$ is given by a function varying, along the water column, with the depth and biomass concentration. The behaviour of the phytoplankton biomass, along the water column, is the results of three processes: growth, loss, and movement. The phytoplankton growth rate depends on I and R [16, 18, 24, 28, 91]. The limitation in phytoplankton growth is described by the Monod kinetics [92]. The gross phytoplankton growth rate per capita is given by $\min\{f_I(I), f_R(R)\}$, where $f_I(I)$ and $f_R(R)$ are obtained by the Michaelis-Menten formulas

$$f_I(I) = rI/(I + K_I), \tag{2.1}$$

$$f_R(R) = rR/(R + K_R). \tag{2.2}$$

In Eqs. (2.1), (2.2), r is the maximum growth rate, while K_I and K_R are the half-saturation constants for light intensity and nutrient concentration, respectively. Varying K_R and K_I allows to model, for instance, a species (or group) which is better adapted to the light (smaller values of K_I) or nutrient (smaller values of K_R). More specifically, we consider a group with small K_I and large K_R that corresponds to good life conditions at large depth. These constants depend on the metabolism of the specific microorganism considered.

The biomass loss, connected with respiration, death, and grazing, occurs at a rate m [13, 15, 16, 17, 18]. The gross per capita growth rate is defined as

$$g(z,t) = \min(f_R(R(z,t)), f_I(I(z,t))). \tag{2.3}$$

The effect of the turbulence, responsible for passive movement of the phytoplankton, is modeled in differential equation by using diffusion term. Specifically, the turbulence is described assuming that the vertical diffusion coefficient is uniform with the depth and characterized by a low value ($D_b = D_R = 0.5$). This choice is motivated by the fact that in sites L1129b and L1105 the phytoplankton peaks, located at 87 m and 111 m respectively, are quite far from the thermocline (see Fig. 1.4).

The movement of the phytoplankton depend on biological conditions, and is described by the advection term. In general, phytoplankton should go up (or down) if the biological conditions are more suitable for growth above (below) than below (above), while no migration should occur if the biomass concentrations are the same at different depths [16]. However, in this study, the advection term takes in account

only the downwards movements due to gravitational force (passive movement), in agreement with other authors [17, 18].
These assumptions about growth, loss, and movement, allow to obtain the following differential equation for the dynamics of the biomass concentration b [16, 17]

$$\frac{\partial b(z,t)}{\partial t} = g(z,t)b(z,t) - mb(z,t) + D_b\frac{\partial^2 b(z,t)}{\partial z^2} - v\frac{\partial b(z,t)}{\partial z}. \tag{2.4}$$

The positive phytoplankton velocity v is oriented downward (sinking), in the direction of positive z. Phytoplankton does not enter or leave the water column. This is set by using no-flux boundary conditions at $z = 0$ and $z = z_b$

$$\left[D_b\frac{\partial b}{\partial z} - vb\right]\Big|_{z=0} = \left[D_b\frac{\partial b}{\partial z} - vb\right]\Big|_{z=z_b} = 0. \tag{2.5}$$

Eddy diffusion is responsible for mixing of the nutrient concentration along the water column, with vertical turbulent diffusivity D_R. The nutrient consumed by the phytoplankton is also obtained from recycled dead phytoplanktonic microorganisms. The dynamics of the nutrient concentration can be therefore modeled as follows

$$\frac{\partial R(z,t)}{\partial t} = -\frac{b(z,t)}{Y}g(z,t) + D_R\frac{\partial^2 R(z,t)}{\partial z^2} + \varepsilon m\frac{b(z,t)}{Y}. \tag{2.6}$$

Here Y is the phytoplankton biomass produced per unit of nutrient consumed, and ε is the nutrient recycle coefficient. Since the nutrient is not supplied by the sea surface but comes from the seabed, its concentration is set to the constant value R_{in} in the sediment and, as a consequence, to the value $R(z_b)$ in the bottom of the water column. In fact the nutrient diffuses across the sediment-water interface with a rate proportional to the concentration difference between the solid phase (seabed) and the deepest water layer (bottom of the water column). Accordingly, the boundary conditions are given by

$$\frac{\partial R}{\partial z}\bigg|_{z=0} = 0, \quad \frac{\partial R}{\partial z}\bigg|_{z=z_b} = h(R_{in} - R(z_b)), \tag{2.7}$$

where h is the permeability of the interface. Finally, taking into account Lamber-Beer's law [35, 93], the light intensity is characterized by an exponential decrease modeled as follows

$$I(z) = I_{in}\exp\left\{-\int_0^z \left[ab(Z) + a_{bg}\right]dZ\right\}, \tag{2.8}$$

where a and and a_{bg} are the attenuation coefficients due to the phytoplankton biomass and background, respectively. Equations (2.4)-(2.8) form the biophysical model used in this analysis.

2.1.2 Simulation setting

In order to reproduce the spatial distributions obtained from the real data for the phytoplankton biomass (see Fig. 1.4), for the environmental and biological parameters we choose values which satisfy the monostability condition given by the presence of a deep chlorophyll maximum [13, 16, 17, 18]. Moreover, the values of the biological parameters r, K_I, K_R, v, have been chosen to reproduce the characteristics of the picoeukaryotes and simulate their behaviour. The numerical values assigned to the parameters are shown in Table 2.1.

Here it is worth noting that the vertical turbulent diffusivity is kept constant along the water column. In fact, in systems characterized by a constant value of the diffusion coefficient, the stationary state does not depend on the initial conditions, according to previous studies [16, 18].

The values of the light intensity resulted to be quite high in both sites, since the sampling occurred during the summer (August 2006). In this period the light intensity at the water surface is larger than 1300 μmol photons m^{-2} s^{-1}. Moreover, the sinking velocity is set to the value estimated by other authors [17] for picophytoplankton ($v = 0.1$ m day^{-1}). The diffusion coefficient is fixed at the value $D_b = 0.5$ cm^2 sec^{-1}, which corresponds to the condition of poorly mixed waters. By solving Eqs. (2.4)-(2.8) we obtain the biomass concentration expressed in cells/m^3 along the water column. Depths of the water column used in the model were set according to the measured depths in the corresponding marine sites. Moreover the light intensities, I_{in}, are fixed using data available on the NASA web site[1]. Finally, nutrient concentrations at the seabed were set at values such as to obtain, for each site, a peak of biomass concentration at the same position of the peak experimentally observed. All the other parameters are the same in both sites. The growth rate obtained from Eq. (4.3) agrees with the values measured by other authors [94].

Preliminary analysis (data not shown) revealed that the monostability condition

[1]http://eosweb.larc.nasa.gov/sse/RETScreen/

Symbol	Interpretation	Units	Site L1129b	Site L1105
I_{in}	Incident light intensity	μmol photons m^{-2} s^{-1}	1404.44	1383.19
a_{bg}	Background turbidity	m^{-1}	0.045	0.045
a	Absorption coefficient of phytoplankton	m^2 cell^{-1}	6×10^{-10}	6×10^{-10}
z_b	Depth of the water column	m	186	575
$D_b = D_R$	Vertical turbulent diffusivity	cm^2 s^{-1}	0.5	0.5
r	Maximum specific growth rate	h^{-1}	0.08	0.08
K_I	Half-saturation constant of light-limited growth	μmol photons m^{-2} s^{-1}	20	20
K_R	Half-saturation constant of nutrient-limited growth	mmol nutrient m^{-3}	0.0425	0.0425
m	Specific loss rate	h^{-1}	0.01	0.01
$1/Y$	Nutrient content of phytoplankton	mmol nutrient cell^{-1}	1×10^{-9}	1×10^{-9}
ϵ	Nutrient recycling coefficient	dimensionless	0.5	0.5
v	Buoyancy velocity	m h^{-1}	-0.0042	-0.0042
R_{in}	Nutrient concentration at z_b	mmol nutrient m^{-3}	26.0	36.0
h	Sediment-water column permeability	m^{-1}	0.01	0.01

Table 2.1: Parameters used in the model. The values of the biological and environmental parameters are those typical of picophytoplankton and summer period in Mediterranean Sea, respectively.

was satisfied only for some values assigned to two parameters: incident light intensity and nutrient concentration at seabed. In particular, large values of I_{in} (incident light intensity at the water surface) led to stationary conditions characterized by DCM, while large values of R_{in} (nutrient concentration in the sediment) determined an upper chlorophyll maximum (UCM). Finally, for intermediate values of I_{in} and R_{in} the chlorophyll maximum could be localized close to the surface or at different depths, depending on the values of the other parameters [18]. In this work, the stationary solution is characterized by DCM which is localized in deeper layers, in agreement with experimental data collected during the summer period.

2.1.3 Results of the deterministic model

The time evolution of the system is studied by analyzing the spatio-temporal dynamics of biomass and nutrient concentrations. Using a numerical method, implemented by a program in C++ language and based on an explicit finite difference scheme, equations (2.4)-(2.8) are solved. In particular, we used a centered-in-space differencing for the diffusion term and a forward differencing for the advection term. The increment of the spatial variable is set at 0.5 m, while the size of the time step is chosen, for fixed values of vertical turbulent diffusion and sinking velocity, such as to respect the von Neumann's stability conditions for both differencing terms [95, 96, 97]. For linear systems with constant coefficient, the theorem of Lax establishes the equivalence of stability and convergence provided that the following conditions apply: the initial-value problem must be well posed, in the sense of Hadamard; the finite difference equation must be consistent with the partial difference equation; the stability must be defined in L_2 norm. All these conditions are satisfied for the linear part of our differential equations [95, 97]. Moreover, the results arising from linear theory are used in general as guidelines to non-linear problems [95]. Specifically, previous works have shown that the contribute of non-linear growth term can be omitted in the stability analysis [98, 99, 100]. Therefore, we can consider guaranteed the convergence of the finite difference equations in this study. In order to obtain the steady spatial distribution, the equations were integrated numerically over a time interval long enough to observe the stationary solution. In particular, the numerical results were obtained using a maximum simulation time

$t_{max} = 10^5\ h$. Simulations (see Fig. 2.2) performed within the deterministic approach show that the stationary regime is reached at $t \approx 3 \cdot 10^4\ h$. This indicates that, to reach the steady state, it is sufficient to solve the equations of our model with a maximum time $t_{max} = 4 \cdot 10^4\ h$.

As initial conditions we consider that the phytoplankton biomass is concentrated

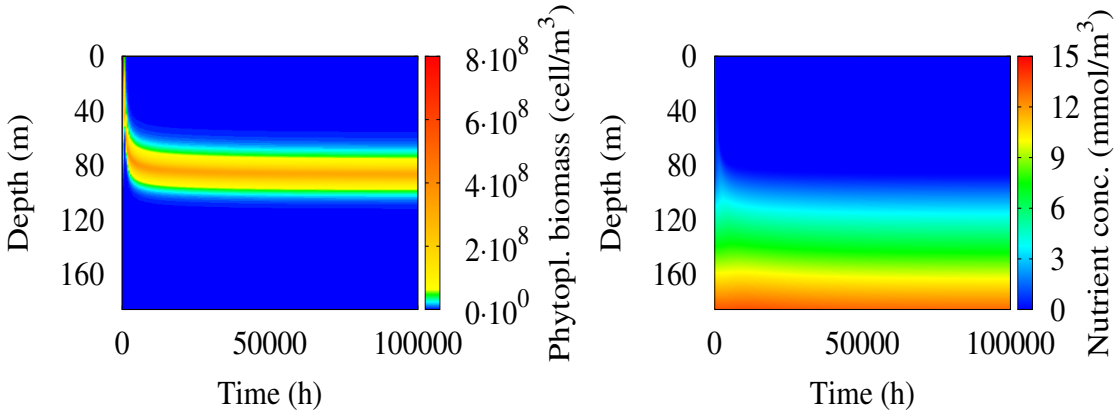

Figure 2.2: Contour map for phytoplankton biomass (left panel) and nutrient concentration (right panel) as a function of depth and time for CTD collected in site L1129b. The values of the parameters are those of table 2.1.

in the layer where the maximum of the experimental chlorophyll distribution is observed. On the other side, the nutrient concentration is approximately constant from the water surface to the DCM, and increases linearly below this point up to the seabed.

By solving Eqs. (2.4)-(2.8), we get the stationary profiles, both for biomass concentration and light intensity, shown in Fig. 2.3. Here, it is possible to note the presence of a biomass peak as found in the experimental data, and the typical exponential behaviour of the light intensity. To compare the theoretical results with the experimental data, we exploit the curve of Fig. 1.3 to convert the cell concentrations, obtained from the model and expressed in cell/m^3, into *chl a* concentrations expressed in μg/l. It is worth to recall that about 43% of the total quantity of *chl a* [17, 67] is due to nano- and micro-phytoplankton (20% of the total *chl a* on average), and Synechococcus (23% of the total *chl a* on average), quite uniformly distributed along the water column. Since our model accounts for the dynamics of

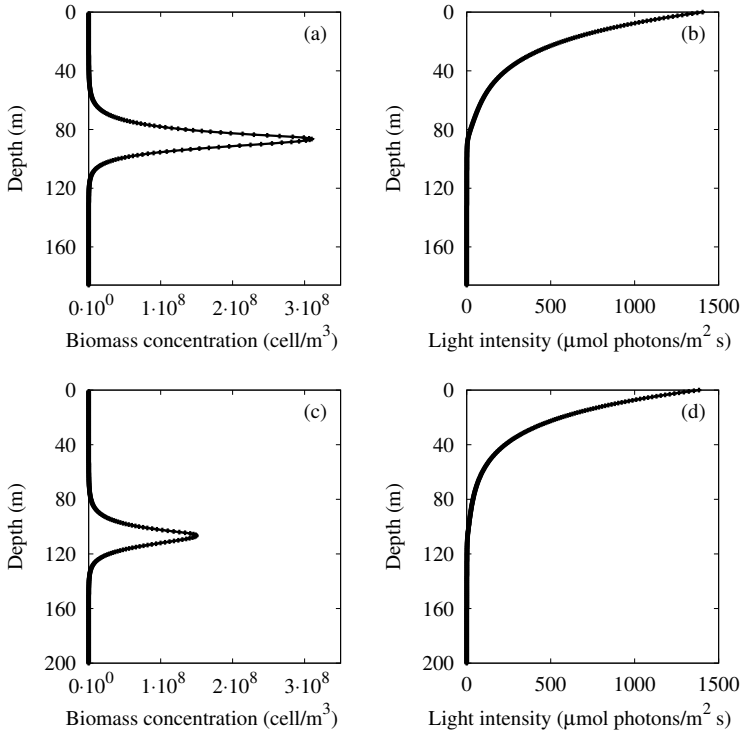

Figure 2.3: Stationary distributions of the biomass concentration and light intensity in sites L1129b (panels a, b) and L1105 (panels c, d) as a function of depth.

picoeukaryotes, to compare the numerical results with the experimental data, we consider the 43% of the total biomass and divide it by depth, obtaining for each site the value $\Delta b_{chl\,a}$, which represents a constant concentration due to other phytoplankton species present in the water column. Finally along the water column we add the theoretical concentration with $\Delta b_{chl\,a}$ and obtain, for the distributions of *chl a* concentration, the stationary theoretical profiles consistent with those of the experimental data. The results are shown in Fig. 2.4. Here it is possible to observe

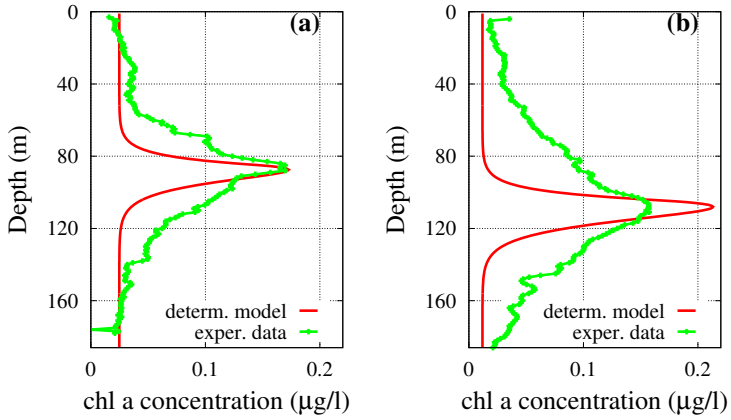

Figure 2.4: Stationary distribution of the chlorophyll a concentration as a function of depth calculated (red line) by the deterministic model and measured (green line) in sites (a) L1129b and (b) L1105.

that in both sites the deep chlorophyll maxima obtained from the model are located at the same depth of those observed experimentally. However, the shape of the theoretical *chl a* distributions is quite different from the experimental profiles. Finally, we note that in site L1105 the magnitude of the theoretical DCM is significantly different from that observed in real data.

2.2 Stochastic approach

In the previous section, it has been used a deterministic model to fit the experimental distributions of *chl a* concentration. The results obtained reproduce partially the characteristics of the experimental profiles. In order to get a good agreement between real data and theoretical results, we recall that the sea is a complex system. This implies the presence of non-linear interactions among its parts [51, 101, 102, 103, 104, 105] and a continuous interaction between the ecosystem and environment. In particular, the system dynamics is affected not only by deterministic forces but also random perturbations coming from the environment. In this context environmental variables, due to their random fluctuations, can act as noise sources, causing phytoplankton to be subject to a stochastic dynamics. Therefore, in order to perform an analysis that takes account for real conditions of the ecosystem, it is necessary to modify the deterministic model, including the noise effects.

2.2.1 Description of the model

In previous works it has been observed that the fluctuations of temperature, food resources, and other environmental parameters can be modeled by including multiplicative noise sources [47, 48, 51, 106], that can effectively reproduce experimental data in population dynamics [107, 108, 109].

The same arguments hold for nutrients, whose random fluctuations should be modeled by terms of multiplicative noise, according to the approach widely used to describe stochastic dynamics not only in physics, but also in biology, ecology, economy, or social sciences [108]. This agrees with the observation that the effects of fluctuations have to be proportional to the activity densities [110, 111, 112, 113, 114], which are in our system the biomass and nutrient concentrations.

In marine ecosystems, the multiplicative noise, used in population dynamics and reaction-diffusion problems [107, 115, 116, 117], describes changes mainly generated by two sources of fluctuations: i) vertical mixing along the water column due to the random variations of the velocity field, ii) gain or loss of biomass and nutrient concentrations among different water columns due to random horizontal movement. These noise sources are responsible for the real behaviour of the ecosystem, charac-

terized by an intrinsically non-deterministic dynamics.
Therefore, in order to reproduce the dynamics of the picoeukaryotes group and nutrient concentration, taking into account the role of the environmental fluctuations, we modify the model given by Eqs. (2.4)-(2.8), including terms of multiplicative noise. In the following we analyze two different situations.
Case 1. The environmental noise affects only the biomass concentration. Therefore, Eqs. (2.4)-(2.8) are maintained unaltered, while Eq. (2.4) becomes

$$\frac{\partial b}{\partial t} = gb - mb + D_b \frac{\partial^2 b}{\partial z^2} - v\frac{\partial b}{\partial z} + b\,\xi_b(z,t) \tag{2.9}$$

Case 2. The environmental noise affects only the nutrient concentration. In this case, Eqs. (2.4),(2.5),(2.7),(2.8) are maintained unaltered, while Eq. (2.6) is replaced by

$$\frac{\partial R}{\partial t} = [m\varepsilon - g]\frac{b}{Y} + D_R \frac{\partial^2 R}{\partial z^2} + R\,\xi_R(z,t). \tag{2.10}$$

In Eqs. (2.9) and (2.10), $\xi_b(z,t)$ and $\xi_R(z,t)$ are statically independent white Gaussian noises with the usual properties $\langle \xi_b(z,t)\rangle = 0$, $\langle \xi_R(z,t)\rangle = 0$, $\langle \xi_b(z,t)\xi_b(z',t')\rangle = \sigma_b\delta(z-z')\delta(t-t')$, $\langle \xi_R(z,t)\xi_R(z',t')\rangle = \sigma_R\delta(z-z')\delta(t-t')$, where σ_b and σ_R are the noise intensities. We note that the two noise sources are spatially uncorrelated, that is at the generic point z no effects is present due to random fluctuations occurring in $z' \neq z$.

2.2.2 Simulation setting

In order to reproduce the chlorophyll spatial distributions obtained from the experimental data, we choose for the environmental and biological parameters the same values used in the deterministic model.
Afterwards the stochastic dynamics is analyzed, solving the equations of the modified model, where multiplicative noise terms has been inserted, and averaging over several realizations. It is worth noting that the ecosystem is characterized by nonlinear interactions among its parts. Because of this feature the response of the system to external solicitations is also non-linear. Therefore, one can not expect that the presence of a symmetric noise with zero mean, i.e. Gaussian noise used in

the model, produces in average the same effect as a deterministic dynamics [118]. On the other side, the use of a random function, i.e. noise source, to simulate the spatio-temporal behaviour of the system, makes the single realization unpredictable and unique, and therefore non-representative of the real dynamics. As a consequence, one possible choice to describe correctly the time evolution of the system is to calculate the average of several realizations. This procedure, indeed, allows to take into account different "trajectories" obtained by the integration of the stochastic equations, without focusing on a specific realization [51]. Therefore, in our simulations, we fixed a number of realizations such as to obtain phytoplankton distributions in agreement with experimental data and without "spikes" of biomass concentration.

2.2.3 Results of the stochastic model

In this sub-section we solve numerically, within the Ito scheme, the equations of the stochastic model for different values of the noise intensities. About the numerical integration, it is worth to recall that the calculus of stochastic differential equations with terms of white noise can be based on different definitions, i.e. Ito and Stratonovich schemes. This situation has led to a long controversy in physical literature. In particular, the Stratonovich's choice is the only definition of stochastic integral leading to a calculus with classic rules within the context of functional analysis. Moreover, a principle of invariance of the equation under "coordinate transformation" is invoked to pick the Stratonovich integral as the "right" one and reject the Ito integral as the "wrong" one. The principle refers to an invariance of the form of the stochastic differential equation under a non-linear transformation of the system. This invariance does not posses any physical virtue, but it is only a different way to say that the Stratonovich calculus obeys the familiar classic rules [119]. The only quantities that have to be invariant under a coordinate transformation are the probabilities. This condition is of course guaranteed in both calculi [119, 120]. On this basis we conclude that the specific problem can be treated by performing the integration of the stochastic differential equations within the Ito scheme.
In particular we obtain, for different values of the noise intensities, the concentration profiles averaged over 1000 realizations [51, 118]. The presence of noise sources does not determine significant variations in the time necessary to reach the steady state. Therefore, in according to the discussion of sub-section 2.1.3, the solutions are cal-

culated for a maximum simulation time $t_{max} = 4 \cdot 10^4$ h, while initial conditions are the same of the deterministic model.

The numerical results for case 1 are shown in Figs. 2.5 and 2.6. Here we note that, in both sites, for higher noise intensities the peaks of the two average *chl a* distributions show: (i) a decrease of their magnitude; (ii) a small displacement along the water column. For suitable values of the noise intensity the peaks of the average *chl a* distributions obtained from the model match very well the experimental data. We observe also that the two DCMs are located at 90 m (site L1129b) and 106 m (site L1105) of depth (in Figs. 2.5d and 2.6d are compared theoretical (red line) and experimental (green line) profiles). A quantitative comparison of each theoretical *chl a* distribution (red line) with the corresponding experimental one (green line) was carried out by performing χ^2 goodness-of-fit test. The results are shown in Tables 2.2, where $\tilde{\chi}^2$ indicates the reduced chi-square. Results of the χ^2 test show that the smallest difference between theoretical and experimental *chl a* distributions is obtained for $\sigma_b = 0.22$ in site L1129b and $\sigma_b = 0.15$ in site L1105. Finally, it is possible to note that the depths of the DCMs are almost the same as in the deterministic case.

In order to better analyze this aspect, we study for both sites the behaviour of the magnitude, depth, and width of the DCM as a function of σ_b. The results, shown in Fig. 2.7, indicate that the depth of the DCM is almost constant for $\sigma_b \leq 0.4$, while it increases for higher values of the noise intensity (see panels b, e of Fig. 2.7). Conversely, the width of the DCM is characterized by a non-monotonic behaviour for increasing noise intensities. In particular, we note that the width of the DCM exhibits a maximum in both sites (for $\sigma_b \leq 0.4$ in site L1129b and $\sigma_b \leq 0.3$ in site L1105). For higher noise intensities the width tends to zero for site L1129b, while a minimum is present for site L1105 at $\sigma_b \leq 0.5$. However, for $\sigma_b > 0.4$, the values of the DCM width are less significant, since the *chl a* concentration along the water column and in particular in the DCM decreases strongly, as can be checked in panels a, d. In particular, random fluctuations, cause the reduction of biomass concentration and its displacement along the water column, determining the extinction of the picophytoplankton in the presence of higher intensities of noise. In this condition a clear determination of the DCM becomes more difficult. As a consequence, the values of depth and width for the DCM are less reliable. This analysis shows that

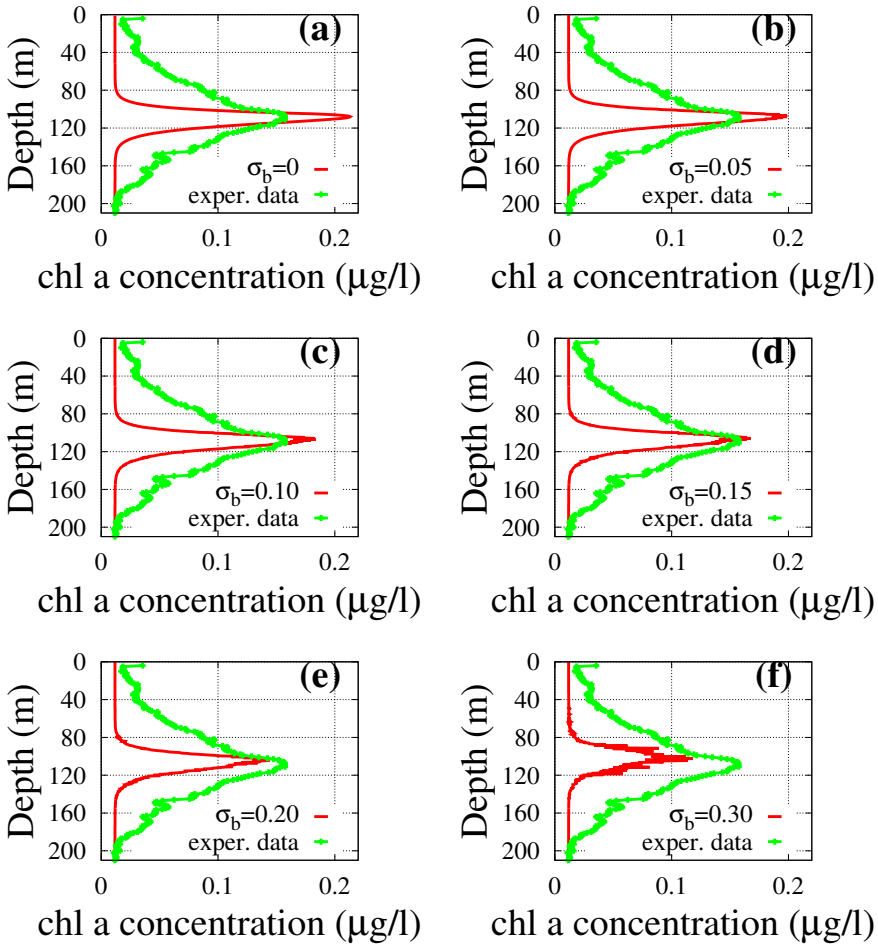

Figure 2.5: Average *chl a* concentration calculated (red line) for different values of σ_b by the stochastic model (case 1, see Eqs. (2.5), (2.6), (2.7), (2.8), (2.9)) as a function of depth. Results are compared with *chl a* distributions measured (green line) in site L1129b. The theoretical values were obtained averaging over 1000 numerical realizations. The values of the parameters are those shown in Table 2.1. The noise intensities are: (a) $\sigma_b = 0$ (deterministic case), (b) $\sigma_b = 0.10$, (c) $\sigma_b = 0.20$, (d) $\sigma_b = 0.22$, (e) $\sigma_b = 0.25$ and (f) $\sigma_b = 0.30$.

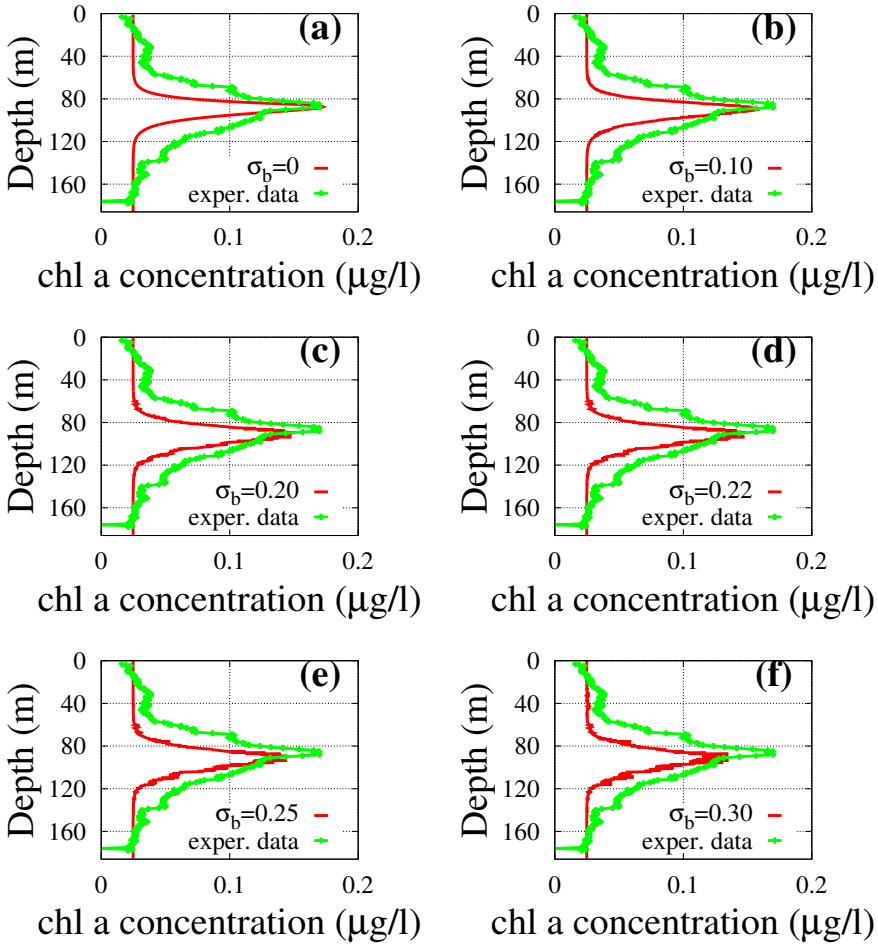

Figure 2.6: Average *chl a* concentration calculated (red line) for different values of σ_b by the stochastic model (case 1, see Eqs. (2.5), (2.6), (2.7), (2.8), (2.9)) as a function of depth. Results are compared with *chl a* distributions measured (green line) in site L1105. The theoretical values were obtained averaging over 1000 numerical realizations. The values of the parameters are those shown in Table 2.1. The noise intensities are: (a) $\sigma_b = 0$ (deterministic case), (b) $\sigma_b = 0.05$, (c) $\sigma_b = 0.10$, (d) $\sigma_b = 0.15$, (e) $\sigma_b = 0.20$ and (f) $\sigma_b = 0.30$.

Site L1129b

R_{in}	σ_b	χ^2	$\tilde{\chi}^2$
26	0.00	4.43	0.0253
26	0.10	3.79	0.0216
26	0.20	3.45	0.0197
26	0.22	3.44	0.0196
26	0.25	3.46	0.0198
26	0.30	3.60	0.0206

Site L1105

R_{in}	σ_b	χ^2	$\tilde{\chi}^2$
36	0.00	22.87	0.0407
36	0.05	22.72	0.0404
36	0.10	22.55	0.0401
36	0.15	22.50	0.0400
36	0.20	22.95	0.0408
36	0.30	27.14	0.0483

Table 2.2: Results of χ^2, reduced chi-square ($\tilde{\chi}^2$) goodness-of-fit test for site L1129b (left panel) and site L1105 (right panel) for different values of σ_b (stochastic dynamics - case 1). The number of samples along the water column is n = 176 for site L1129b and n = 563 for site L1105.

the stationary conditions of the system depends strongly on the environmental fluctuations, which play a critical role in determining the best life conditions for the picophytoplankton species.

The analysis of the stochastic dynamics is completed by considering the noise source which affects directly the nutrient concentration (case 2). By numerically solving the corresponding equations of the motion (see Eqs. (2.4),(2.5),(2.7),(2.8),(2.10)) and averaging over 1000 realizations, we obtain the average *chl a* distributions shown in Figs. 2.8 and 2.9. The results show that also for low noise intensities (σ_R between 0.001 and 0.005), a decrease and a deeper localization of the DCMs are present. The shape of the *chl a* peaks exhibits, for both sites, a better agreement with the corresponding experimental DCMs respect to the deterministic case. In particular, for site L1129b the best value of the χ^2 test is obtained for $\sigma_R = 0.0020$, while for site L1105 the best fitting results for $\sigma_R = 0.0015$ (see Table 2.3). It is worth noting that in site L1129b the best agreement between experimental and numerical distributions is obtained, both in case 1 and case 2, for values of the noise intensity, σ_b and σ_R, higher than those of site L1105. This can be explained by the fact that in site L1129b the DCM is localized at a depth shallower than in site L1105 (88

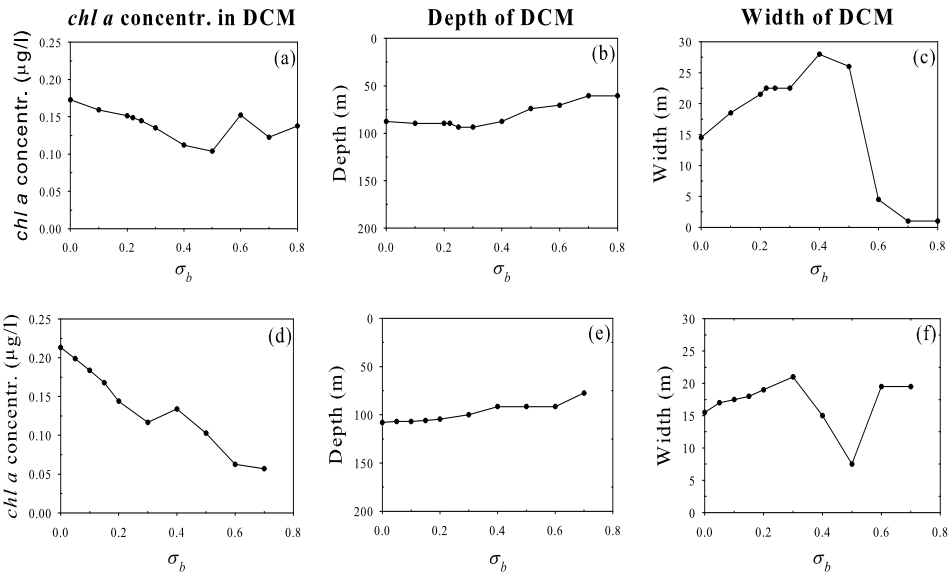

Figure 2.7: Magnitude, depth, and width of the DCM as a function of σ_b obtained from the model for site L1129b (panels a, b, c) and site L1105 (panels d, e, f).

Site L1129b

R_{in}	σ_R	χ^2	$\tilde{\chi}^2$
26	0.0000	4.43	0.0253
26	0.0010	3.18	0.0182
26	0.0015	3.03	0.0173
26	0.0020	3.01	0.0172
26	0.0025	3.04	0.0174
26	0.0050	3.57	0.0204

Site L1105

R_{in}	σ_R	χ^2	$\tilde{\chi}^2$
36	0.0000	22.87	0.0407
36	0.0010	17.98	0.0320
36	0.0015	17.86	0.0318
36	0.0020	18.35	0.0327
36	0.0025	19.18	0.0341
36	0.0050	25.47	0.0453

Table 2.3: Results of χ^2, reduced chi-square ($\tilde{\chi}^2$) goodness-of-fit test for site L1129b (left panel) and site L1105 (right panel) for different values of σ_R (stochastic dynamics - case 2). The number of samples along the water column is n = 176 for site L1129b and n = 563 for site L1105.

m vs. 111 m), causing the environmental variables to be subject to more intense random fluctuations due to the closer sea surface. As a consequence, the *chl a* peak in site L1129b (88 m) is more strongly affected by the environmental noise than in

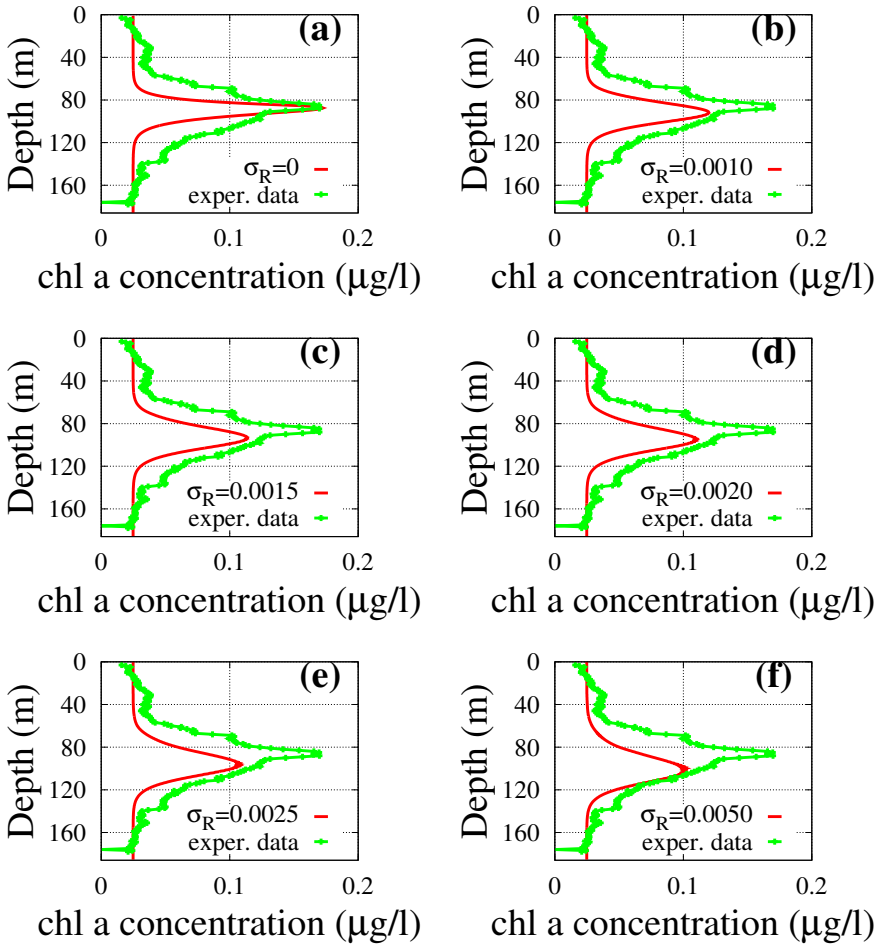

Figure 2.8: Average *chl a* concentration calculated (red line) for different values of σ_R by the stochastic model (case 2, see Eqs. (2.4), (2.5), (2.7), (2.8), (2.10)) as a function of depth. Results are compared with *chl a* distributions measured (green line) in site L1129b. The theoretical values were obtained averaging over 1000 numerical realizations. The values of the parameters are those shown in Table 2.1. The noise intensities are: (a) $\sigma_R = 0$ (deterministic case), (b) $\sigma_R = 0.0010$, (c) $\sigma_R = 0.0015$, (d) $\sigma_R = 0.0020$, (e) $\sigma_R = 0.0025$ and (f) $\sigma_R = 0.0050$.

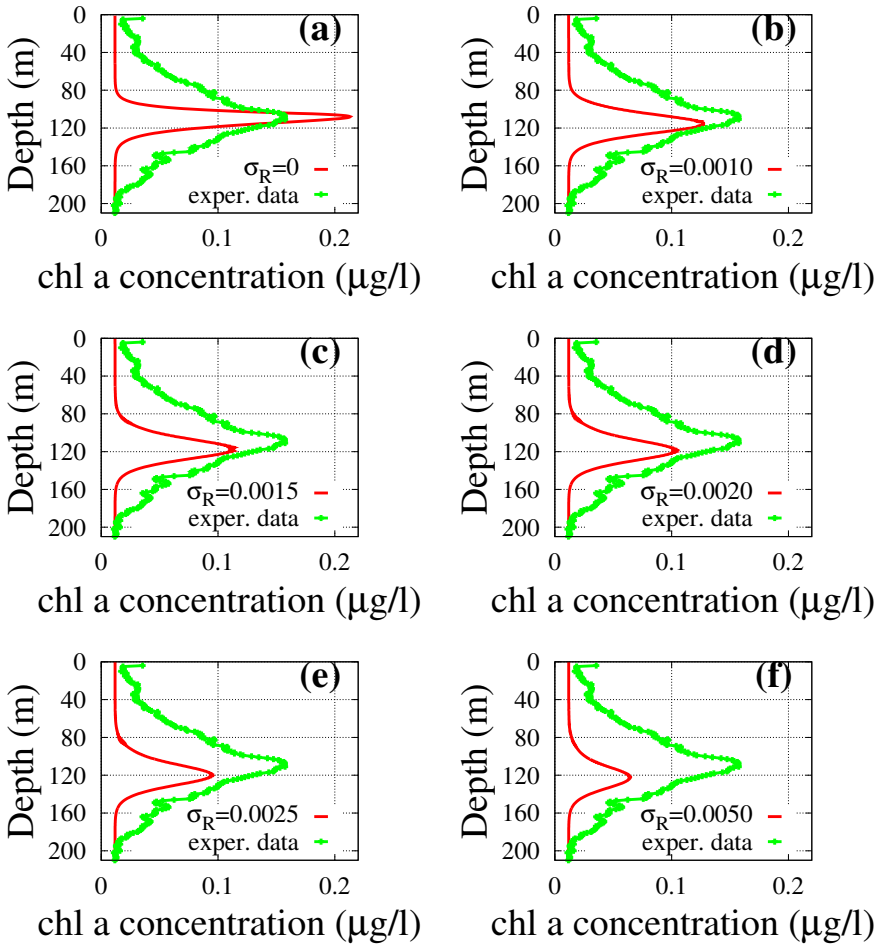

Figure 2.9: Average *chl a* concentration calculated (red line) for different values of σ_R by the stochastic model (case 2, see Eqs. (2.4), (2.5), (2.7), (2.8), (2.10)) as a function of depth. Results are compared with *chl a* distributions measured (green line) in site L1105. The theoretical values were obtained averaging over 1000 numerical realizations. The values of the parameters are those shown in Table 2.1. The noise intensities are: (a) $\sigma_R = 0$ (deterministic case), (b) $\sigma_R = 0.0010$, (c) $\sigma_R = 0.0015$, (d) $\sigma_R = 0.0020$, (e) $\sigma_R = 0.0025$ and (f) $\sigma_R = 0.0050$.

site L1105 (111 m).

To better understand the dependence of the biomass concentration on the random fluctuations of the nutrient, according to the procedure followed for case 1, we study for both sites the behaviour of the depth, width, and magnitude of the DCM as a function of σ_R. The results, shown in Fig. 2.10, indicate that the depth of the DCM

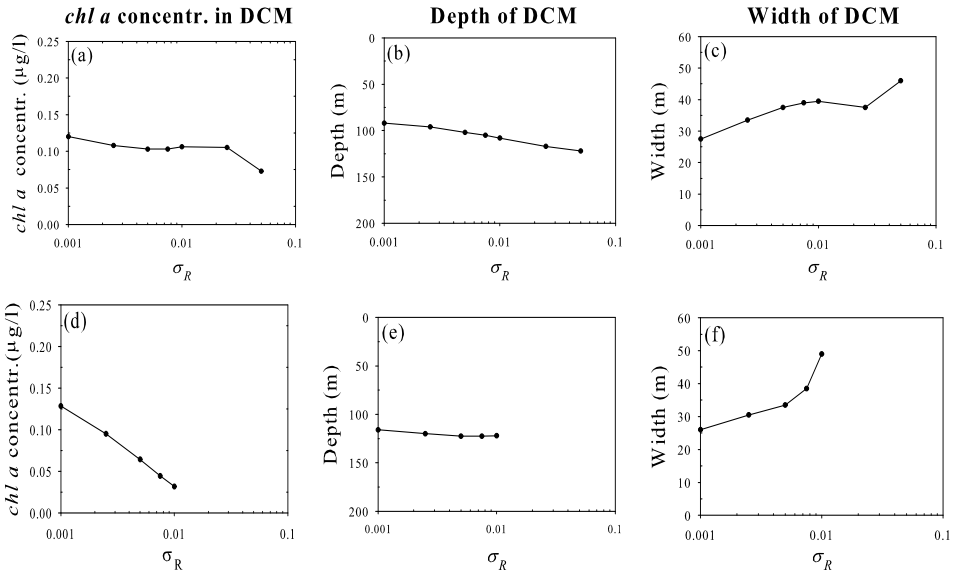

Figure 2.10: Theoretical values of the magnitude, depth, and width of the DCM as a function of σ_R obtained from the model for site L1129b (panels a, b, c) and site L1105 (panels d, e, f). The values shown have been calculated at the steady state.

slightly increases in both sites as a function of the noise intensity (see panels b, e of Fig. 2.10). We note also that a decrease of the *chl a* concentration is observed in the DCMs of the two sites. This decrease is more rapid in site L1105 (panel d), where a *chl a* concentration ~ 0.025 is reached for $\sigma_R \sim 0.01$. Analogously we observe an increase, faster in site L1105, of the width of the DCM. The spread of DCM and reduction of its magnitude are strictly connected with each other. In fact, the decrease of *chl a* concentration determines a flattening of the DCM with a consequent increase of its width. In conclusion the results shown in Fig. 2.10 indicate that the phytoplankton biomass tends to disappear for $\sigma_R \sim 0.01$, a value lower than those used in case 1, where no extinction occurs up to $\sigma_b \sim 0.7$ (see panels a, d of Fig. 2.7). This indicates that the stability of the nutrient concentration is a critical factor in the dynamics of the ecosystem. Indeed, random fluctuations of the nutrient concen-

tration can produce dramatic effects such as the collapse of phytoplankton biomass considered in the model studied.

The previous analysis indicates that stochastic model is able to reproduce the phytoplankton distributions observed in real data, without the model taking into account explicitly the environmental variables, such as temperature, salinity and velocities field. However, we observe that, in case 2, the spatio-temporal dynamics of the nutrients has been modeled by introducing noise sources, which can be interpreted as the effect of random fluctuations of environmental variables, among which salinity, temperature, and food resources, i.e. phosphorus concentration.

Chapter 3

Models for population dynamics of two picophytoplankton groups

In this chapter, we introduce an advection-reaction-diffusion model to simulate the spatio-temporal behaviuor of two picophytoplankton groups in the Strait of Sicily. Following the same procedure as in chapter 2, the population dynamics of picoeukaryotes and Prochlorococcus is analyzed by using mathematical models based on two different approaches, i.e. deterministic and stochastic.

In the first part of the chapter, we use a deterministic model to obtain the distributions of biomass concentration for picoeukariotes and Prochlorococcus along the weakly mixed water column. The numerical results obtained are compared with the experimental data.

In the second section of the chapter, the random fluctuations of the environmental variables are taken into account by inserting terms of multiplicative Gaussian noise into the differential equations of the model. As a first step, a term of multiplicative noise is added only in the differential equation for the nutrient concentration. Afterwards, terms of multiplicative noise are inserted also into the equations for the biomass concentrations of picoeukariotes and Prochlorococcus. By this way, the effects of the environmental noise on picophytoplankton distributions are analyzed.

3.1 Deterministic approach

In this section, the spatio-temporal behaviour of the two picophytoplankton groups is analyzed by using a deterministic approach. In particular, the analysis is performed by taking in account the intraspecific competition of both picophytoplankton groups for light and nutrients in deep chlorophyll maximum. The mathematical tool used to simulate the picophytoplankton dynamics is a model based on a system with three differential equations and an auxiliary equation. By solving this system, we obtain the vertical distributions of picophytoplankton groups as a function of the depth. In Fig. 3.1 we give a schematic representation of the mechanism underlying the phytoplankton dynamics.

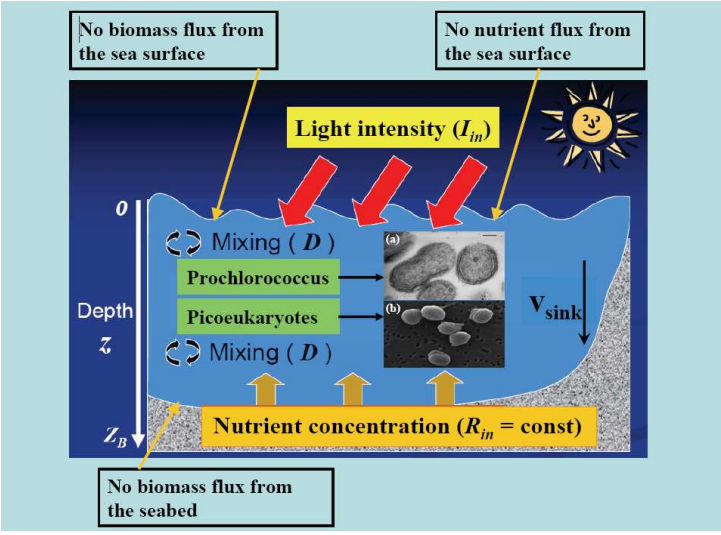

Figure 3.1: Scheme of the mechanism responsible for the phytoplankton dynamics (modified from original figure by Alexey Ryabov). Inset: (a) Prochlorococcus PCC 9511 (courtesy of Rippka et al., 2000 (Ref. [121])), (b) Micromonas NOUM17 (courtesy of Augustin Engman, Rory Welsh, and Alexandra Worden).

3.1.1 Description of the model

In this paragraph, we consider a deterministic advection-reaction-diffusion model [13, 15, 16, 17, 18] to analyze the dynamics of the two picophytoplanktonic groups, distributed along the same one-dimensional spatial domain (z-direction) used in the

one-population analysis performed in the previous chapter. In particular, we assume that the interaction of these two populations with the environment occurs through the same two factors that limit the growth of the aquatic microorganisms: light intensity and nutrient, i.e. phosphorus. The model allows to obtain the dynamics of the biomass concentrations of picoeukaryotes and Prochlorococcus, $b_1(z,t)$ and $b_2(z,t)$, nutrient concentration $R(z,t)$ and light intensity $I(z,t)$. Also in this case, a crucial role in the phytoplankton dynamics is played by growth and loss of biomass concentration, movement of the single microorganisms, and the growth rates of the two picophytoplankton groups. These are strictly connected with I and R, whose characteristics of limiting factors [16, 24, 28, 91] are implemented in the model by the Monod kinetics [92]. Specifically, the gross phytoplankton growth rates per capita are given by $\min\{f_{I_i}(I), f_{R_i}(R)\}$, where $f_{I_i}(I)$ and $f_{R_i}(R)$ are obtained by the Michaelis-Menten formulas

$$f_{I_i}(I) = r_i I/(I + K_{I_i}), \tag{3.1}$$

$$f_{R_i}(R) = r_i R/(R + K_{R_i}). \tag{3.2}$$

where r_i is the maximum growth rate, and K_{I_i} and K_{R_i} are the half-saturation constants for light intensity and nutrient concentration, respectively, of the *i-th* picophytoplankton group. These constants depend on the metabolism of the specific microorganisms considered. In particular, K_{R_i} and K_{I_i} contribute to determine the position along the water column (depth) of the maximum (peak) of biomass concentration for each species. The biomass loss of the *i-th* picophytoplankton group, connected with respiration, death, and grazing, occurs at a rate m_i [16, 17, 18]. The gross per capita growth rates are defined as

$$g_i(z,t) = \min(f_{R_i}(R(z,t)), f_{I_i}(I(z,t))). \tag{3.3}$$

The movement of phytoplankton groups depends on turbulence, responsible for a passive movement of the phytoplankton. Turbulence is modeled by vertical diffusion coefficient D, which we assume uniform with the depth in both sites. Sinking velocities of the two picophytoplankton groups, v_1 and v_2, describe another passive movement of picoeukaryotes and Prochlorococcus along water column towards deeper layers [7, 16, 69]. Positive velocities are oriented downward (sinking) for both

groups, and are set equal to those observed in experimental data [17, 18].
Taken together, these assumptions about growth, loss, and movement result in the following differential equations for the dynamics of the biomass concentrations of picoeukaryotes $b_1(z,t)$ and Prochlorococcus $b_2(z,t)$ [7, 17, 18]

$$\frac{\partial b_1(z,t)}{\partial t} = b_1 min(f_{I_1}(I), f_{R_1}(R)) - m_1 b_1 + D\frac{\partial^2 b_1(z,t)}{\partial z^2} - v_1\frac{\partial b_1(z,t)}{\partial z} \tag{3.4}$$

$$\frac{\partial b_2(z,t)}{\partial t} = b_2 min(f_{I_2}(I), f_{R_2}(R)) - m_2 b_2 + D\frac{\partial^2 b_2(z,t)}{\partial z^2} - v_2\frac{\partial b_2(z,t)}{\partial z}. \tag{3.5}$$

Boundary conditions for concentrations of picoeukaryotes and Prochlorococcus biomass describe no-flux in both surface layer $z = 0$ and seabed $z = z_b$:

$$\left[D\frac{\partial b_i}{\partial z} - v_i b_i\right]\Big|_{z=0} = \left[D\frac{\partial b_i}{\partial z} - v_i b_i\right]\Big|_{z=z_b} = 0. \tag{3.6}$$

The nutrient concentration $R(z,t)$ is consumed by both the picophytoplankton groups, and a further quantity of nutrient is obtained from dead phytoplankton by a recycling process. Furthermore, turbulence is also responsible for mixing of the nutrient concentration along the water column and it is described by the vertical diffusion coefficient D. All these processes are modeled by the following equation

$$\begin{aligned}\frac{\partial R(z,t)}{\partial t} &= -\sum \frac{b_i(z,t)}{Y_i}\cdot min(f_{I_i}(I), f_{R_i}(R)) + D\frac{\partial^2 R(z,t)}{\partial z^2} \\ &+ \sum \varepsilon_i m_i \frac{b_i(z,t)}{Y_i}\end{aligned} \tag{3.7}$$

where ε_i and $1/Y_i$ are nutrient recycling coefficient and nutrient content of the *i-th* picophytoplankton group, respectively.
Nutrients do not come from the top of the water column but are supplied from the bottom. In particular, nutrient concentration at the bottom of the water column, $R(z_b)$, is fixed at the value R_{in}, which is different in the two sites investigated. Thus the boundary conditions are described by the following equations:

$$\frac{\partial R}{\partial z}\Big|_{z=0} = 0, \qquad R(z_b) = R_{in}. \tag{3.8}$$

The light intensity is assumed to decrease exponentially according to Lamber-Beer's law [19, 35, 93]

$$I(z) = I_{in}\exp\left\{-\int_0^z \left[\sum a_i b_i(Z) + a_{bg}\right] dZ\right\} \tag{3.9}$$

where a_i are the absorption coefficients of the *i-th* picophytoplankton group, a_{bg} is the background turbidity, and I_{in} is the incident light intensity at the water surface.

3.1.2 Simulation setting

In this paragraph, we describe the procedure to set the values of the environmental and biological parameters used in the model to simulate the experimental distributions of the total concentration of *chl a* and *Dvchl a* (see Fig. 1.4). As in the one-species model, the parameters have been fixed in order to obtain the monostability condition, which corresponds in this case to the presence of a DCM for both picophytoplankton groups [13, 16, 17, 18, 29]. This choice is in agreement with experimental findings, which show as these groups coexist in the same layers of the water column, even if the maximum concentration for each group is localized at a different depth [19]. The numerical values assigned to the parameters are shown in Table 3.1.

The values of the biological parameters have been chosen to reproduce the behaviour of picoeukaryotes and Prochlorococcus. In particular, for both groups, the maximum specific growth rates are in agreement with ones measured from other authors [67, 68, 94], and the sinking velocity is set to the value used by Huisman et al. for picophytoplankton, $v = 0.1$ m day^{-1} [17, 122]. The half-saturation constants, K_{R_i} and K_{I_i}, for the two groups are set to obtain a suitable position of production layers and a certain depth for the position of the peak of biomass concentration. Since picoeukariotes consist of picophytoplankton species that are better adapted to lower light intensity than Prochlorococcus, we fix $K_{I_1} < K_{I_2}$. Viceversa, since Prochlorococcus is better adapted to lower nutrient concentration than picoeukariotes group, we set $K_{R_2} < K_{R_1}$. As a consequence, the peak of picoeukaryotes concentration along the water column tends to be deeper than the peak of Prochlorococcus concentration. It is worth noting that the nutrient content of the picoeukaryotes, $1/Y_1$, is set to different values in the two sites investigated in this work. This choice can be explained recalling that, in the Mediterranean Sea, the picoeukaryotes group located in the DCM includes several species. As a consequence, depending of the marine site analyzed, different ecotypes of this group prevail and nutrient content changes accordingly [20, 123]. Viceversa, the nutrient content of picoprokaryotes ($1/Y_2$) is set equal in both sites because Prochlorococcus is the only species of its group present in the DCM. We recall that the parameters $1/Y_1$ and $1/Y_2$ contribute to determine the steady distributions of the picophytoplankton concentrations. Experimental findings indicate that (i) the peak of biomass con-

Symbol	Interpretation	Units	Site L1129b	Site L1105
I_{in}	Incident light intensity	μmol photons m^{-2} s^{-1}	1404.44	1383.19
a_{bg}	Background turbidity	m^{-1}	0.045	0.045
a_1	Absorption coefficient of picoeukaryotes	m^2 cell^{-1}	6×10^{-10}	3.3×10^{-10}
a_2	Absorption coefficient of Prochlorococcus	m^2 cell^{-1}	2.4×10^{-15}	2.4×10^{-15}
z_b	Depth of the water column	m	186	575
D	Vertical turbulent diffusivity	cm^2 s^{-1}	1.0	3.0
r_1	Maximum specific growth rate of picoeukaryotes	h^{-1}	0.08	0.08
r_2	Maximum specific growth rate of Prochlorococcus	h^{-1}	0.07	0.07
K_{I_1}	Half-saturation constant of light-limited growth of picoeukaryotes	μmol photons m^{-2} s^{-1}	20	20
K_{R_1}	Half-saturation constant of nutrient-limited growth of picoeukaryotes	mmol nutrient m^{-3}	0.0425	0.0425
K_{I_2}	Half-saturation constant of light-limited growth of Prochlorococcus	μmol photons m^{-2} s^{-1}	98	98
K_{R_2}	Half-saturation constant of nutrient-limited growth of Prochlorococcus	mmol nutrient m^{-3}	0.0150	0.0150
m_1	Specific loss rate of picoeukaryotes	h^{-1}	0.01	0.01
m_2	Specific loss rate of Prochlorococcus	h^{-1}	0.01	0.01
$1/Y_1$	Nutrient content of picoeukaryotes	mmol nutrient cell^{-1}	1×10^{-9}	0.6×10^{-9}
$1/Y_2$	Nutrient content of Prochlorococcus	mmol nutrient cell^{-1}	4×10^{-15}	4×10^{-15}
ϵ_1	Nutrient recycling coefficient of picoeukaryotes	dimensionless	0.5	0.5
ϵ_2	Nutrient recycling coefficient of Prochlorococcus	dimensionless	0.5	0.5
v_1	Sinking velocity of picoeukaryotes	m h^{-1}	0.0042	0.0042
v_2	Sinking velocity of Prochlorococcus	m h^{-1}	0.0042	0.0042
R_{in}	Nutrient concentration at z_b	mmol nutrient m^{-3}	5.0	6.0

Table 3.1: Parameters used in the model. The values of the biological and environmental parameters are those typical of two picophytoplankton groups and summer period in Mediterranean Sea, respectively.

centration of Prochlorococcus is shallower than that of picoeukaryotes and (ii) the cell concentration of Prochlorococcus is much higher than that of picoeukaryotes. In these conditions a smaller amount of nutrient is available for Prochlorococcus localized in the biomass peak. Therefore, in order to obtain for the two picophytoplankton groups, the correct cell concentrations as found in field observations, $1/Y_2$ is set at a value much smaller than $1/Y_1$ (see Table 3.1). The absorption coefficient of Prochlorococcus, fixed in our model, is very different from that of the picoeukaryotes. In fact, due to the low nutrient concentration in the higher layers and different average cell concentration of the two groups (0.6×10^3 cells ml^{-1} for picoeukariotes and 5.2×10^4 cells ml^{-1} for Prochlorococcus), we had to exploit an absorption coefficient for Prochlorococcus lower than that used for picoeukaryotes. In particular, in order to obtain the same gradient of light intensity inside the production layers [7], we set $a_2 = 2.4 \times 10^{-15}$m^2 cell^{-1}. All the other biological parameters are the same in both sites in agreement with ones used from other authors [17, 18].

As done for the one-population model (see chapter 2), the values of the environmental parameters have been chosen to reproduce marine ecosystem of the Sicily Channel in summer, i.e. oligotrophic water and high light intensity. The water column depths used in the model are fixed according to those measured in the corresponding marine sites. The diffusion coefficients are set at typical values of weakly mixed water ($D = 1.0$ cm^2 s^{-1} for site L1129b and $D = 3.0$ cm^2 s^{-1} for site L1105). This choice is due to the fact that the site L1129b is placed on the Libyan continental shelf, not far from the coast, where turbulence is low. Conversely, the site L1105 is located in the middle of Sicily Channel, where vertical diffusion coefficient is greater respect to the Libyan coast because the flows of the Modified Atlantic Water (MAW) and Levantine Intermediate Water (LIW) are responsible for a bigger turbulence. Moreover, in both sites we set the light intensity at the water surface, I_{in}, at values larger than 1300 μmol photons m^{-2} s^{-1}. This is due to the fact that the sampling of the experimental data occurred during summer (August 2006), when the light intensity achieves maximum values in Mediterranean Sea. In particular, the light intensities used in this study were fixed using data available on the NASA web site[1]. Finally, nutrient concentrations at depth z_b were fixed at values such as to obtain, for each site, a peak of biomass concentration at the same position of the

[1]http://eosweb.larc.nasa.gov/sse/RETScreen/

peak experimentally observed.

A preliminary analysis (results here not shown) indicated that large values of I_{in} lead to stationary conditions characterized by the presence of a DCM, where two species can coexist, while large values of R_{in} (nutrient concentration close to seabed) determine an upper chlorophyll maximum (UCM) [18], where picoeukaryotes prevail and Prochlorococcus undergoes a strong reduction. In particular, for fixed values of I_{in} and D, an increase of R_{in} generates a displacement of picoeukaryotes towards higher layers, where the production layer of Prochlorococcus is located. As a consequence of light limitation, Prochlorococcus moves upward in the direction of surface layers of the water column. If R_{in} is very high, we can observe an upper chlorophyll maximum (UCM) due to the picoeukaryotes group and the disappearance of Prochlorococcus. These results are in agreement with those shown in Ref. [7].

3.1.3 Results of the deterministic model

In order to obtain the theoretical distributions of biomass concentrations for the two picophytoplankton populations, we solved numerically Eqs. (3.4)-(4.9). According to the procedure followed in the previous chapter for the one-population model, the numerical method, whose computer implementation consists in a C++ program, is based on an explicit finite difference scheme with centered-in-space differencing for the diffusion term and forward differencing for the advection term. The increment of the spatial variable is fixed at 0.5 m, while the size of the time step is chosen, for fixed values of vertical turbulent diffusion and sinking velocity, such as to obtain the convergence of the finite difference equations [96, 99, 100], according to the discussion of paragraph 2.1.3.
As initial conditions, we set that the two picophytoplankton groups are both concentrated in the DCM where the maximum of the experimental chlorophyll distribution is observed. As in the one-population model, the nutrient concentration is approximately constant from the water surface to the DCM, and increases linearly below this point down to the seabed.

The equation system (3.4)-(4.9) is solved for the maximum simulation time $t_{max} = 6 \cdot 10^4\ h$, even if the stationary solution already appears for $t \approx 3 \cdot 10^4\ h$(see Fig. 4.2). Therefore, in order to obtain the stationary distributions for the biomass

concentrations of picoeukaryotes and Prochlorococcus, and the profile of light intensity, it is sufficient to set $t_{max} = 4 \cdot 10^4\ h$. The results are shown in Fig. 3.3. We observe the presence of a picoeukaryotes biomass peak (panels a, d of Fig. 3.3) in correspondence of the two experimental DCMs (see Fig. 1.4). Moreover, a Prochlorococcus biomass peak (panels b, e of Fig. 3.3) is observed close to the two experimental DCMs (see again Fig. 1.4). Finally the typical exponential behaviour of the light intensity is found (panels c, f of Fig. 3.3).

We recall that our experimental data are expressed in μg/l (see Fig. 1.4), which

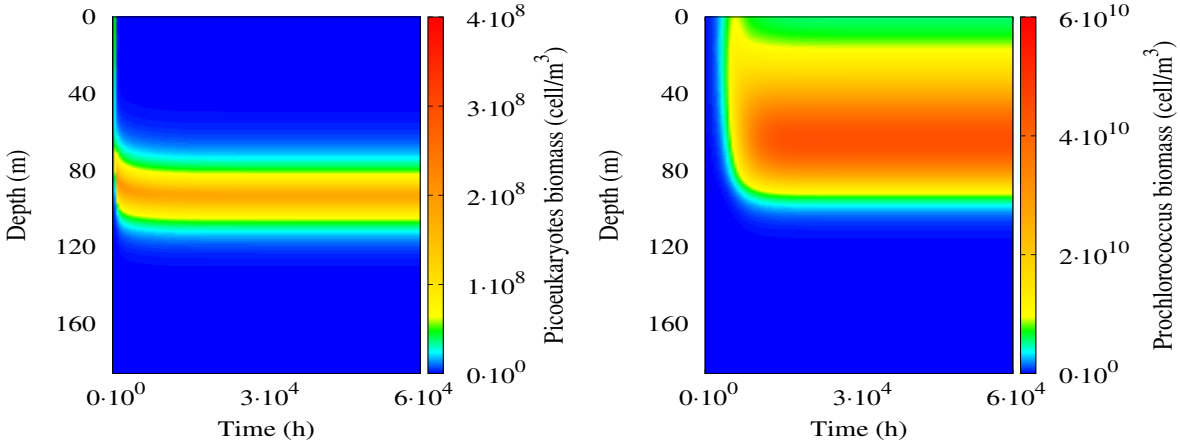

Figure 3.2: Contour map for picoeukaryotes (left panel) and Prochlorococcus (right panel) biomass concentration as a function of the depth and time for CTD collected in site L1129b. The values of the parameters are those of table 3.1.

is the unit of measure used for *chl a* and *Dvchl a* concentrations. Therefore, to compare the numerical results with experimental profiles, the theoretical cell concentrations of picoeukaryotes and Prochlorococcus (expressed in cell/m^3) have been converted into *chl a* and *Dvchl a* concentrations (expressed in μg/l) by using the curves of mean vertical profile obtained by Brunet et al. [67, 68]. Since the structure of the *chlorophyll a* molecule is almost identical to that of *Divinyl chlorophyll a*, we summed their concentrations to get theoretical equilibrium profiles consistent with those obtained from the experimental data. It is important to recall that in the Sicily Channel nano–phytoplankton, micro-phytoplankton and Synechococcus account about for 43% of the total quantity of *chl a* and *Dvchl a* [67, 68]. This quantity is quite uniformly distributed along the water column. Therefore, following the

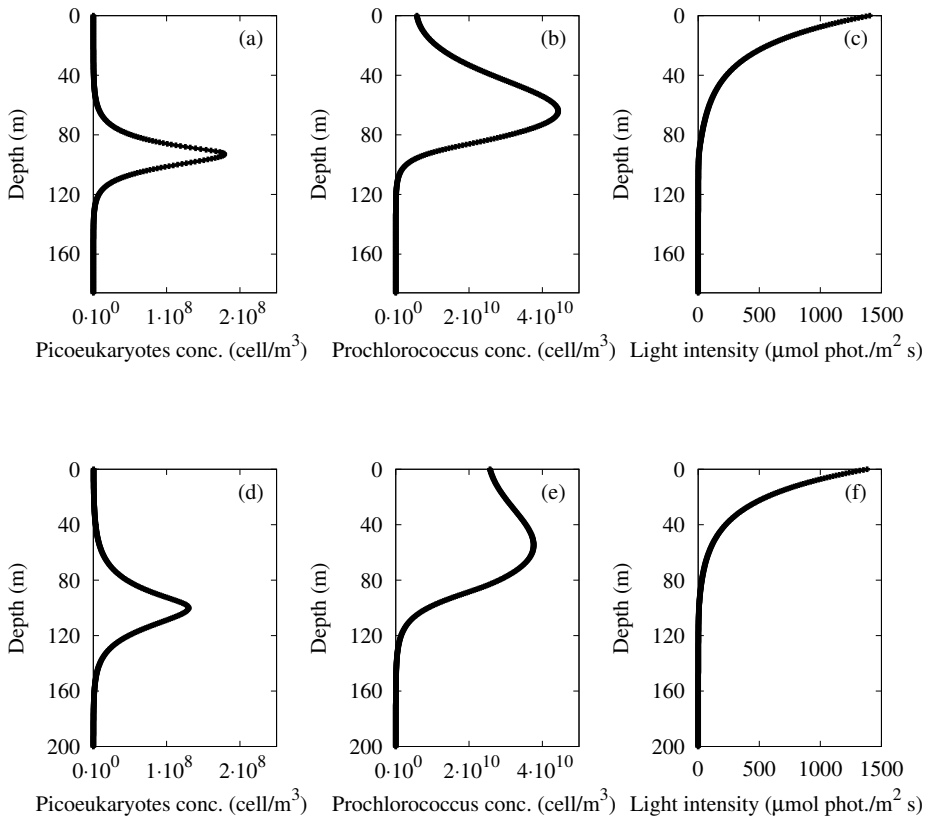

Figure 3.3: Stationary distributions of picoeukaryotes and Prochlorococcus biomass concentrations and light intensity: site L1129b (panels a, b, c) and site L1105 (panels d, e, f) as a function of the depth.

same procedure as for the one-population analysis, we considered this fraction of the total biomass and divided it by depth, obtaining for each site the value $\Delta b_{(Dv)chl\,a}$, which represents a constant concentration along the whole water column, due to other phytoplankton species present in the marine ecosystem [29]. Then, along the water column, we added the numerical concentrations with $\Delta b_{(Dv)chl\,a}$ and obtained, for both sites, the stationary theoretical profiles consistent with the experimental ones. The results, shown in Fig. 3.4, indicate the presence of a fairly good agreement

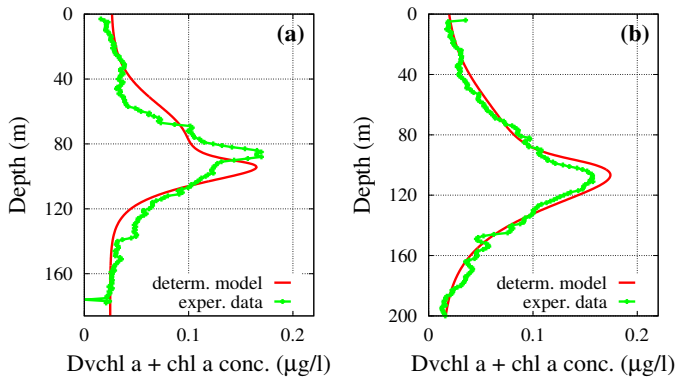

Figure 3.4: Theoretical distributions (red line) of the total *chl a* and *Dvchl a* concentration in stationary conditions. The profiles, obtained by the deterministic model and given as a function of the depth, are compared with experimental distributions (green line) sampled in sites L1129b (panel a) and L1105 (panel b).

between experimental data (green line) and numerical results (red line). Only in site L1129b the theoretical distribution of total *chl a* and *Dvchl a* is characterized by a shape which exhibits some differences respect to the experimental profile. Moreover, in site L1105 we note that the magnitude of the theoretical DCM is larger than that obtained from the real data. Finally, we performed a quantitative comparison based on the goodness-of-fit test χ^2. The results indicate that, respect to the one-population model (see chapter 2), this description provides in both sites theoretical results in a better agreement with the experimental findings [29, 37].

3.2 Stochastic approach

The theoretical model discussed in the previous section is based on a deterministic approach. However, a study on population dynamics in aquatic ecosystem implies that external solicitations, coming from the environment, are taken into account. In fact, it is worth to recall that the marine ecosystems are complex systems, which are open systems characterized by non-linear interactions [29, 51, 62, 101, 102, 103, 104, 105, 106, 124, 125]. In particular, each picophytoplankton group not only interacts with all other populations, but is also subject to environmental variables, such as turbulence and availability of food resources, which affects the ecosystem dynamics through deterministic and random perturbations. In this context, random variations of species concentrations [44, 45, 46, 55, 58] are fundamental aspects that can not be neglected when seeking a better understanding of the dynamics of complex living systems.

In previous works it has been shown that the effects of random fluctuations have to be proportional to the activity densities [110, 111, 112, 113, 114], which are in our system the biomass and nutrient concentrations.
In particular, we recall that problems, which involve absorbing states, are described by equations whose noise amplitude is proportional to the square root of the space and time dependent activity density. Such systems include propagating epidemics, autocatalytic reactions, and reaction-diffusion problems [108]. As a consequence, according also to the study performed in the one-population case (see chapter 2), the fluctuations of environmental parameters have been modeled by including multiplicative noise sources [47, 48, 51, 106] in view of obtaining theoretical results that better reproduce experimental data.

3.2.1 Description of the model

In this paragraph, a stochastic model is used to study the dynamics of the two picophytoplankton populations [17, 18] distributed along a one-dimensional spatial domain (z-direction). As in the previous section, we assume that the interaction of these microorganisms with the marine environment occurs through the two factors which limit the growth of the planktonic communities: light intensity (I) and

nutrient (R), i.e. phosphorus. Moreover, we also take into account random fluctuations and their effect on the phytoplankton dynamics. In particular, we modify the deterministic model given by Eqs. (3.4)-(4.9), by inserting in the three differential equations terms of spatially uncorrelated multiplicative noise, distinguishing the stochastic analysis in two different cases.

Case 1. The environmental noise affects only the nutrient concentration. In this case, Eqs. (3.4),(3.5),(3.6),(4.8),(4.9) remain unchanged, while Eq. (4.7) is replaced by

$$\begin{aligned}\frac{\partial R(z,t)}{\partial t} &= -\sum \frac{b_i(z,t)}{Y_i} \cdot min(f_{I_i}(I), f_{R_i}(R)) + D\frac{\partial^2 R(z,t)}{\partial z^2} \\ &+ \sum \varepsilon_i m_i \frac{b_i(z,t)}{Y_i} + R\,\xi_R(z,t). \end{aligned} \tag{3.10}$$

Case 2. The environmental noise affects the concentrations of picoeukaryotes biomass, Prochlorococcus biomass and nutrient. Therefore, Eqs. (3.6),(4.8),(4.9) remain unaltered, while Eqs. (3.4),(3.5) and (4.7) become

$$\begin{aligned}\frac{\partial b_1(z,t)}{\partial t} &= b_1 min(f_{I_1}(I), f_{R_1}(R)) - m_1 b_1 + D\frac{\partial^2 b_1(z,t)}{\partial z^2} - v_1\frac{\partial b_1(z,t)}{\partial z} \\ &+ b_1\,\xi_{b_1}(z,t) \end{aligned} \tag{3.11}$$

$$\begin{aligned}\frac{\partial b_2(z,t)}{\partial t} &= b_2 min(f_{I_2}(I), f_{R_2}(R)) - m_2 b_2 + D\frac{\partial^2 b_2(z,t)}{\partial z^2} - v_2\frac{\partial b_2(z,t)}{\partial z} \\ &+ b_2\,\xi_{b_2}(z,t) \end{aligned} \tag{3.12}$$

$$\begin{aligned}\frac{\partial R(z,t)}{\partial t} &= -\sum \frac{b_i(z,t)}{Y_i} \cdot min(f_{I_i}(I), f_{R_i}(R)) + D\frac{\partial^2 R(z,t)}{\partial z^2} \\ &+ \sum \varepsilon_i m_i \frac{b_i(z,t)}{Y_i} + R\,\xi_R(z,t). \end{aligned} \tag{3.13}$$

Here, $\xi_{b_1}(z,t)$, $\xi_{b_2}(z,t)$ and $\xi_R(z,t)$ are statically independent and spatially uncorrelated white Gaussian noises with the following properties: $\langle \xi_{b_i}(z,t)\rangle = 0$, $\langle \xi_R(z,t)\rangle = 0$, $\langle \xi_{b_i}(z,t)\xi_{b_i}(z',t')\rangle = \sigma_{b_i}\delta(z-z')\delta(t-t')$, $\langle \xi_R(z,t)\xi_R(z',t')\rangle = \sigma_R\delta(z-z')\delta(t-t')$, with $i = 1, 2$. Here, σ_{b_i} and σ_R are the intensities of the noise sources which act on the *i-th* picophytoplanktonic group and nutrient, respectively.

3.2.2 Simulation setting

The inputs of stochastic model are chosen to reproduce the experimental profile of *chl a* and *DVchl a* concentration, collected in the two marine sites studied. In particular, as in deterministic model, the values of the environmental and biological parameters are set so that the presence of a deep chlorophyll maximum for both picophytoplankton groups is guaranteed [17, 18, 42]. Moreover, the values of the biological parameters have been fixed to simulate the behaviour of picoeukaryotes and Prochlorococcus. The numerical values assigned to the parameters are shown in Table 3.1.

Finally, it is worth noting that, in order to describe correctly the time evolution of the system in the presence of noise sources, the equations of the model are solved taking in account the average of an enough large amount of numerical realizations [51]. Specifically, preliminary analysis indicated that the theoretical distributions of the total chlorophyll a and divinyl-chlorophyll a concentration are not affected by the fluctuations of the single numerical realization, when the mean profiles are calculated averaging over $N \geq 800$ realizations.

3.2.3 Results of the stochastic model

In this section the analysis of the stochastic model is performed by numerically solving the system equations for different values of the noise intensities. As in the one-population model, the stochastic differential equations have been solved by using the Ito scheme, according to the discussion of paragraph 2.2.3. In particular, in order to obtain phytoplankton distributions statistically meaningful, e.g. without "spikes" of biomass concentration, the phytoplankton profiles are calculated by averaging over 1000 realizations [51, 118].

Also in this case, we note that the presence of noise sources does not determine significant changes respect to the deterministic model in the time necessary to reach the stationary state. Therefore, accordingly to the deterministic analysis, in order to get the stationary solution, the equations of the stochastic model have been solved fixing as a maximum time $t_{max} = 4 \cdot 10^4\ h$. Finally, it is worth recalling that initial conditions are the same of the deterministic model in all simulations.

Case 1. The average theoretical distributions of the total phytoplankton biomass

concentration have been obtained in each site and transformed in *chl a* and *Dvchl a* concentration profiles by exploiting the usual conversion curves (see Fig. 1.3). The numerical results (see Figs. 3.5 and 3.6) show that a decrease and a deeper localization of the DCMs respect to the deterministic case, are present also for low noise intensities (σ_R between 0.001 and 0.010).

In order to evaluate the agreement of each theoretical distribution (red line) with the corresponding experimental one (green line), we use two comparative methods: χ^2 goodness-of-fit test and Kolmogorov-Smirnov (K-S) test. The results are shown in Tables 3.2, where $\tilde{\chi}^2$ indicates the reduced chi-square, while $D(K-S)$ and $P(K-S)$ are the maximum difference between the cumulative distributions and the corresponding probability for the K-S test, respectively. The quantitative

Site L1129b

R_{in}	σ_R	χ^2	$\tilde{\chi}^2$	D (K-S)	P (K-S)
5	0.0000	0.74	0.0042	0.1136	0.193
5	0.0010	0.69	0.0039	0.1136	0.193
5	0.0025	0.65	0.0037	0.1136	0.193
5	0.0050	0.66	0.0038	0.1136	0.193
5	0.0075	0.71	0.0041	0.1136	0.193
5	0.0100	0.78	0.0045	0.1136	0.193

Site L1105

R_{in}	σ_R	χ^2	$\tilde{\chi}^2$	D (K-S)	P (K-S)
6	0.0000	0.23	0.0012	0.0812	0.517
6	0.0010	0.20	0.0010	0.0660	0.771
6	0.0020	0.18	0.0009	0.0609	0.847
6	0.0025	0.18	0.0009	0.0660	0.771
6	0.0050	0.19	0.0010	0.0711	0.687
6	0.0100	0.32	0.0016	0.1066	0.201

Table 3.2: Results of χ^2, reduced chi-square ($\tilde{\chi}^2$), and Kolmogorov-Smirnov goodness-of-fit tests for site L1129b (left panel) and site L1105 (right panel) for different values of σ_R (stochastic dynamics - case 1). D(K-S) and P(K-S) are the maximum difference between the cumulative distributions and the corresponding probability for the K-S test, respectively. The number of samples, used for the tests and distanced of 1 m, is n = 176 for site L1129b, corresponding to consider the whole water column, and n = 200 for site L1105, corresponding to consider from the surface the first 200 m of depth.

comparison, based on the χ^2 goodness-of-fit test, shows a good agreement between theoretical and experimental profiles for both sites, better than in the deterministic case. In particular, the best value of the χ^2 test is obtained, in site L1129b, setting $\sigma_R = 0.0025$ and, in site L1105, using two different values of the noise intensity, i.e.

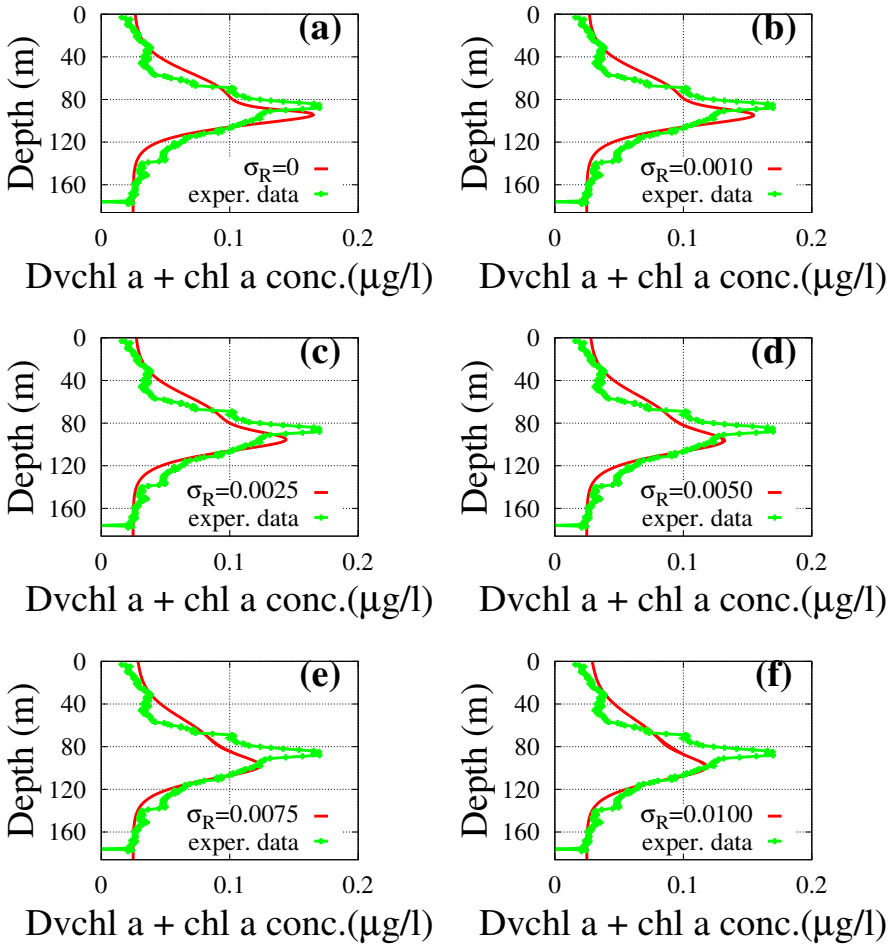

Figure 3.5: Theoretical distributions (red line) of the total *chl a* and *Dvchl a* concentration (stochastic approach). The profiles were obtained in stationary regime for different values of σ_R (case 1 of the stochastic model) as a function of the depth. The results are compared with the distributions of the total *chl a* and *Dvchl a* concentration measured (green line) in site L1129b. The theoretical values were obtained averaging over 1000 numerical realizations. The values of the parameters are those shown in Table 3.1. The noise intensities are: (a) $\sigma_R = 0$ (deterministic case), (b) $\sigma_R = 0.0010$, (c) $\sigma_R = 0.0025$, (d) $\sigma_R = 0.0050$, (e) $\sigma_R = 0.0075$ and (f) $\sigma_R = 0.0100$.

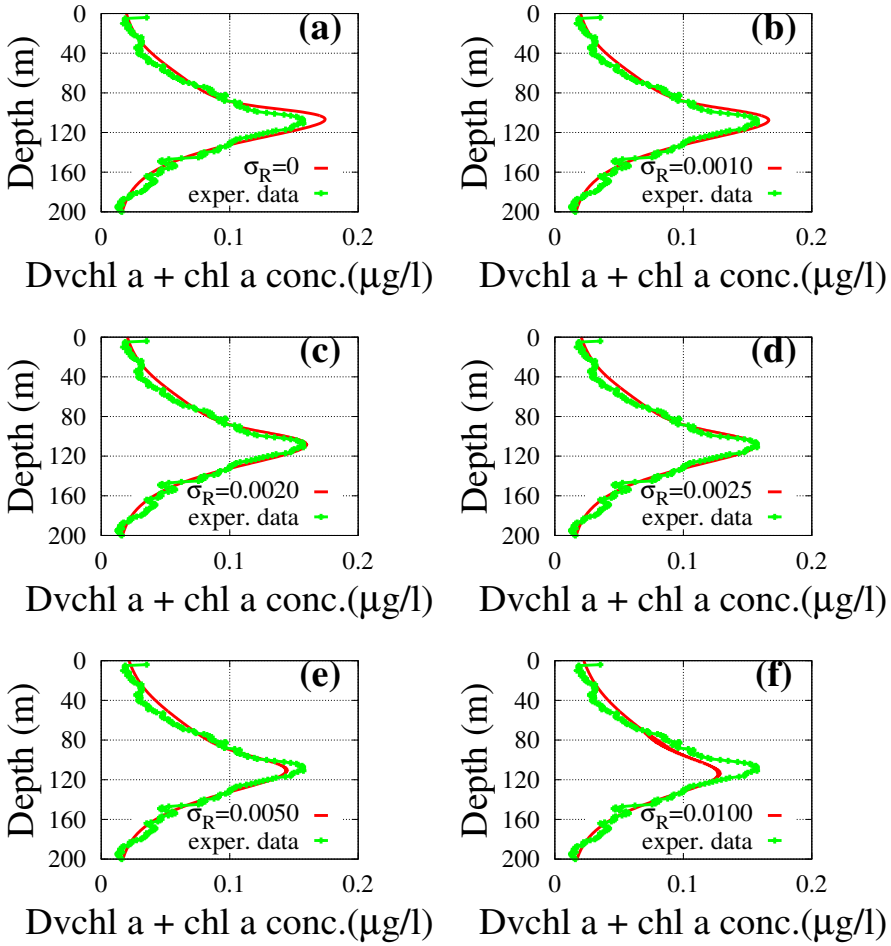

Figure 3.6: Theoretical distributions (red line) of the total *chl a* and *Dvchl a* concentration (stochastic approach). The profiles were obtained in stationary regime for different values of σ_R (case 1 of the stochastic model) as a function of the depth. The results are compared with the distributions of the total *chl a* and *Dvchl a* concentration measured (green line) in site L1105. The theoretical values were obtained averaging over 1000 numerical realizations. The values of the parameters are those shown in Table 3.1. The noise intensities are: (a) $\sigma_R = 0$ (deterministic case), (b) $\sigma_R = 0.0010$, (c) $\sigma_R = 0.0020$, (d) $\sigma_R = 0.0025$, (e) $\sigma_R = 0.0050$ and (f) $\sigma_R = 0.0100$.

$\sigma_R = 0.0020$ and $\sigma_R = 0.0025$. Analyzing the results of the Kolmogorov-Smirnov test we get, in site L1105, the best agreement between experimental and theoretical distributions for $\sigma_R = 0.0020$, while in site L1129b the parameters $D(K - S)$ and $P(K - S)$ remain unchanged as σ_R varies. Finally, it is possible to note that the best agreement in site L1105 is obtained for a value of the noise intensity σ_R lower than that used in site L1129b as observed in the previous one-population analysis (see chapter 2). This can be explained by the fact that in site L1105 the DCM is deeper than in site L1129b (111 m vs. 88 m). As a consequence, in site L1105 the environmental variables, and therefore the peak of total *chl a* and *Dvchl a* concentration, are subject to less intense random perturbations respect to site L1129b, which is closer to the water surface.

In order to better understand the dependence of the biomass concentration on the random fluctuations of the nutrient, we studied for both sites the behaviour of the depth, width, and magnitude of the DCM as a function of σ_R. The results, shown in Fig. 3.7, indicate that the depth of the DCM slightly increases in both sites as a function of the noise intensity (see panels b, e). We note also that a decrease of the total concentration of *chl a* and *Dvchl a* is observed in the DCMs of the two sites (see panels a, d). At the same time we observe an increase, slightly faster in site L1105, of the width of the DCM (see panels c, f). The spread of the DCM and reduction of its magnitude appear therefore to be strictly connected with each other (an effect observed also in the one-population model). Results here not reported indicate that the phytoplankton biomass tends to disappear for $\sigma_R > 0.01$. On this basis the present analysis confirm the result found in the one-population study: the nutrient concentration also in this case plays a crucial role in the stability of the phytoplankton populations. Finally, we note that the presence of noise sources directly acting on the nutrient concentration could explain, in real ecosystems, events as the disappearance of the picophytoplankton biomass.

Case 2. According to the procedure followed for case 1, we obtained in both sites the profiles of the total concentration of *chl a* and *Dvchl a* for suitable values of the noise intensity ($\sigma_{b_1} = 0.22$, $\sigma_{b_2} = 0.08$ and $\sigma_R = 0.0025$ for site L1129b; $\sigma_{b_1} = 0.15$, $\sigma_{b_2} = 0.10$ and $\sigma_R = 0.0020$ for site L1105). The results are shown in Fig. 3.8. In this case, the reduced chi-square test (see Table 3.3) exhibits values ($\tilde{\chi}^2 = 0.0019$ for site L1129b and $\tilde{\chi}^2 = 0.0008$ for site L1105) much lower than the

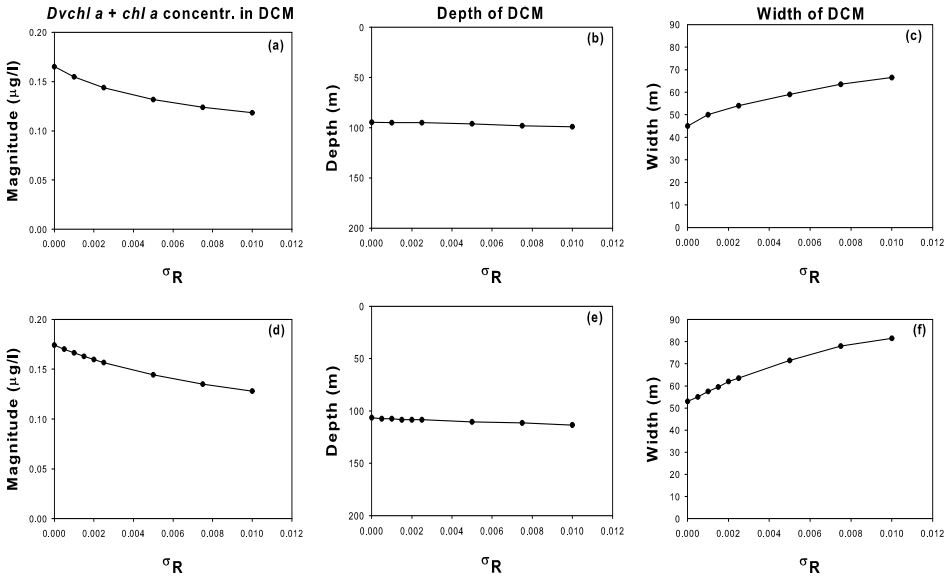

Figure 3.7: Theoretical values of the magnitude, depth, and width of the DCM as a function of σ_R obtained from the model for site L1129b (panels a, b, c) and site L1105 (panels d, e, f). The values shown have been calculated at the steady state.

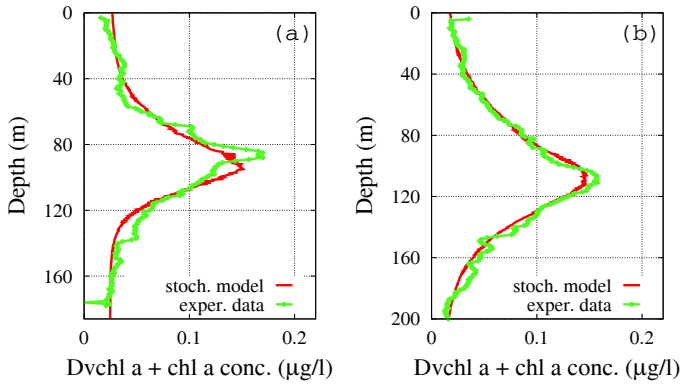

Figure 3.8: Theoretical distributions (red line) of the total *chl a* and *Dvchl a* concentration (stochastic approach). The profiles were obtained in stationary regime for a given set of noise intensities (case 2 of the stochastic model) as a function of the depth, and are compared with the corresponding experimental distributions (green line) in sites L1129b (panel a) and L1105 (panel b). The theoretical values were obtained averaging over 1000 numerical realizations. The values of the parameters are those shown in Table 3.1. The noise intensities are: (a) $\sigma_{b_1} = 0.22$, $\sigma_{b_2} = 0.08$ and $\sigma_R = 0.0025$ for site L1129b; (b) $\sigma_{b_1} = 0.15$, $\sigma_{b_2} = 0.10$ and $\sigma_R = 0.0020$ for site L1105.

Site	R_{in}	σ_R	σ_{b_1}	σ_{b_2}	χ^2	$\tilde{\chi}^2$	D (K-S)	P (K-S)
L1129b	5	0.0025	0.22	0.08	0.33	0.0019	0.1136	0.193
L1105	6	0.0020	0.15	0.10	0.16	0.0008	0.0914	0.3670

Table 3.3: Results of χ^2, reduced chi-square ($\tilde{\chi}^2$), and Kolmogorov-Smirnov goodness-of-fit tests for sites L1129b and L1105, at fixed values of σ_{b_1}, σ_{b_2} and σ_R (stochastic dynamics - case 2). D(K-S) and P(K-S) are the maximum difference between the cumulative distributions and the corresponding probability for the K-S test, respectively. The number of samples, used for the tests and distanced of 1 m, is n = 176 for site L1129b, corresponding to consider the whole water column, and n = 200 for site L1105, corresponding to consider from the surface the first 200 m of depth.

values previously obtained from the stochastic approach in case 1. Viceversa the statistical parameters, $D(K-S)$ and $P(K-S)$, of the Kolmogorov-Smirnov test remain unchanged for site L1129b, while indicate in site L1105 a worse agreement, with respect to case 1, between numerical results and experimental data. On the basis of these results we can conclude that in site L1129b the presence of noise sources, which act on the phytoplankton biomass, allows to further improve the agreement between theoretical results and experimental findings. Contrasting indications are provided, in site L1105, by the $\tilde{\chi}^2$ and K-S tests, about the role played by the noise sources ξ_{b_1} and ξ_{b_2} from the point of view of a better agreement between theoretical and experimental distributions.

In conclusion, the results obtained from the stochastic model indicate that the environmental fluctuations, connected with the random modifications of physical and chemical variables, such as temperature, velocities field, and food resources, i.e. phosphorus concentration, can give rise to interesting effects: (i) "shift" of the DCM towards a greater depth; (ii) "disappearance" of picoeukaryotes and Prochlorococcus for higher noise intensity. These results could explain the time evolution of picophytoplankton populations in real ecosystems whose dynamics is continuously influenced by random fluctuations of the environmental variables [44, 45, 46].

Chapter 4

Model for population dynamics of five picophytoplankton species

In this chapter, we introduce a reaction-diffusion-taxis model to simulate the spatio-temporal behaviuor of five picophytoplankton species in the Tyrrhenian Sea during three different periods of the year. Specifically, the population dynamics of the picophytoplankton populations is analyzed by using mathematical models based on deterministic approach.

In the first part of the chapter, the mechanism responsible for the phytoplankton dynamics is shown. In particular, we describe the locations of the five species along the water column due to their different ability to grow in presence of different environmental conditions.

In the second part of the chapter, we use a deterministic model to get the distributions of biomass concentration for five species belonging to two picophytoplankton groups, i.e. picoeukariotes and picoprokaryotes. In particular, the behaviour of the vertical profiles obtained is analyzed in presence of a water column mixed in upper layer and weakly mixed in deeper layers. The numerical results converted in the total concentration of *chl a* and *Dvchl a* are compared with the experimental data.

4.1 Mechanism responsible for the phytoplankton dynamics

In this study the spatio-temporal behaviour of the five picophytoplankton species is analyzed by using a deterministic approach. In particular, the analysis is performed by taking into account the intraspecific competition of every population for light and nutrients inside the Modified Atlantic Water (from the surface down to 200 m). This is located above the Levantine Intermediate Water (LIW) and corresponds to the euphotic zone of the water column, where the growth of phytoplankton is allowed.
The real conditions of marine ecosystem are reproduced by considering the water column stratification. Specifically, we assume that the diffusivity $D(z)$ takes a larger value D_U in the upper layer (from the surface down to the thermocline) and a smaller value D_D in the deeper layers [18]. The former changes as a function of the time, while the latter remains constant during the whole solar year. By this way, the influence of the upper mixed layer on population dynamics has been studied by modifying the vertical turbulent diffusivity and thermocline position depending on the period of the year.
In previous works it has been shown that phytoplankton should move along the water column upward if growing conditions are better above than below, downward if growing conditions are better below than above, and should not move if growing conditions are worse above and below [16]. As a consequence, in order to better simulate the behaviour of phytoplankton species, the active movement is modeled by a taxis term, where the swimming velocity v_i of each population changes direction according to the value of gradient of its net growth rate.
The mathematical tool used to reproduce the picophytoplankton dynamics is a model based on a system with six differential equations and an auxiliary equation. By solving this system, we obtain the vertical distributions of five picophytoplankton populations as a function of the depth. The location of the production layer of each picophytoplankton population is shown in Fig. 4.1, where a schematic representation of the mechanism underlying the phytoplankton dynamics is given.

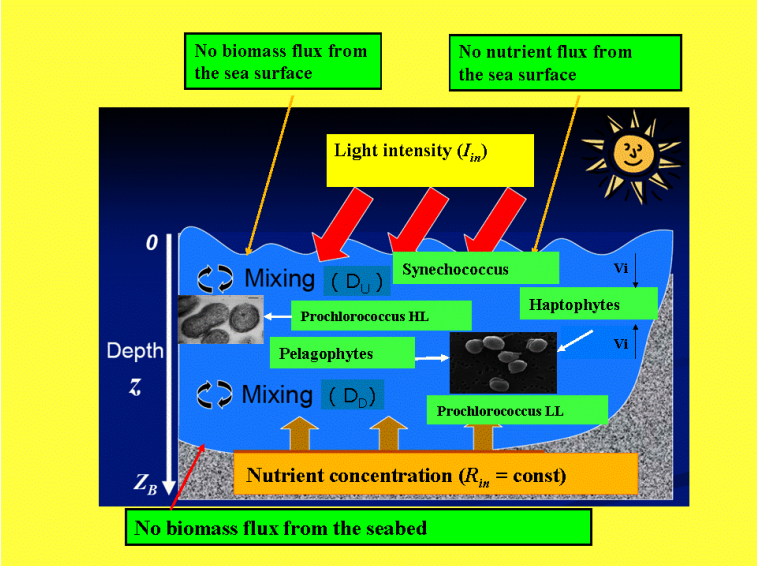

Figure 4.1: Scheme of the mechanism responsible for the phytoplankton dynamics (modified from original figure by Alexey Ryabov). Inset: (a) Prochlorococcus PCC 9511 (courtesy of Rippka et al., 2000 (Ref. [121])), (b) Micromonas NOUM17 (courtesy of Augustin Engman, Rory Welsh, and Alexandra Worden).

4.2 The five-population model

4.2.1 Description of the model

In this paragraph we describe the dynamics of the five picophytoplankton populations by using a deterministic reaction-diffusion-taxis model [16, 17, 18]. As in previous chapters, the populations analyzed are distributed along a one-dimensional spatial domain (z-direction) in the euphotic zone of the water column. In particular, we assume that the interaction of these five populations with the environment occurs through the same two factors that limit the growth of the aquatic microorganisms: light intensity and nutrient, i.e. phosphorus. The model allows to obtain the dynamics of the biomass concentrations of Synechococcus, Haptophytes, Prochlorococcus HL, Pelagophytes and Prochlorococcus LL given by $b_1(z,t)$, $b_2(z,t)$, $b_3(z,t)$,$b_4(z,t)$ and $b_5(z,t)$, respectively. Moreover, the vertical distributions of the nutrient concentration $R(z,t)$ and light intensity $I(z,t)$ are obtained. In the numerical solutions a crucial role in the phytoplankton dynamics is played by the specific loss rate of biomass concentration, the active movement of the single microorganisms, and the

growth rates of the five picophytoplankton populations. In particular, the growth rates depend on I and R, whose characteristics of limiting factors [16, 24, 28, 91] are described in the model by the Monod kinetics [92]. In particular, the gross phytoplankton growth rates per capita are given by $\min\{f_{I_i}(I), f_{R_i}(R)\}$, where $f_{I_i}(I)$ and $f_{R_i}(R)$ are obtained by the Michaelis-Menten formulas

$$f_{I_i}(I) = r_i I/(I + K_{I_i}), \tag{4.1}$$

$$f_{R_i}(R) = r_i R/(R + K_{R_i}), \tag{4.2}$$

where r_i is the maximum growth rate, and K_{I_i} and K_{R_i} are the half-saturation constants for light intensity and nutrient concentration, respectively, of the *i-th* picophytoplankton species. As for previous analysis (one- and two-population models), the constants depend on the metabolism of the specific microorganisms considered. Specifically, the values of K_{R_i} and K_{I_i} determine, along the water column, the boundaries of the production layer and the position of the maximum of biomass concentration for each population. The specific loss rate of the *i-th* picophytoplankton species, due to respiration, death, and grazing, is given by m_i [16, 17, 18]. In particular, the loss rates have been estimated by using the experimental results obtained by other authors [78, 126, 127, 128]. The net per capita growth rates are defined as

$$G_i(z,t) = \min(f_{R_i}(R(z,t)), f_{I_i}(I(z,t))) - m_i. \tag{4.3}$$

The passive movement of all phytoplankton species depends on the turbulence, which is modeled by a vertical turbulent diffusivity with coefficient $D(z)$. This is assumed uniform in the upper mixed layer ($D(z) = D_U$), while decreases as a function of the depth from the thermocline down to deeper layers, where reaches the value D_D [18]. The gradual transition from one area to another has been described in terms of a generalized Fermi function

$$D(z) = D_D + \frac{D_U - D_D}{1 + \exp^{(z-Z_t)/w}}, \tag{4.4}$$

where Z_t is the depth of the thermocline and the parameter w is the width of the transient layer.

The active movement of each population is described by the swimming velocity v_i, which is a function of the gradient of net growth rate $(\partial G_i(z,t)/\partial z)$ [16]. In the model, positive velocities are oriented downward in the direction of positive z. Moreover, the magnitude of swimming velocity v_i^s for each population is estimated by using the same criteria adopted by other authors [82]. Therefore, in order to reproduce the active movement of the *i-th* picophytoplankton species, we use a step function [16], defined as $v_i = +v_i^s$ if $\partial G_i(z,t)/\partial z > 0$, $v_i = -v_i^s$ if $\partial G_i(z,t)/\partial z < 0$, and $v_i = 0$ if $\partial G_i(z,t)/\partial z = 0$.

By taking in account these assumptions about growth, loss, and movement, we obtain the following differential equations for the population dynamics of the different species of phytoplankton [7, 16, 17, 18]

$$\frac{\partial b_i(z,t)}{\partial t} = b_i min(f_{I_i}(I), f_{R_i}(R)) - m_i b_i + \frac{\partial}{\partial z}\left[D(z)\frac{\partial b_i(z,t)}{\partial z}\right] - v_i\left(\frac{\partial G_i(z,t)}{\partial z}\right)\frac{\partial b_i(z,t)}{\partial z} \tag{4.5}$$

As boundary conditions for the concentration of the *i-th* picophytoplankton species, we assume, according to one- and two population analysis, no-flux in both surface layer $z = 0$ and interface MAW-LIW $z = z_b$:

$$\left[D(z)\frac{\partial b_i}{\partial z} - v_i b_i\right]\Bigg|_{z=0} = \left[D(z)\frac{\partial b_i}{\partial z} - v_i b_i\right]\Bigg|_{z=z_b} = 0. \tag{4.6}$$

The nutrient concentration $R(z,t)$ is consumed by all the picophytoplankton species, and a further quantity of nutrient is obtained from dead phytoplankton by a recycling process. Furthermore, turbulence is also responsible for mixing of the nutrient along the water column and it is described by the vertical turbulent diffusivity $D(z)$. The dynamics of the nutrient concentration can be therefore modeled as follows

$$\begin{aligned}\frac{\partial R(z,t)}{\partial t} &= -\sum \frac{b_i(z,t)}{Y_i} \cdot min(f_{I_i}(I), f_{R_i}(R)) + \frac{\partial}{\partial z}\left[D(z)\frac{\partial R(z,t)}{\partial z}\right] \\ &+ \sum \varepsilon_i m_i \frac{b_i(z,t)}{Y_i},\end{aligned} \tag{4.7}$$

where ε_i and $1/Y_i$ are nutrient recycling coefficient and nutrient content of the *i-th* picophytoplankton species, respectively.

According to the conditions fixed fro one- and two- population models, nutrients do not come from the top of the water column but are supplied from the bottom. In particular, nutrient concentration at the bottom of the water column, $R(z_b)$, is fixed

at the average value R_{in} for all periods of the solar year. The boundary conditions are therefore modeled by the following equations

$$\left.\frac{\partial R}{\partial z}\right|_{z=0} = 0, \qquad R(z_b) = R_{in}. \tag{4.8}$$

The biomass concentration $b_i(z,t)$ is then converted in chlorophyll concentration $chla_i(z,t)$ for each phytoplankton species. As a consequence, we take into account the shading due to the chlorophyll molecules in the Lamber-Beer's law [19, 35, 93], with the light intensity being characterized by the usual exponential decrease

$$I(z) = I_{in} \exp\left\{ - \int_0^z \left[\sum a_i \cdot chla_i(Z) + a_{bg} \right] dZ \right\}, \tag{4.9}$$

where a_i are the *chl a*-normalized average absorption coefficients of the *i-th* picophytoplankton species, a_{bg} is the background turbidity, and I_{in} is the incident light intensity at the water surface.

4.2.2 Simulation setting

In this paragraph, we describe the procedure to set the values of the environmental and biological parameters used in the model to obtain the experimental distributions of the total concentration of *chl a* and *Dvchl a* (see Fig. 1.5). As in the previous chapters, the parameters have been fixed in order to obtain the monostability condition, which corresponds to the presence of a DCM in the site investigated. This condition is valid in Tyrrhenian Sea during the period included between the early spring and late autumn [16, 17, 18, 29]. The DCM is also present during the winter season, even if an strong increase of the total *chl a* and *Dvchl a* concentration is observed in the surface layer during the late winter. In this period, the vertical distribution assumes the shape of UCM profile due to upwelling of nutrients, which reach the shallower layers of the water column by supporting the growth of phytoplankton species. As a consequence, to obtain the numerical results in agreement with experimental data for all periods of the year, we used different values of some environmental parameters to simulate seasonal changes. The numerical values assigned to the parameters are shown in Table 4.1. Here, the values of the biological parameters have been chosen to reproduce the behaviour of the five picophytoplankton species. In particular, as in previous chapters, the maximum specific growth rates have been chosen in agreement with those measured by other authors [78, 94, 126], accordingly, the specific

Symbol	Interpretation	Units	Autumn	Winter	Spring
I_{in}	Incident light intensity	μmol photons m^{-2} s^{-1}	421.67	601.85	1454.40
a_{bg}	Background turbidity	m^{-1}	0.060	0.060	0.060
$a_1 = a_3 = a_5$	Average absorption coefficient of picoprokaryotes	m^2 mg chl-a $^{-1}$	0.016	0.016	0.016
$a_2 = a_4$	Average absorption coefficient of picoeukaryotes	m^2 mg chl-a $^{-1}$	0.012	0.012	0.012
a_6	Average absorption coefficient of phytoplankton $> 3\mu m$	m^2 mg chl-a $^{-1}$	0.015	0.015	0.015
z_b	Depth of the water column	m	200	200	200
D_U	Vertical turbulent diffusivity in UML	m^2 h^{-1}	3.198	10.381	2.745
D_D	Vertical turbulent diffusivity in deep layer	m^2 h^{-1}	0.540	0.540	0.540
r_1	Maximum specific growth rate of Synechococcus	h^{-1}	0.058	0.058	0.058
r_2	Maximum specific growth rate of Haptophytes	h^{-1}	0.079	0.079	0.079
r_3	Maximum specific growth rate of Prochlorococcus HL	h^{-1}	0.088	0.088	0.088
r_4	Maximum specific growth rate of Pelagophytes	h^{-1}	0.096	0.096	0.096
r_5	Maximum specific growth rate of Prochlorococcus LL	h^{-1}	0.031	0.031	0.031
K_{I_1}	Half-saturation constant of light-limited growth of Synechococcus	μmol photons m^{-2} s^{-1}	80.00	80.00	80.00
K_{I_2}	Half-saturation constant of light-limited growth of Haptophytes	μmol photons m^{-2} s^{-1}	80.00	80.00	80.00
K_{I_3}	Half-saturation constant of light-limited growth of Prochlorococcus HL	μmol photons m^{-2} s^{-1}	36.00	36.00	36.00
K_{I_4}	Half-saturation constant of light-limited growth of Pelagophytes	μmol photons m^{-2} s^{-1}	19.75	19.75	19.75
K_{I_5}	Half-saturation constant of light-limited growth of Prochlorococcus LL	μmol photons m^{-2} s^{-1}	1.00	1.00	1.00
K_{R_1}	Half-saturation constant of nutrient-limited growth of Synechococcus	mmol nutrient m^{-3}	0.0010	0.0010	0.0010
K_{R_2}	Half-saturation constant of nutrient-limited growth of Haptophytes	mmol nutrient m^{-3}	0.0040	0.0034	0.0230
K_{R_3}	Half-saturation constant of nutrient-limited growth of Prochlorococcus HL	mmol nutrient m^{-3}	0.0160	0.0058	0.0850
K_{R_4}	Half-saturation constant of nutrient-limited growth of Pelagophytes	mmol nutrient m^{-3}	0.1050	0.0163	0.2150
K_{R_5}	Half-saturation constant of nutrient-limited growth of Prochlorococcus LL	mmol nutrient m^{-3}	0.0610	0.0535	0.0900
m_1	Specific loss rate of Synechococcus	h^{-1}	0.014	0.014	0.014
$m_2 = m_4$	Specific loss rate of picoeukaryotes	h^{-1}	0.010	0.010	0.010
$m_3 = m_5$	Specific loss rate of Prochlorococcus	h^{-1}	0.011	0.011	0.011
$1/Y_1$	Nutrient content of Synechococcus	mmol nutrient $cell^{-1}$	5×10^{-14}	5×10^{-14}	5×10^{-14}
$1/Y_2 = 1/Y_4$	Nutrient content of picoeukaryotes	mmol nutrient $cell^{-1}$	2×10^{-12}	2×10^{-12}	2×10^{-12}
$1/Y_3 = 1/Y_5$	Nutrient content of Prochlorococcus	mmol nutrient $cell^{-1}$	2.5×10^{-14}	2.5×10^{-14}	2.5×10^{-14}
ε_1	Nutrient recycling coefficient of Synechococcus	dimensionless	0.51	0.51	0.51
$\varepsilon_2 = \varepsilon_4$	Nutrient recycling coefficient of picoeukaryotes	dimensionless	0.52	0.52	0.52
$\varepsilon_3 = \varepsilon_5$	Nutrient recycling coefficient of Prochlorococcus	dimensionless	0.52	0.52	0.52
v_1^s	Magnitude of swimming velocity of Synechococcus	m h^{-1}	0.000088	0.000088	0.000088
$v_2^s = v_4^s$	Magnitude of swimming velocity of picoeukaryotes	m h^{-1}	0.000098	0.000098	0.000098
$v_3^s = v_5^s$	Magnitude of swimming velocity of Prochlorococcus	m h^{-1}	0.000039	0.000039	0.000039
R_{in}	Nutrient concentration at z_b	mmol nutrient m^{-3}	0.204	0.204	0.204

Table 4.1: Parameters used in the model. The values of the biological and environmental parameters are those typical of five picophytoplankton species that coexist in the Tyrrhenian Sea during three different periods of the year.

loss rates have been estimated on the basis of the experimental results described in previous works [78, 126, 127, 128]. Conversely, the swimming velocity and nutrient recycling coefficients have been chosen by following different criteria respect to previous chapters. Specifically, the magnitudes of swimming velocities of all picophytoplankton species are set equal to the values obtained by Raven for spherical phytoplankton cells [82], while nutrient recycling coefficients have been calculated by taking into account the assimilation efficiencies of the planktonic species estimated by Thingstad [127].

The half-saturation constants, K_{R_i} and K_{I_i}, for the five populations are set to obtain a suitable position of production layers and a certain depth for the position of the peak of biomass concentration. In particular, we fix that the half-saturation constants for nutrient assume low values for those populations, i.e. Synechococcus and Haptophytes, that are better adapted to low nutrient concentration. Viceversa, the half-saturation constants for light intensity are set to low values for those populations, i.e. Pelagophytes and Prochlorococcus LL, that are better adapted to low light intensity. As a consequence, the peaks of biomass concentration of the Pelagophytes and Prochlorococcus LL are localized, along the water column, deeper than those of the Synechococcus and Haptophytes. In this study, different values of the half-saturation constants for nutrient concentration have been used to mimics the genetic plasticity of picophytoplankton species, which modify their capacity to absorb nutrient in correspondence to the seasonal variations of the environmental conditions. In fact, the half-saturation constants for nutrient depend on the turbulent kinetic energy dissipation rate ϵ, which changes its value as a function of the depth of the thermocline and friction velocity in air. Since these environmental variables assume different values during the year, the half-saturation constants for nutrient cannot be considered constant in the three periods investigated.

It is worth nothing that we set half-saturation constants, K_{R_i} and K_{I_i}, by taking into account the invasibility criterion used by Ryabov and Blasius [69] to guarantee the coexistence of two or more species in the same layers of the water column. This choice allows to obtain numerical results in agreement with the experimental data, even if the maximum concentration for each species is localized at a different depth [19].

In this study, the nutrient contents of the picophytoplankton species, $1/Y_i$, are fixed

to the same values in the three periods investigated (see Table 4.1). These parameters have been estimated for Synechococcus and Pelagophytes by using previous works [129, 130], while no data are available for the other phytoplankton species. Therefore, in order to obtain cell concentrations in agreement with the experimental findings, we set the nutrient contents of Haptophytes and Prochlorococcus (both the ecotypes) such as to respect the ratios between the average concentrations of the picophytoplankton species studied [67, 68].
The *chl a*-normalized average absorption coefficients have been estimated by using the light absorption spectra obtained by other authors on picophytoplankton cultures [19, 89]. The values used in the model are in agreement with the absorption coefficients measured by Brunet et al. in Gulf of Naples [83].
Finally, it is worth underline that all the biological parameters, except the half-saturation constants for nutrient concentration, are the same in the three periods studied.

The values of the environmental parameters have been chosen to reproduce the marine ecosystem of the Tyrrhenian Sea in autumn, winter and late spring. The water column depth used in the model is fixed equal to that estimated for the MAW (200 m). The vertical turbulent diffusivity in the deep layers is set at a typical value of weakly mixed water ($D_D = 1.5$ cm^2 s^{-1}) for all periods investigated [18, 42, 43]. Viceversa, the diffusivity in the upper mixed layer D_U assumes different values during the year. These values can be estimated by exploiting the several methods adopted by other authors in marine ecosystems [131, 132, 133, 134, 135]. Specifically, to obtain D_U in winter and late spring, we used the expression of Denman and Gargett [131] defined as

$$D_U = 0.25\epsilon N^{-2}, \tag{4.10}$$

where ϵ and N are the turbulent kinetic energy dissipation rate and the buoyancy frequency, respectively. The former is calculated by using the friction velocity in the water estimated by remote sensing, and the vertical profile of temperature acquired in situ for each period considered. The latter has been calculated by using the vertical profile of water density measured together with the temperature profile by the CTD probe.
In the autumn season, the vertical turbulent diffusivity in the upper layer has been

fixed to the maximum value obtained using the following expression by Oakey [132, 133]

$$D_U = (1.0 \pm 0.5) \cdot 0.24\epsilon N^{-2}, . \tag{4.11}$$

This choice is due to the fact that, in the preliminary analysis, the theoretical biomass concentrations were underestimated in the upper mixed layer respect to the experimental data, when the expression of Denman and Gargett was used.
By following the same procedure of previous chapters, we set the light intensity at the water surface, I_{in}, at values corresponding to the periods investigated. In particular, the light intensities used in this study have been fixed using data available on the NASA web site[1]. Finally, nutrient concentrations at depth z_b were fixed at the average value of phosphorus concentration obtained by analyzing the bottle samples collected in the site investigated during the three oceanographic surveys.

4.2.3 Results of the deterministic model

The theoretical distributions of biomass concentrations for the five picophytoplankton populations are obtained by solving numerically Eqs. (4.5)-(4.9). Following the same procedure described in the previous chapters, we used a numerical method, whose computer implementation consists in a C++ program, based on an explicit finite difference scheme with centered-in-space differencing for the diffusion term and upwind differencing for the taxis term. The increment of the spatial variable and the time step are set at 0.5 m and 0.05 h, respectively. Also in this case, these values are chosen such as to obtain the stability conditions for both differencing terms. Moreover, on the basis of the analysis performed in paragraph 2.1.3, the convergence of the whole finite difference equations is guaranteed [96, 99, 100].
As initial conditions, we assumed for each picophytoplankton species a small biomass concentration uniformly distributed along the water column. Moreover, the nutrient concentration is fixed equal to zero from the water surface to the thermocline, while increases linearly below this point down to the interface MAW-LIW.

The equation system (4.5)-(4.9) is solved for the three period of the year, with

[1] http://eosweb.larc.nasa.gov/sse/RETScreen/

the maximum simulation time $t_{max} = 10^5\ h$, even if the stationary solution already appears for $t \approx 5 \cdot 10^4\ h$ (see Fig. 4.2). Therefore, in order to obtain the stationary distributions for the biomass concentrations of the five populations, and the profiles of nutrient concetration, it is sufficient to set $t_{max} = 6 \cdot 10^4\ h$.

The numerical results for the autumnal period are shown in Fig. 4.3. Here, it is

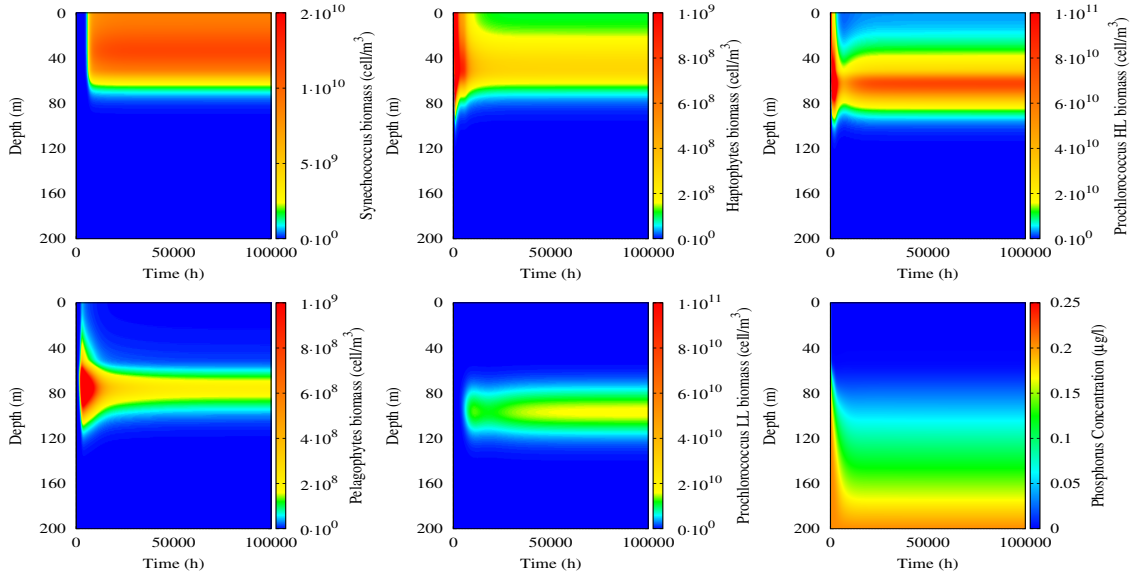

Figure 4.2: Contour map for Synechococcus, Haptophytes and Prochlorococcus HL (top panels from left to right), Pelagophytes, Prochlorococcus LL and nutrient concentration (bottom panels from left to right) as a function of the depth and time. The parameters are set to the autumn values of table 4.1.

possible to observe the presence of the biomass peak for Haptophytes, Prochlorococcus HL and Pelagophytes (see panels b, c, d of Fig. 4.3) in correspondence of the experimental DCM (see Fig. 4.4). This theoretical result is obtained also for the other periods of the year investigated, and is in agreement with the experimental data reported in previous works [65, 67, 68]. Moreover, a Synechococcus biomass peak (panel a of Fig. 4.3) is observed close to the surface water in correspondence of the upper mixed layer, where the total average *chl a* and *Dvchl a* concentration reaches a value equal to 0.08 μg/l in autumn (see again Fig. 4.4). This value increases during the winter season and decreases in late spring, in according to the behaviour of the biomass concentration of Synechococcus. Conversely, the peak of Prochlorococcus LL biomass concentration is localized in deeper layers, where the

total average *chl a* and *Dvchl a* concentration assumes low values during the whole solar year (see panels b, d, f of Fig. 1.5). Finally, we note that the nutrient concentration show the typical behaviour experimentally observed.

Also in this case the experimental data are expressed in μg/l (see Fig. 1.5), which

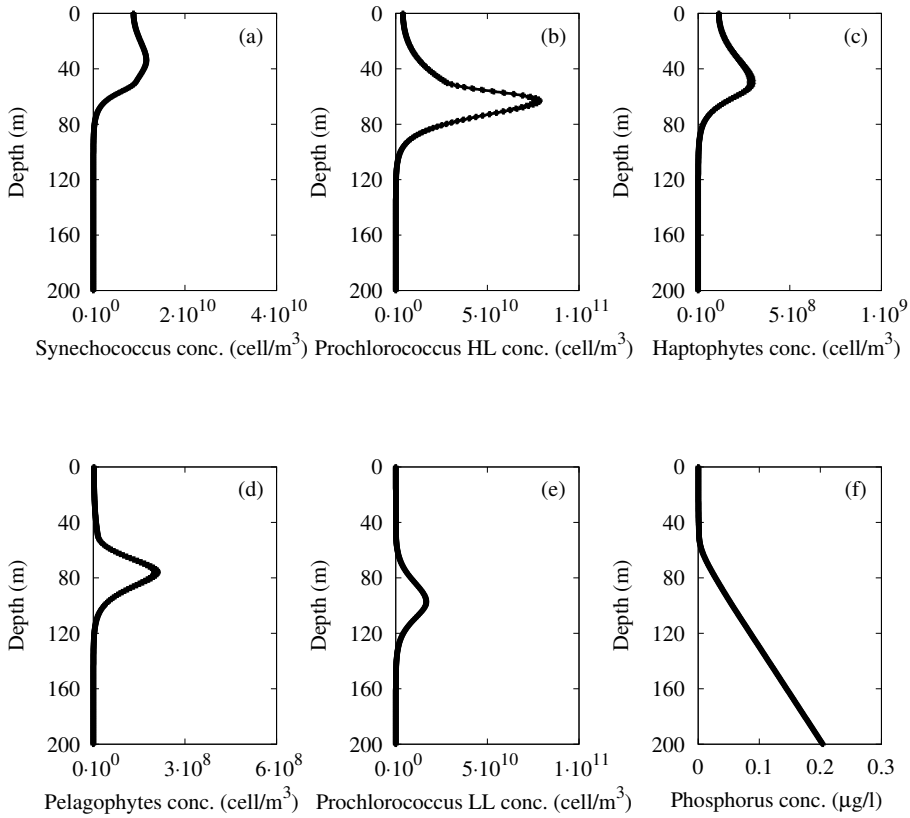

Figure 4.3: Stationary distributions of Synechococcus (panel a), Haptophytes (panel b), Prochlorococcus HL (panel c), Pelagophytes (panel d) and Prochlorococcus LL (panel e) biomass concentrations, and nutrient concentration (panel f) as a function of the depth. The numerical profiles simulate the experimental data acquired in the sampling site (39^o $30'.00$N, $13^o30'.00$E), during the oceanographic survey VECTOR-TM1 (24 November 2006). The values of the parameters are those of table 4.1 for autumn.

is the unit of measure used for *chl a* and *Dvchl a* concentrations. As a consequence, in order to compare the theoretical profiles of Fig. 4.3 with the experimental find-

ings, the numerical cell concentrations of the five populations (expressed in cell/m^3) were converted into *chl a* and *Dvchl a* concentrations (expressed in μg/l) by setting the cellular content of Synechococcus equal to 2 fg *chl a* cell^{-1} [70], and using the curves of mean vertical profile for the other species [67, 68]. It is worth recalling that the structure of the *chlorophyll a* molecule is almost identical to that of *Divinyl chlorophyll a*, therefore we can sum their concentrations (without introducing significat errors) to obtain theoretical equilibrium profiles the total *chl a* and *Dvchl a* concentration. By analyzing the bottle samples collected in the same site of the Tyrrhenian Sea during different periods of the year, diatoms, cryptophytes and dinophytes resulted to be present in traces. As a consequence their contribution to the total chlorophyll-a concentration can be neglected. Conversely, it has been estimated that the fraction of the nano- and micro-phytoplankton ($> 3\mu m$) account about for 20% of the total quantity of *chl a* and *Dvchl a*. This quantity is quite uniformly distributed along the water column. Thus, following the same procedure as for the two-population analysis, we considered the biomass fraction of the nano- and micro-phytoplankton and divided it by depth, obtaining the value $\Delta b_{(Dv)chl\,a}$, which represents a constant concentration along the whole water column, due to other phytoplankton species present in the site investigated [29, 43]. Therefore, along the water column, we added the numerical concentrations with $\Delta b_{(Dv)chl\,a}$ and obtained, for all seasons, the stationary theoretical profiles which can be compared with experimental ones.

The results, shown in Fig. 4.4, indicate the presence of a very good agreement between experimental data (green line) and numerical results (red line) in late spring. In particular, by performing the goodness-of-fit test χ^2, we obtained for the reduced chi-square $\tilde{\chi}^2 = 0.0045$. Viceversa, the theoretical profiles obtained for other periods are not in total agreement with the experimental distributions. Specifically, the numerical results show a magnitude of the total *chl a* and *Dvchl a* concentration underestimated in the upper mixed layer, while a good agreement with experimental data is obtained in deeper layers. This behaviour is due to two different reasons: the difficulty to find the correct vertical turbulent diffusivity in autumn and winter, since the methods used in this study can give values lower than those postulated for the real marine ecosystems; the increase of the nano- and micro-phytoplankton fraction in the upper mixed layer during the winter season as observed by performing

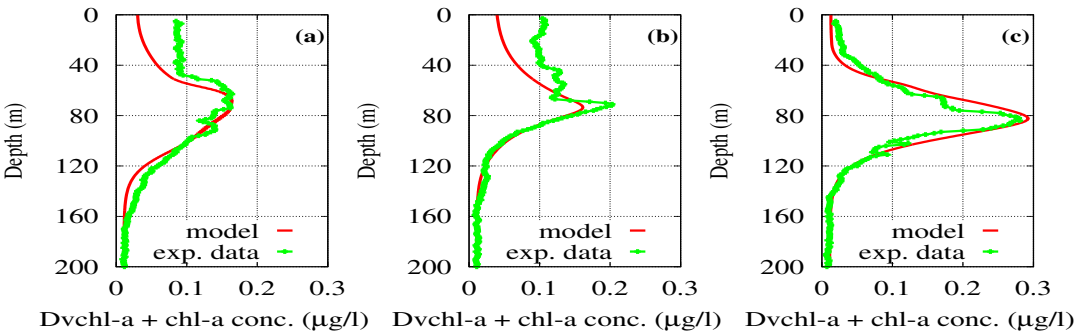

Figure 4.4: Theoretical distributions (red line) of the total *chl a* and *Dvchl a* concentration in stationary conditions. The profiles, obtained by the five-population model and given as a function of the depth, are compared with the experimental distributions (green line) collected in the sampling site (39^o $30'.00$N, $13^o30'.00$E), during the oceanographic surveys VECTOR-TM1 (24 November 2006, panel a), VECTOR-TM2 (3 February 2007, panel b) and VECTOR-TM4 (9 June 2007, panel c).

the analysis on the bottle samples. As a consequence, the magnitude of the total *chl a* and *Dvchl a* concentration obtained by the model in correspondence of the surface layer is underestimated.

In conclusion, the five-population model is able to reproduce the behaviour of the picophytoplankton species analyzed in the deeper layers, i.e. below the thermocline, during the whole solar year. On the other hand, the study indicates that the model needs of further modifications to obtain theoretical profiles of the total *chl a* and *Dvchl a* concentration in agreement with experimental data in the upper mixed layer.

Conclusions

The studies presented in this thesis consisted in analyzing the dynamics of picophytoplankton species by using deterministic and stochastic models [37, 29, 106, 125] and comparing the results with real data coming from three different sites of the Mediterranean Sea. In particular, first we investigated the phytoplankton dynamics in two sites of the Strait of Sicily in the summer period, when the waters are prevalently oligotrophic, i.e. with low nutrient concentrations. Afterwards, we analyzed the spatio-temporal behaviour of phytoplankton in a site of the Tyrrhenian Sea during three different periods of the year, by taking into account the seasonal changes of the environmental variables. The phytoplankton species analyzed belong to two groups, i.e. picoeukaryotes and picoprokaryotes, which account about for 80% of total chlorophyll on average in Mediterranean Sea and represent the whole smaller size fraction (less than 3 μm) of the phytoplankton, i.e. picophytoplankton.

The sites analyzed in this thesis are characterized by oligotrophic waters, typical of Mediterranean Sea, where the surface mixed layer is depleted of nutrients and the subsurface maxima of chlorophyll concentration are often found. Such deep chlorophyll maxima (DCMs) are permanent features in large parts of the tropical and subtropical oceans [14, 136, 137, 138, 139]. Furthermore, seasonal DCMs commonly develop in temperate regions [138, 140, 141] and even in polar oceans [142], when nutrients are depleted in the surface layer with the onset of the summer season. Here we extend the useful recent phytoplankton models [16, 39, 122, 143, 144] to show that the phytoplankton distributions, due to random changes, can exhibit fluctuations.

The studies performed by using mathematical models consists in the analysis and subsequent modeling of data coming from Mediterranean Sea, where the climatic conditions are those typical of a temperate region, and the DCMs show stable fea-

tures for given conditions of light and food resources. For values of depth ranging from 50 to 110 meters, the presence in the experimental data of a deep chlorophyll maximum indicates the existence of favourable life conditions for phytoplankton, according to other experimental findings [67], where higher biomass concentrations were observed between 60 and 90 meters. At the depths considered in this thesis the light intensity is strongly reduced respect to the surface value (about 1% of the surface irradiance at 75 m). The low light intensity however does not prevent the presence of the phytoplankton community [66, 88], since in deeper layers the high concentration of nutrients determines the most favourable life conditions for many species of phytoplankton [145]. Differences in the composition of phytoplankton between the surface and the DCMs are evident mainly for the smaller size class (less than 3 μm), which exhibits greater bio-diversity at depths between 50 and 100 meters. This could be due to the fact that different species of phytoplankton exhibit different responses to the limiting conditions. This behaviour is observed in the Mediterranean Sea, where the incident light intensity is characterized by high values in the summer period. In particular, close to the surface the low nutrient concentration represents a limiting condition for all the phytoplankton species, so that the biomass concentration increases with the depth. For larger values of depth however the light intensity becomes a main limiting factor for some species, such as Synechococcus, which show a low degree of adaptability to smaller values of light intensity [66, 89]. This causes Prochlorococcus and picoeukaryotes, which show a high degree of genetic plasticity [146] and tolerate lower light intensities [79, 89, 147], to exhibit a dominance in the deep chlorophyll maximum [68].

In the models presented here, the values of the biological parameters were those estimated by other authors for the species belonging to two picophytoplankton groups, i.e. picoeukaryotes and picoprokaryotes, while the environmental parameters were set at values typical of the oligotrophic waters. Moreover, the models includes well established facts, such as the greater photoacclimation ability of picophytoplankton species respect to nano- and micro-phytoplankton [66, 67, 68, 79, 83, 88], and the strong contribution of picoeukaryotes, specifically Pelagophytes and Haptophytes [148, 149], to the phytoplankton biomass, as observed also in culture [79, 88, 94].

In chapters 2 and 3, we introduced two stochastic models (one- and two pop-

ulation approaches, devised starting from previous deterministic models [17, 150] by these tools the spatio-temporal dynamics of the picophytoplankton biomass was studied along the water column in two different sites of the Sicily Channel in the summer period. In these analysis, for fixed sinking velocity v, we chose values of the vertical turbulent diffusivity both for biomass and nutrient concentration ($D_b = D_R = D$) which determine the absence of intrinsic oscillations of the picophytoplankton biomass, maintaining the system far from the chaos. In the one-population model we used the condition $D = 0.5\, cm^2/s$, corresponding to poorly mixed waters along the whole water column, which causes the phytoplankton peak to have a width of few meters. Similarly, in the two-population model, we set the condition $D \leq 3.0\, cm^2/s$, corresponding to weakly mixed waters, which causes the phytoplankton peak to have a width of some meters. In both models, the numerical results showed that the thickness of DCM was comparable with that observed in the experimental data. Moreover, we also considered the presence of an upper mixed layer, above the thermocline, characterized by a higher value of the diffusion coefficients ($D = 50\, cm^2/s$), keeping $D_b = D_R$ constant for greater depth [18]. The results (not shown in this thesis) did not evidence, in both cases, any variations in the picophytoplankton distributions respect to the case of uniform diffusion coefficients along the whole water column. This can be explained noting that during the summer the mixed layer, due to the depth of the thermocline, is not thick enough to influence the DCMs of the chlorophyll distributions.

In both models (one- and two-population approaches), to compare the numerical results with the experimental data, the theoretical biomass concentrations were converted into *chl a* and *Dvchl a* concentration by using the mean vertical profile curves of Brunet at al. [68]. These curves come from the analysis on the chlorophyll content per picophytoplankton cell, which is highly variable as a function of the depth. This result does not agree with other works, where a linear trend has been postulated in the shallower layers of the water column. However, from the comparison with experimental findings it was found that the values of *chl a* concentration obtained from the model are in a good agreement not only with the data sampled in the Sicily Channel but also with those measured by Brunet et al. [68]. Moreover, it is worth noting that the theoretical results for the picoeukaryotes and Prochlorococcus concentrations expressed in number of cells/m^3 match the corresponding experimental

data presented in Refs. [67, 68].

More specifically the analysis based on the one- and two-population models was performed, as a first step, by following a deterministic approach. The results of the one-population model showed a qualitative agreement with the real data, even if strong discrepancies were observed between the characteristics of the *chl a* concentration profiles provided by the model and those obtained from the real data. Conversely, the results obtained by solving the two-population model showed a good quantitative agreement with the field observations, even if the theoretical and experimental distributions of the total *chl a* and *Dvchl a* concentration present some differences. In particular, the shape of the theoretical distribution of the total *chl a* and *Dvchl a* concentration resulted quite different from the experimental profile in site L1129b, while the magnitude of the theoretical DCM in site L1105 was higher than the experimental value. However, a quantitative comparison based on the χ^2 goodness-of-fit test confirmed an agreement between the theoretical results and experimental data better than that obtained by the one-population model.

As a second step, in order to improve the agreement between theoretical and experimental distributions, the one- and two-population analysis were performed by following a stochastic approach (see chapters 2 and 3). In particular, the random fluctuations of the environmental variables were taken into account by adding terms of multiplicative Gaussian noise in the differential equations for the phytoplankton biomass and nutrient concentration.

In the one-population model, the results obtained indicated that the presence of random fluctuations acting directly on the phytoplankton biomass determines *chl a* stationary distributions more similar to the experimental ones. In particular, we found that in the sites investigated both the position and magnitude of the DCMs resulted to be in a very good agrement with the experimental findings. On the other side, adding a noise source which acts directly on the dynamics of the nutrients, suitable noise intensities (much lower than those used in the equation for the phytoplankton biomass)determined further improvement of the theoretical distributions of the *chl a* concentration respect to the experimental ones.

In the two-population model, the theoretical results showed that the presence of a noise source, which acts directly on the dynamics of the nutrient, allows to reproduce, in stationary conditions and for both marine sites analyzed, average profiles

of the total *chl a* and *Dvchl a* concentration in a better agreement with the experimental findings respect to the deterministic case. In particular, on the basis of two comparative methods (χ^2 goodness-of-fit test and Kolmogorov-Smirnov test) it has been found that position, shape and magnitude of the DCMs agree very well with the experimental ones in both sites investigated. Moreover, the results of the statistical tests are much better than those obtained by using the one-population stochastic model. Afterwards, the model has been modified by considering also the effects of two multiplicative Gaussian noise sources, which act directly on the two picophytoplankton groups, i.e. picoeukaryotes and Prochlorococcus. In these conditions, for suitable noise intensities, the χ^2 goodness-of-fit test exhibit in both sites values much lower than those obtained by the previous stochastic analysis (noise source only in the equation for the nutrient). On the other side, the values obtained from the Kolmogorov-Smirnov test became worse respect to the deterministic model in one of the two marine sites analyzed, but remained unaltered for the other site, indicating that the random fluctuations which affect the nutrient dynamics play a main role in the dynamics of the ecosystem.
Finally, in all stochastic models analyzed, it has been found that, for higher noise intensities, a rapid extinction of the picophytoplankton community is observed.

In chapter 4 the five-population deterministic model was presented. Reproducing the behaviour of the vertical turbulent diffusivity along the water column by the use of the methods adopted in other works [18, 131, 132, 133]. In particular, the vertical diffusivity in the upper mixed layer, D_U, was estimated by taking into account the seasonal changes of the environmental variables, while a constant value D_D was fixed in the deeper layers. The other environmental variables were obtained by analyzing the experimental data acquired during the three periods of the year investigated. Finally, the biological parameters were estimated on the basis of experimental findings presented in previous works [78, 126, 127, 128, 129, 130].
By following the procedure described in chapter 4, the theoretical results were converted in *chl a* and *Dvchl a* concentration [68, 70]. The theoretical results, according to the experimental data, showed different behaviours in the three periods investigated. From a quantitative point of view, the χ^2 goodness-of-fit test indicated the presence of a very good agreement between experimental and theoretical findings in late spring. Conversely, the statistical test showed that the model is not able to

reproduce the distributions of the total *chl a* and *Dvchl a* concentration because of a mismatch between model results and experimental data in the upper mixed layer during the autumn and winter seasons. These results are due to two different reasons: the difficulty to determine the correct value of the vertical turbulent diffusivity in autumn and winter; the increase of the nano- and micro-phytoplankton fraction in the upper mixed layer during the winter season.

In conclusion, the models presented in this thesis showed to be valid candidates to reproduce and predict the effects of environmental conditions on marine ecosystems, and in particular their influence on the dynamics of phytoplankton populations. Although the models were focused on oligotrophic marine ecosystems, the analysis performed could be applied to other contexts with different levels of eutrophication. By this way, it would be possible to study the phytoplankton behaviour close to coasts. Moreover a possible further extensions of these models could be the inclusion of zooplankton populations and higher trophic levels in view of reproducing the seasonal dynamics of fish species [18]. Finally, from a general point of view, the results presented in this thesis could contribute to devise a new class of models, based on stochastic approach and able to predict future changes in the marine ecosystems.

Bibliography

1. Brauer F, Castillo-Chavez C (2001) Mathematical Models in Population Biology and Epidemiology. Springer-Verlag, New York.

2. Smith JM (1968) Mathematical Ideas in Biology. Cambridge University Press.

3. Pybus OG, Rambaut A (2009) Evolutionary analysis of the dynamics of viral infectious disease. Nat Rev Genet 10: 540-550.

4. Houston A, Clark C, McNamara J, Mangel M (1988) Dynamic models in behavioural and evolutionary ecology. Nature 332: 29-34.

5. Ryabov AB, Blausius B (2008) Population growth and persistence in a heterogeneous environment: the role of diffusion and advection. Math Model Nat Phenom 3: 42-86.

6. Jennings S, Kaiser MJ, Reynolds JD (2001) Marine Fisheries Ecology. Blackwell Science, Oxford.

7. Ryabov A (2012) Phytoplankton competition in deep biomass maximum. Theor Ecol 5: 373-385.

8. Cuttitta A, Carini V, Patti B, Bonanno A, Basilone G, et al. (2003) Anchovy egg and larval distribution in relation to biological and physical oceanography in the Strait of Sicily. Hydrobiologia 503: 117-120.

9. Weston K, Fernand L, Mills DK, Delahunty R, Brown J (2005) Primary production in the deep chlorophyll maximum of the central North Sea. J Plankton Res 27: 909-922.

10. Karsenti E, Acinas S, Bork P, Bowler C, Vargas CD, et al. (2011) A holistic approach to marine eco-systems biology. PLoS Biol 9(10): e1001177.

11. Melbourne-Thomas J, Constable A, Wotherspoon S, Raymond B (2013) Testing paradigms of ecosystem change under climate warming in antarctica. PLoS ONE 8(2): e55093.

12. Basilone G, Guisande C, Patti B, Mazzola S, Cuttitta A, et al. (2004) Linking habitat conditions and growth in the european anchovy (Engraulis encrasicolus). Fish Res 68: 9-19.

13. Huisman J, Weissing FJ (1994) Light-limited growth and competition for light in well-mixed aquatic environments: An elementary model. Ecology 75: 507-520.

14. Mann KH, Lazier JRN (1996) Dynamics of marine ecosystems. Malden, MA, USA: Blackwell Publishing.

15. Huisman J, Weissing F (1999) Biodiversity of plankton by species oscillations and chaos. Nature 402: 407-410.

16. Klausmeier CA, Litchman E (2001) Algal games: the vertical distribution of phytoplankton in poorly mixed water columns. Limnol Oceanogr 46: 1998-2007.

17. Huisman J, Thi NNP, Karl DM, Sommeijer B (2006) Reduced mixing generates oscillations and chaos in the oceanic deep chlorophyll maximum. Nature 439: 322-325.

18. Ryabov AB, Rudolf L, Blasius B (2010) Vertical distribution and composition of phytoplankton under the influence of an upper mixed layer. J Theor Biol 263: 120-133.

19. Hickman A, Dutkiewicz S, Williams R, Follows M (2010) Modelling the effects of chromatic adaptation on phytoplankton community structure in the oligotrophic ocean. Mar Ecol Prog Ser 406: 1-17.

20. Beversdorf L, Miller T, McMahon K (2013) The role of nitrogen fixation in cyanobacterial bloom toxicity in a temperate, eutrophic lake. PLoS ONE 8(2): e56103.

21. Bopp L, Monfray P, Aumont O, Dufresne JL, Treut HL, et al. (2001) Potential impact of climate change on marine export production. Global Biogeochem Cy 15: 81-99.

22. Sarmiento JL, Slater R, Barber R, Bopp L, Doney SC, et al. (2004) Response of ocean ecosystems to climate warming. Global Biogeochem Cy 18.

23. Schmittner A (2005) Decline of the marine ecosystem caused by a reduction in the Atlantic overturning circulation. Nature 434: 628-633.

24. Mei ZP, Finkel ZV, Irwin AJ (2009) Light and nutrient availability affect the size-scaling of growth in phytoplankton. J Theor Bio 259: 582-588.

25. Patti B, Guisande C, Bonanno A, Basilone G, Cuttitta A, et al. (2010) Role of physical forcings and nutrient availability on the control of satellite-based chlorophyll *a* concentration in the coastal upwelling area of the Sicilian Channel. Sci Mar 74(3).

26. Behrenfeld M, O'Malley R, Siegel D, McClain C, Sarmiento J, et al. (2006) Climate-driven trends in contemporary ocean productivity. Nature 444.

27. Barale V, Jaquet JM, Ndiaye M (2008) Algal blooming patterns and anomalies in the Mediterranean Sea as derived from the SeaWiFS data set (1998-2003). Remote Sens Environ 112: 3300-3313.

28. Klausmeier CA, Litchman E, Levin SA (2007) A model of flexible uptake of two essential resources. J Theor Biol 246: 278-289.

29. Denaro G, Valenti D, La Cognata A, Spagnolo B, Bonanno A, et al. (2013) Spatio-temporal behaviour of the deep chlorophyll maximum in mediterranean sea: Development of a stochastic model for picophytoplankton dynamics. Ecol Complex 13: 21-34.

30. Thingstad TF, Rassoulzadegan F (1995) Nutrient limitations, microbial food webs, and biological C-pumps: suggested interactions in a P-limited Mediterranean. Mar Ecol Prog Ser 117: 299306.

31. Ribera d'Alcalà M, Civitarese G, Conversano F, Lavezza R (2003) Nutrient ratios and fluxes hint at overlooked processes in the Mediterranean Sea. J Geophys Res 108.

32. Riley GA, Stommel HM, Bumpus DF (1949) Quantitative ecology of the plankton of the western North Atlantic. Bulletin of the Bingham Oceanographic Collection. Yale University.

33. Radach G, Maier-Reimer E (1975) The vertical structure of phytoplankton growth dynamics, a mathematical model. Mem Soc R Sci Liege 7: 113-146.

34. Platt T, Denman KL, Jassby AD (1977) Modeling the productivity of phytpoplankton (807-856). In: The Sea. John Wiley, New York.

35. Shigesada N, Okubo A (1981) Effects of competition and shading in planktonic communities. J Math Biol 12: 311-326.

36. Klausmeier CA (1999) Regular and irregular patterns in semiarid vegetation. Science 284: 1826-1828.

37. Valenti D, Denaro G, La Cognata A, Spagnolo B, Bonanno A, et al. (2012) Picophytoplankton dynamics in noisy marine environment. Acta Phys Pol B 43: 1227-1240.

38. Diehl S (2002) Phytoplankton, light, and nutrients in a gradient of mixing depths: theory. Ecology 83: 386-398.

39. Huisman J, Sharples J, Stroom JM, Visser PM, Kardinaal WEN, et al. (2004) Changes in turbulent mixing shift competition for light between phytoplankton species. Ecology 85: 2960-2970.

40. Dutkiewicz S, Follows MJ, Bragg JG (2009) Modeling the coupling of ocean ecology and biogeochemistry. Global Biogeochem Cycles : GB4017.

41. Yoshiyama K, Mellard J, Litchman E, Klausmeier C (2009) Phytoplankton competition for nutrients and light in a stratified water column. Am Nat 174.

42. Denaro G, Valenti D, Spagnolo B, Bonanno A, Basilone G, et al. (2013) Stochastic dynamics of two picophytoplankton populations in a real marine ecosystem. Acta Phys Pol B : 977-990.

43. Denaro G, Valenti D, Spagnolo B, Basilone G, Mazzola S, et al. (2013) Dynamics of two picophytoplankton groups in mediterranean sea: Analysis of the deep chlorophyll maximum by a stochastic advection-reaction-diffusion model. PLoS ONE 8(6): e66765.

44. Grenfell BT, Wilson K, Finkenstädt BF, Coulson TN, Murray S, et al. (1998) Noise and determinism in synchronized sheep dynamics. Nature 394: 674-677.

45. Zimmer C (1999) Life after chaos. Science 284: 83-86.

46. Bjørnstad ON, Grenfell BT (2001) Noisy clockwork: Time series analysis of population fluctuations in animals. Science 293: 638-643.

47. Spagnolo B, Cirone M, La Barbera A, de Pasquale F (2002) Noise induced effects in population dynamics. J Phys 14: 2247-2255.

48. La Barbera A, Spagnolo B (2002) Spatio-temporal patterns in population dynamics. Physica A 314: 120-124.

49. Spagnolo B, La Barbera A (2002) Role of the noise on the transient dynamics of an ecosystem of interacting species. Physica A 315: 114-124.

50. Spagnolo B, Fiasconaro A, Valenti D (2003) Noise induced phenomena in Lotka-Volterra systems. Fluct Noise Lett 3: L177-L185.

51. Spagnolo B, Valenti D, Fiasconaro A (2004) Noise in ecosystems: A short review. Math Biosci Eng 1: 185-211.

52. Valenti D, Fiasconaro A, Spagnolo B (2004) Pattern formation and spatial correlation induced by the noise in two competing species. Acta Phys Pol B 35: 1481-1489.

53. Spagnolo B, Valenti D, Fiasconaro A (2005) Transient behavior of a population dynamical model. Prog Theor Phys Supp 157: 312-316.

54. Caruso A, Gargano ME, Valenti D, Fiasconaro A, Spagnolo B (2005) Cyclic fluctuations, climatic changes and role of noise in planktonic foraminifera in the Mediterranean Sea. Fluct Noise Lett 5: L349-L355.

55. Chichigina O, Valenti D, Spagnolo B (2005) A simple noise model with memory for biological systems. Fluct Noise Lett 5: L243-L250.

56. Fiasconaro A, Valenti D, Spagnolo B (2006) Asymptotic regime in N random interacting species. Eur Phys J B 50: 189-194.

57. Valenti D, Schimansky-Geier L, Sailer X, Spagnolo B (2006) Moment Equations for a Spatially Extended System of Two Competing Species. Eur Phys J B 50: 199-203.

58. Chichigina OA (2008) Noise with memory as a model of lemming cycles. Eur Phys J B 65: 347-352.

59. La Cognata A, Valenti D, Dubkov A, Spagnolo B (2010) Dynamics of two competing species in the presence of levy noise sources. Phys Rev E 81: 011121(1-8).

60. Chichigina OA, Dubkov AA, Valenti D, Spagnolo B (2011) Stability in a system subject to noise with regulated periodicity. Phys Rev E 84: 021134(1-10).

61. Goryachev A, Toh DJ, Wee KB, Lee T, Zhang HB, et al. (2005) Transition to quorum sensing in an agrobacterium population: A stochastic model. PLoS Comput Biol 1(4): e37.

62. Maye A, Hsieh CH, Sugihara G, Brembs B (2007) Order in spontaneous behavior. PLoS ONE 2(5): e443.

63. Valenti D, Spagnolo B, Bonanno G (2007) Hitting time distributions in financial markets. Physica A 382: 311-320.

64. Olson RJ, Zettler ER, DuRand MD (1993) Phytoplankton analysis using flow cytometry (pgs. 175-186). In: Handbook of methods in aquatic microbial ecology. Lewis Publishers, Boca Raton, FL, USA, 175-186 pp.

65. Casotti R, Landolfi A, Brunet C, D'Ortenzio F, Mangoni O, et al. (2003) Composition and dynamics of the phytoplankton of the Ionian Sea (Eastern Mediterranean). J Geophys Res 108.

66. Brunet C, Casotti R, Vantrepotte V (2008) Phytoplankton diel and vertical variability in photobiological responses at a coastal station in the Mediterranean Sea. J Plankton Res 30: 645-654.

67. Brunet C, Casotti R, Vantrepotte V, Corato F, Conversano F (2006) Picophytoplankton diversity and photoacclimation in the Strait of Sicily (Mediterranean Sea) in summer. I. Mesoscale variations. Aquat Microb Ecol 44: 127-141.

68. Brunet C, Casotti R, Vantrepotte V, Conversano F (2007) Vertical variability and diel dynamics of picophytoplankton in the Strait of Sicily, Mediterranean Sea, in summer. Mar Ecol Prog Ser 346: 15-26.

69. Ryabov A, Blasius B (2011) A graphical theory of competition on spatial resource gradients. Ecol Lett 14: 220-228.

70. Morel A (1997) Consequences of a Synechococcus bloom upon the optical properties of oceanic (case 1) waters. Limnol Oceanogr 42(8): 1746-1754.

71. Budillon G, Gasparini GP, Schroeder K (2008) Persistence of an eddy signature in the central Tyrrhenian basin. Deep-Sea Res Pt II .

72. Ribera d'Alcalà M, Brunet C, Conversano F, Corato F, Lavezza R (2009) Nutrient and pigment distributions in the southern Tyrrhenian Sea during mid-summer and late fall 2005. Deep-Sea Res Pt II 56: 676-686.

73. Ferla RL, Maimone G, Azzaro M, Conversano F, Brunet C, et al. (2012) Vertical distribution of the prokaryotic cell size in the Mediterranean Sea. Helgol Mar Res 66: 635-650.

74. Bethoux J, Morin P, Ruiz-Pino D (2002) Temporal trends in nutrient ratios: chemical evidence of mediterranean ecosystem changes driven by human activity. Deep-Sea Res Pt II 49: 2007-2016.

75. Brankart JM (1994) The modb local quality control. Technical Report, University of Liege .

76. Grasshoff K (1976) Methods of seawater analysis. Verlang Chemie, New York.

77. Casotti R, Brunet C, Aronne B, Ribera d'Alcalà M (2000) Mesoscale features of phytoplankton and planktonic bacteria in a coastal area as induced by external water masses. Mar Ecol Prog Ser 195: 15-27.

78. Raven JA, Finkel ZV, Irwin AJ (2005) Picophytoplankton: bottom-up an top-down controls on ecology and evolution. J Geophys Res 55: 209-205.

79. Dimier C, Corato F, Saviello G, Brunet C (2007) Photophysiological properties of the marine picoeukaryotes picochlorum rcc 237 (Trebouxiophyceae chlorophyta). J Phycol 43: 275283.

80. Worden AZ, Not F (2008) Microbial Ecology of the Oceans, Second Edition. John Wiley & Sons, Inc.

81. Mendonça A, Arístegui J, Vilas J, Montero M, Ojeda A, et al. (2012) Is there a seamount effect on microbial community structure and biomass? The case study of Seine and Sedlo Seamounts (Northeast Atlantic). PLoS ONE 7(1): e29526.

82. Raven JA (1998) The twelfth tansley lecture. small is beautiful: The picophytoplankton. Funct Ecol 12: 503.

83. Brunet C, Casotti R, Aronne B, Vantrepotte V (2003) Measured photophysiological parameters used as tools to estimate vertical water movements in the coastal Mediterranean. J Plankton Res 25: 1413-1425.

84. Finkel ZV, Irwin AJ (2005) Picophytoplankton: Bottom-up and top-down controls on ecology and evolution. Vie Milieu 55: 209-215.

85. Mella-Flores D, S M, Humily F, Partensky F, Mah F, et al. (2011) Is the distribution of Prochlorococcus and Synechococcus ecotypes in the mediterranean sea affected by global warming? Biogeosciences 8: 2785-2804.

86. Garczarek L, Dufresne A, Rousvoal S, West NJ, Mazard S, et al. (2007) High vertical and low horizontal diversity of prochlorococcus ecotypes in the Mediterranean Sea in summer. FEMS Microbiol Ecol 60: 189-206.

87. Denis M, Thyssen M, Martin V, Manca B, Vidussi F (2010) Ultraphytoplankton basin-scale distribution in the eastern mediterranean sea in winter: link to hydrodynamism and nutrients. Biogeosciences 7: 2227-2244.

88. Dimier C, Saviello G, Tramontano F, Brunet C (2009) Comparative ecophysiology of the xanthophyll cycle in six marine phytoplanktonic species. Protist 160: 397-411.

89. Moore LR, Goericke R, Chisholm SW (1995) Comparative physiology of synechococcus and prochlorococcus: influence of light and temperature on growth, pigments, fluorescence and absorptive properties. Mar Ecol Prog Ser 116: 259-275.

90. Partensky F, Hess W, Vaulot D (1999) Prochlorococcus, a marine photosyntheic prokaryote of global significance. Microbiol Mol Biol R 63: 106-127.

91. Bougaran G, Bernard O, Sciandra A (2010) Modeling continuous cultures of microalgae colimited by nitrogen and phosphorus. J Theor Biol 265: 443454.

92. Turpin DH (1988) Physiological mechanisms in phytoplankton resource competition (316-368). In: Growth and reproductive strategies of freshwater phytoplankton. Cambridge University Press.

93. Kirk JTO (1994) Light and Photosynthesis in Aquatic Ecosystems (2^{nd} edition). Cambridge University Press.

94. Dimier C, Brunet C, Geider R, Raven J (2009) Growth and photoregulation dynamics of the picoeukaryote *Pelagomonas calceolata* in fluctuating light. Limnol Oceanogr 54: 823-836.

95. Roache PJ (1976) Computational fluid dynamics. Hermosa Publishers, Albuquerque, New Mexico.

96. Roache PJ (1998) Fundamentals of Computational Fluid Dynamics. Hermosa Publishers, Albuquerque, New Mexico.

97. Tveito A, Winther R (1998) Introduction to Partial Differential Equations: A Computational Approach. Springer-Verlag, New York.

98. Veldman AEP (2001) Computational Fluid Dynamics. Lecture Notes. University of Groningen, The Netherlands.

99. Hundsdorfer W, Verwer JG (2003) Numerical Solution of Time-Dependent Advection-Diffusion-Reaction Equations. Springer Series in Computational Mathematics. Springer-Verlag, Berlin.

100. Thi NNP, Huisman J, Sommeijer BP (2005) Simulation of three-dimensional phytoplankton dynamics: competition in light-limited environments. J Comput Appl Math 174: 57-77.

101. Huppert A, Blasius B, Olinkya R, Stone L (2005) A model for seasonal phytoplankton blooms. J Theor Biol 236: 276-290.

102. Ebeling W, Spagnolo B (2005) Noise in condensed matter and complex systems. Fluct Noise Lett 5: L159-L161.

103. Provata A, Sokolov I, Spagnolo B (2008) Editorial: Ecological complex systems. Eur Phys J B 65: 307-314.

104. Spagnolo B, Dubkov AA (2008) Editorial of critical phenomena and diffusion in complex systems. Int J Bifurcat Chaos 18: 2643-2647.

105. Valenti D, Tranchina L, Cosentino C, Brai M, Caruso A, et al. (2008) Environmental metal pollution considered as noise: Effects on the spatial distri-

bution of benthic foraminifera in two coastal marine areas of Sicily (Southern Italy). Ecol Model 213: 449-462.

106. Valenti D, Fiasconaro A, Spagnolo B (2004) Stochastic resonance and noise delayed extinction in a model of two competing species. Physica A 331: 477-486.

107. Mikhailov AS, Loskutov AY (1996) Foundations of Synergetics II: Chaos and Noise. Springer Series in Synergetics. Springer, Berlin.

108. Muñoz MA, Colaiori F, Castellano C (2005) Mean-field limit of systems with multiplicative noise. Phys Rev E 72: 056102.

109. Manor A, Shnerb N (2009) Multiplicative noise and second order phase transitions. Phys Rev Lett 103: 030601.

110. Schenzle A, Brand H (1979) Multiplicative stochastic processes in statistical physics. Phys Rev A 20: 1628-1647.

111. Graham R, Schenzle A (1982) Carleman imbedding of multiplicative stochastic processes. Phys Rev A 25: 1731-1754.

112. García-Ojalvo J, Sancho JM (1999) Noise in Spatially Extended Systems. Springer, New York.

113. Redner S (1990) Random multiplicative processes: An elementary tutorial. Am J Phys 58: 267-273.

114. Sornette D (2000) Critical Phenomena in Natural Sciences. Springer Series in Synergetics. Springer, Heidelberg.

115. Barrera P, Ciuchi S, Spagnolo B (1993) Generating function for a multiplicative noise with group analysis. J Phys A: Math Gen 26: L559-L565.

116. Ciuchi S, de Pasquale F, Spagnolo B (1993) Nonlinear relaxation in the presence of an absorbing barrier. Phys Rev E 47: 3915-3926.

117. Ciuchi S, de Pasquale F, Spagnolo B (1996) Self-regulation mechanism of an ecosystem in a non-gaussian fluctuation regime. Phys Rev E 54: 706-716.

118. Giuffrida A, Valenti D, Ziino G, Spagnolo B, Panebianco A (2009) A stochastic interspecific competition model to predict the behaviour of *Listeria monocytogenes* in the fermentation process of a traditional sicilian salami. Eur Food Res Technol 228.

119. Horsthemke W, Lefever R (1984) Noise-Induced Transitions: Theory and Applications in Physics, Chemistry, and Biology. Springer-Verlag, Berlin Heidelberg.

120. Gardiner CW (1985) Handbook of Stochastic Methods. Springer-Verlag, Berlin Heidelberg.

121. Rippka R, Coursin T, Hess W, Lichtle C, Scanlan DJ, et al. (2000) *Prochlorococcus marinus* Chisholm et al. 1992 subsp. *pastoris* subsp. nov. strain PCC 9511, the first axenic chlorophyll a_2/b_2-containing cyanobacterium (*Oxyphotobacteria*). Int J Syst Evol Micr 50: 1833-1847.

122. Huisman J, Arrays M, Ebert U, Sommeijer B (2002) How do sinking phytoplankton species manage to persist? Am Nat 159: 245-254.

123. Moon-Van Der Staay SY, De Wachter R, Vaulot D (2001) Oceanic 18S rDNA sequences from picoplankton reveal unsuspected eukaryotic diversity. Nature 409: 607-610.

124. Spagnolo B, Spezia S, Curcio L, Pizzolato N, Fiasconaro A, et al. (2009) Noise effects in two different biological systems. Eur Phys J B 69: 133-146.

125. Liu QX, Jin Z, Li BL (2008) Resonance and frequency-locking phenomena in spatially extended phytoplankton-zooplankton system with additive noise and periodic forces. J Stat Mech-Theory E 2008.

126. Veldhuis MJW, Timmermans KR, Croot P, Van Der Wagt B (2005) Picophytoplankton; a comparative study of their biochemical composition and photosynthetic properties. J Sea Res 53: 7-24.

127. Thingstad TF, Sakshaugh E (1990) Control of phytoplankton growth in nutrient recycling ecosystems. Theory and terminology. Mar Ecol Prog Ser 63: 261-272.

128. Quevedo M, Anadón R (2001) Protist control of phytoplankton growth in the subtropical north-east Atlantic. Mar Ecol Prog Ser 221: 20-38.

129. Timmermans KR, van der Wagt B, Veldhuis MJW, Maatman A, de Baar HJW (2005) Physiological responses of three species of marine pico-phytoplankton to ammonium, phospahte, iron and light limitation. J Sea Res 53: 109-120.

130. Bertilsson S, Berglund O, Karl DM, Chisholm SW (2003) Elemental composition of marine *Prochlorococcus* and *Synechococcus*: implications for the ecological stoichiometry of the sea. Limnol Oceanogr 48: 1721-1731.

131. Denman KL, Gargett AE (1983) Time and space scales of vertical mixing and advection of phytoplankton in the upper ocean. Limnol Oceanogr 28: 801-815.

132. Oakey NS, Elliott JA (1982) Dissipation within the surface mixed layer. J Phys Oceanogr 12: 171-185.

133. Nishimura H, Nakamura Y (1987) A new method of estimating vertical diffusion coefficient. Cont Shelf Res 7: 1245-1256.

134. Nakamura Y, Hayakawa N (1991) Modelling of thermal stratification in lakes and coastal seas. In: Hydrology of Natural and Manmade Lakes. volume 206, pp. 227-236.

135. Justić D, Rabalais NN, Turner RE (2002) Modeling the impacts of decadal changes in riverine nutrient fluxes on coastal eutrophication near the Mississippi River Delta. Ecol Model 152: 33-46.

136. Venrick EL, McGowan JA, Mantyla AW (1973) Deep maxima of photosynthetic chlorophyll in the Pacific Ocean. Fish Bull 71: 41-52.

137. Cullen JJ (1982) The deep chlorophyll maximum: comparing vertical profiles of chlorophyll a. Can J Fish Aquat Sci 39: 791-803.

138. Longhurst AR (1998) Ecological geography of the sea. San Diego, California, USA: Academic Press.

139. Letelier RM, Karl DM, Abbott MR, Bidigare RR (2004) Light driven seasonal patterns of chlorophyll and nitrate in the lower euphotic zone of the North Pacific Subtropical Gyre. Limnol Oceanogr 49: 508-519.

140. Venrick EL (1993) Phytoplankton seasonatity in the central North Pacific: The endless summer reconsidered. Limnol Oceanogr 38: 1135-1149.

141. Li WKW (1995) Composition of ultraphytoplankton in the central North Atlantic. Mar Ecol Prog Ser 122: 1-8.

142. Holm-Hansen O, Hewes CD (2004) Deep chlorophyll-a maxima (DCMs) in Antarctic waters. I. Relationships between DCMs and the physical, chemical, and optical conditions in the upper water column. Polar Biol 27: 699-710.

143. Fennel K, Boss E (2003) Subsurface maxima of phytoplankton and chlorophyll: Steady-state solutions from a simple model. Limnol Oceanogr 48: 1521-1534.

144. Hodges BA, Rudnick DL (2004) Simple models of steady deep maxima in chlorophyll and biomass. Deep-Sea Res Pt I 51: 999-1015.

145. Reynolds CS (1998) The concept of ecological succession applied to seasonal periodicity of freshwater phytoplankton. Verh Internat Verein Limnol 23: 683-691.

146. Bibby TS, Mary I, Nield J, Partensky F, Barber J (2003) Low light adapted prochloroccus species possess specific antennae for each photosystem. Nature 424: 1051-1054.

147. Moore LR, Rocap G, Chisholm SW (1998) Physiology and molecular phylogeny of coexisting Prochlorococcus ecotypes. Nature 397: 464-467.

148. Olaizola M, Ziemann DA, Bienfang PK, Walsh WA, Conquest LD (1993) Eddy-induced oscillations of the pycnocline affect the floristic composition and depth distribution of phytoplankton in the sub-tropical Pacific. Mar Biol 116: 533-542.

149. Vaillancourt RD, Marra J, Seki MP, Parsons ML, Bidigare RR (2003) Impact of a cyclonic eddy on phytoplankton community structure and photosynthetic competency in the subtropical North Pacific Ocean. Deep Sea Res II 50: 829-847.

150. Litchmann E, Klausmeier CA (2001) Competition of phytoplankton under fluctuating irradiance. Am Nat 157: 170-187.

Appendix A

A.1 List of Pubblications

A.1.1 Papers in ISI Journals

1. D. Valenti, G. Denaro, D. Persano Adorno, N. Pizzolato, S. Zammito, B. Spagnolo, *'Monte Carlo analysis of polymer translocation with deterministic and noisy electric fields'*. Centr. Eur. J. Phys. **10**, 560-567 (2012).

2. D. Valenti, G. Denaro, A. La Cognata, B. Spagnolo, A. Bonanno, G. Basilone, S. Mazzola, S. Zgozi, S. Aronica, *'Picophytoplankton dynamics in noisy marine environment'*. Acta Phys. Pol. B **43**, 1227-1240 (2012).

3. G. Denaro, D. Valenti, A. La Cognata, B. Spagnolo, A. Bonanno, G. Basilone, S. Mazzola, S. Zgozi, S. Aronica, C. Brunet, *'Spatio-temporal behaviour of the deep chlorophyll maximum in Mediterranean Sea: Development of a stochastic model for picophytoplankton dynamics'*. Ecol. Complex. **13**, 21-34 (2013).

4. G. Denaro, D. Valenti, B. Spagnolo, G. Basilone, S. Mazzola, S. Zgozi, S. Aronica, A. Bonanno, *'Dynamics of Two Picophytoplankton Groups in Mediterranean Sea: Analysis of the Deep Chlorophyll Maximum by a Stochastic Advection-Reaction-Diffusion model'*. PLOS ONE **8(6)**, e66765(1)-e66765(14) (2013).

5. G. Denaro, D. Valenti, B. Spagnolo, A. Bonanno, G. Basilone, S. Mazzola, S. Zgozi, S. Aronica, *'Stochastic dynamics of two picophytoplankton populations in real marine ecosystem'*. Acta Phys. Pol. B **44**, 977-990 (2013).

A.2 International conferences

1. Congress presentation: *'Monte Carlo study of external noise influence on polymer translocation'* by D. Valenti, G. Denaro, D. Persano Adorno, N. Pizzolato, S. Zammito and B. Spagnolo, at the *International Conference on Statistical Physics 2011*, held in Larnaca, Cyprus on 2011 July 11-15.
   http://www.sigmaphi2011.org/

2. Congress presentation: *'A stochastic reaction-diffusion-taxis model for pico-phytoplankton dynamics'* by D. Valenti, G. Denaro, A. La Cognata, B. Spagnolo, A. Bonanno, G. Basilone, S. Mazzola, S. Zgozi and S. Aronica, at the *24th Marian Smoluchowski Symposium on Statistical Physics*, held in Zakopane, Poland on 2011 September 17-22.
   http://th-www.if.uj.edu.pl/zfs/smoluchowski/2011/

3. Poster presentation: *'A stochastic reaction-diffusion-taxis model for two pico-phytoplankton populations'* by G. Denaro, D. Valenti, A. La Cognata, B. Spagnolo, A. Bonanno, G. Basilone, S. Mazzola and S. Aronica, at the *25th Marian Smoluchowski Symposium on Statistical Physics*, held in Krakow, Poland on 2012 September 10-13.
   http://th-www.if.uj.edu.pl/zfs/smoluchowski/2012/